STUDY ON COKE FORMATION OVER Mo/HZSM-5 CATALYST IN NON-OXIDATIVE METHANE DEHYDROAROMATIZATION REACTION

July 2015

SONG YANG

Graduate School of Engineering

CHIBA UNIVERSITY

（千葉大学審査学位論文）

STUDY ON COKE FORMATION OVER Mo/HZSM-5 CATALYST IN NON-OXIDATIVE METHANE DEHYDROAROMATIZATION REACTION

July 2015

SONG YANG

Graduate School of Engineering

CHIBA UNIVERSITY

Abstract

Non-oxidative methane dehydroaromatization reaction (MTB) over Mo/HZSM-5 catalyst, as a promising route for direct conversion of methane resources into highly value-added chemicals, has received considerable recent attention. Although many meaningful and inspiring studies were reported in the past two decades, coking-caused catalyst deactivation problem remains still unsolved. This thesis focuses mainly on the coking pathways, coking locations, types of coke formed and coke formation behavior in cyclic CH_4-H_2 switching operation mode. First, by pursuing coke formation behavior over the lifetime of Mo/HZSM-5 catalyst and examining the effect of co-fed H_2 in CH_4 feed on the distribution of coke formed in a multi-layer fixed bed reactor, I have successfully proved that not the aromatic product C_6H_6 but the intermediate C_2H_4 is the dominant source of coke deposition. Second, by pursuing coke accumulation behavior in cyclic CH_4-H_2 switching operation mode and coke removal behavior in pure H_2, I have revealed for the first time that the graphite-like coke formed at the channel mouths of the zeolite is responsible for the catalyst deactivation. Third, by using MoO_3-added carbon materials as reference samples I have also clarified the catalytic role of Mo species on promoting coke burning in TPO process, which in turn enables me to distinguish four types of coke forming on microzeolite-based Mo/HZSM-5 catalyst in the title reaction.

論文概要

Mo/HZSM-5 触媒によるメタンの芳香族化反応は 1993 年に初報告された、メタン資源を石油化学の基幹原料の一つであるベンゼンとクリーンな水素ガスに直接転換する非酸化的触媒反応であり、過去２０年間にわたって多くの基礎及び応用研究が行われてきた。しかしながら触媒の迅速失活を引き起こす炭素析出のメカニズムは未だに解明されていない。本学位論文は炭素析出による Mo/HZSM-5 触媒の失活メカニズムの解明研究に関するもので、析出炭素源となる反応中間体または芳香族生成物の同定、炭素析出サイトの解明、及び析出炭素のタイプの解析に焦点を当てる。本研究により得られた成果は以下である。（１）触媒の完全失活までのその活性、選択性及び析出炭素（コーク）量の経時変化を追跡することと、多層固定触媒層に析出する炭素分布に対する水素の反応ガスへの添加効果を系統的に調べることにより、芳香族生成物のベンゼンではなく反応中間物のエチレンが析出炭素の主な供給源であることを初めて明らかにした。（２）触媒の失活試験と水素によるその再生試験を短い周期で繰り返す所謂周期的切替操作モードでの炭素析出速度の経時変化を追跡することと、水素による析出炭素の連続除去に伴ったメタンの生成速度の経時変化を追跡することにより、触媒の活性低下は主にゼオライト細孔口付近への炭素析出により引き起こされることを明らかにした。（３）酸化モリブデンを担持した参照炭素試料の昇温酸化反応との比較試験により、マイクロサイズゼオライトをベースとする Mo/HZSM-5 触媒には 4 種類の炭素が析出されることを明らかにした。

Content

Chapter 1

Introduction 1

1.1. Background 1

1.1.1. Alternative carbon source for production of petrochemicals 1

1.1.2. Non-oxidative methane dehydroaromatization 1

1.1.3. Catalyst deactivation by coke 1

1.2. Characterization of coke deposit 2

1.2.1. Types of coke 2

1.2.2. Locations of coke 3

1.2.3. Factors to control coking formation 4

1.3. Approaches to suppressing coke formation 4

1.3.1. Zeolite selection 5

1.3.2. Creation of mesopores in zeolites 5

1.3.3. Modification of the acidity of zeolite 6

1.3.4. Synthesis of new zeolites 7

1.3.5. Doping of metal promoters 7

1.3.6. Surface silanation treatment 8

1.3.7. Addition of oxygen-containing gases 8

1.3.8. Reaction coupling 10

1.4. Regeneration of coked catalyst 11

1.4.1. O_2 regeneration 11

1.4.2. H_2 regeneration 12

1.5. Motivation and objectives 13

1.6. Dissertation organization 13

References 14

Chapter 2

Experimental 21

2.1. Catalyst preparation 21

2.1.1. Main chemicals and instruments for catalysts preparation 21

2.1.2. Catalyst preparation approaches 21

2.2. Catalyst characterization 21

2.2.1. FT-IR spectroscopy 21

2.2.2. N_2 adsorption and desorption isotherm 22

2.2.3. X-ray diffraction 22

2.2.4. Scanning Electron Microscope 22

2.2.5. NH_3 adsorption/temperature programmed desorption 22

2.2.6. ^{27}Al NMR spectra 23
2.2.7. X-ray photoelectron spectroscopy 23
2.2.8. Thermal gravimetric analysis 23
2.2.9. Temperature programmed oxidation 24
2.3. Catalyst activity evaluation 24
2.3.1. Apparatus 24
2.3.2. Experimental procedure 25
2.3.3. Methodology 26

Chapter 3

The lifetime performance of Mo/HZSM-5: the pathway of coke formation in the last stage of catalyst deactivation 31

3.1. Introduction 31
3.2. Experimental 34
3.2.1. Catalyst preparation 34
3.2.2. Catalyst characterization 34
3.2.3. Reactor 34
3.2.4. Activity evaluation 35
3.2.5. Coke characterization 36
3.3. Results and discussion 37
3.3.1. Catalyst characterization 37
3.3.2. Activity evaluation 37
3.3.3. Quantification of the coke deposit 41
3.3.4. Characterization of the coke deposit 43
3.3.5. Coke source 46
3.4. Further discussion 50
3.5. Conclusions 51
References 52

Chapter 4

Effect of co-fed H_2 on the distribution of coke formed: the pathway of coke formation in the stable benzene formation stage 63

4.1. Introduction 63
4.2. Experimental 65
4.2.1. Catalyst preparation and characterization 65
4.2.2. Activity evaluation test 65
4.2.3. Coke characterization 66
4.3. Results and discussion 67

4.3.1. Suppressing effect of co-fed H2 on catalyst performance and coke formation 67
4.3.2. Mechanism of the suppressive effect of H_2 72
4.3.3. Dominant coke source 74
4.4. Conclusions 80

Chapter 5

Coke formation over Mo/HZSM-5 in the non-oxidative methane dehydroaromatization reaction under CH_4-H_2 switching mode: identification of the coke responsible for deactivation 96

5.1. Introduction 96
5.2. Experimental 98
5.2.1. Catalyst preparation and characterization 98
5.2.2. Activity evaluation 98
5.2.3. Coke characterization 98
5.3. Results and discussion 99
5.3.1. Activity evaluation 99
5.3.2. Characterization of coked catalyst 101
5.4. Identification of the coke responsible for deactivation 103
5.5. Further discussion deactivation mechanism 106
5.6. Conclusions 107
References 108

Chapter 6

The catalytic role of Mo in the Temperature-Programmed-Oxidation of the coke 114

6.1. Introduction 114
6.2. Experimental 116
6.2.1. Catalyst preparation 116
6.2.2. Catalyst characterization and evaluation 117
6.2.3. Characterization of spent catalyst 118
6.3. Results and discussion 118
6.3.1. Fresh catalyst characterization 118
6.3.2. Catalytic reaction 120
6.3.3. BET of spent catalyst 121
6.3.4. TG of spent catalysts 122
6.4. Discussion 125
6.5. Conclusions 126

References 126

Chapter 7

Conclusions 136

Achievements 137

Acknowledge 139

Chapter 1

Introduction

1.1. Background

1.1.1. Alternative carbon source for production of petrochemicals

At present the chemical industry, which supplies many useful chemical products such as plastic and rubber products to support human's daily life, is mostly based on the fossil oil [1]. However, depletion of petroleum reserves is a strong driver for the search of alternative carbon sources to produce fuels and chemicals. This is the requirement of a new era, where cleaner technologies and renewable resources replace fossil fuels to support modern society life [2]. Methane is considered as a very abundant resource that is widely distributed around the globe. After the shale gas revolution in the United States, researchers pay more attention on the utilization of the methane to produce petrochemicals directly [3-5].

1.1.2. Non-oxidative methane dehydroaromatization

In 1993, Wang et al. [6] first reported the Mo/HZSM-5 catalyzed non-oxidative methane dehydroaromatization reaction (MTB), via which methane can be directly converted to aromatics (mainly C_6H_6) and H_2. This reaction showed a high benzene selectivity in comparison with oxidative methane conversion processes. This reaction provides an alternative way for production of benzene and its industrial application is of great importance. Thereafter, many meaningful and inspiring studies were reported on its fundamentals and applications [7-10]. To date, the title reaction is well recognized to proceed via a bifunctional mechanism: CH_4 is first activated on Mo_2C sites [11] to form the C_2H_4 intermediate and then the oligomerization and cyclization of C_2H_4 on Bronsted acid sites follows to form benzene as well as naphthalene [12-14].

1.1.3. Catalyst deactivation by coke

Due to its low equilibrium conversion, the title reaction should be conducted under high temperature to achieve a high methane conversion. However, under severe conditions, serious coke formation will cause the catalyst to deactivate rapidly. This problem remains still unsolved and a big obstacle to the industrial application of the title reaction. [15, 16]

1.2. Characterization of coke deposit

1.2.1. Types of coke

Coke formation in methane dehydroaromazization is a major obstacle for a better understanding of the fundamentals of the reaction and its practical utilization. The properties of coked catalyst samples were characterized by many techniques such as XPS, UV-Raman and TPO. The XPS study of fresh and spent catalysts by Lunsford and co-workers [17] and Larachi et al. [18] showed that during the conversion of methane to benzene in the absence of oxygen over a 2 wt% Mo/H-ZSM-5 catalyst at 700 ℃, three different types of surface carbon formed in the catalyst: adventitious or graphitic-like C (284.6 eV), carbidic-like C (282.7 eV), and hydrogen-poor sp-type C (283.2 eV). Ma et al [19] reported that there are at least three types of coke: carbidic carbon in molybdenum carbide, molybdenum-associated coke, and aromatic-type coke on acid sites. UV-Raman spectra disclosed that the carbonaceous deposits formed on HZSM-5 are mainly polyolefinic and aromatic, while that on Mo/HZSM-5 catalyst is mainly polyaromatic. Comparing the coke deposits on HZSM-5 with that on Mo/HZSM-5, one can find that the degree of the polymerization and cyclization of coke species on the Mo/HZSM-5 was higher [20].

TPO technique, as a powerful method, was used to investigate the burning behavior of coke deposition over coked catalysts. Some researchers [21-23] have reported a typical CO_x releasing curve during the coke burning in the TPO process, which show two peaks corresponding to coke burning at low and high temperatures, respectively. The coke depositions burning at low and high temperatures in TPO were attributed to coke associated with Mo species and coke deposited on the

Bronsted acid site, respectively. Liu et al [23, 24] reported that the carbonaceous deposits, burnt-off at both low and high temperatures, could react with H_2 and CO_2, and the catalytic activity be restored after temperature-programmed hydrogenation. In the presence of higher concentrations of CO (4.0–12 %) the formation of inert coke was preferentially suppressed to leave the coke more reactive and possibly associated with Mo_2C [25]. TG, ^1H MAS NMR [26] and XAES [27] studies confirmed that the amount of the aromatic carbonaceous deposits greatly increased with the reaction time. Ma and co-workers [28] reported that there were three peaks, excluding COx evolution from oxidation of Mo_2C, in the TPO curves of spent catalysts exposed to CH_4 at high space velocities (≥5400 ml/(g·h)). Nevertheless, as determined by differential thermal analysis (DTA), Matus [29] reported that carbonaceous deposits formed in a 2% Mo/HZSM-5 catalyst with the zeolite of Si/Al = 17 over a 6 h reaction period produced a single exothermic peak, whereas two peaks were observed for the catalysts with their zeolites of Si/Al = 30 and 45. The diversity of burning peak of spent catalysts in the TPO or DTA indicates that identification of the positions and types of the coke formed Mo/HZSM-5 during the MDA reaction still remains under debate.

1.2.2. Locations of coke

Due to deep involvement of the zeolite channel system in aromatics formation, a small amount of coke deposition inside the zeolite channels or at the channel mouths will cause a significant influence on the product selectivity. Therefore identification of the locations of coke deposition is of great importance. However, due to the use of different methods the resultant conclusions were quite confused. In terms of spatial position the coke on the external zeolite surface (external coke) was distinguished from that inside the zeolite channels (internal coke), while in terms of chemical stricture, coke was attributed to the type associated with Mo species or that located on the Bronsted acid site. No matter which methodology is used for coke identification, it would not lead to a clear answer to the question of what type of coke is responsible for catalyst deactivation and not allow us to identify its location in the catalyst. Great controversial and non-uniform conclusions can be found in the following literatures.

The unvarying O1s binding energy observed in the XPS spectra of both fresh and used catalysts suggests that coke formation does not occur on the SiO_4 tetrahedra but rather on the molybdenum sites dispersed on the external surface of ZSM-5[30]. HRTEM results [29] showed that the carbonaceous deposits were formed as graphite layers on the surface of Mo_2C nanoparticles that were >2 nm in size, and as friable layers with a disordered structure on the external surface of the zeolite. Coke characterization using TG analysis and TPO showed that besides the carbidic carbon, two other types of coke formed on Mo/HZSM-5: one associated to molybdenum and the other associated to Bronsted acid sites located both on the catalyst surface and inside zeolite pores [31]. ^{1}H-^{27}Al CP/MAS NMR experiments indicated that most of the coke is deposited on framework aluminum (Bronsted acid site) [32]. By analyzing their TPO data, Ma [19] and Wang [33] believed that the aromatic-type cokes on Bronsted acid sites are responsible for catalyst deactivation. Bai [34] suggested the blockage of the zeolite channels by coke deposition became gradually more serious with prolonged time on stream and was the main cause of catalyst deactivation. Ma [28] concluded that coke deposited on the free Bronsted acid sites, which was derived from naphthalene adsorption, is responsible for the catalyst deactivation.

1.2.3. Factors to control coking formation

The effect of operating conditions on the coke formation such as space velocity [28, 35] and superficial velocity [36] and those of zeolite particle size [37] and binder [38] were also investigated to explore the coking formation behavior in the title reaction.

1.3. Approaches to suppressing coke formation

Because coking causes rapid deactivation of Mo/HZSM-5 catalyst in the MTB process, researchers have attempted to solve this formidable problem and enhance the catalyst stability in extensive researches.

1.3.1. Zeolite selection

After the original report of the title reaction in 1993, researchers realized that not only active metal sites but also zeolite channels must be involved in the reaction. Many efforts have been made to screen various types of zeolites for their application in this reaction, such as HZSM-11, HZSM-8, H-β, HMCM-41, H-SAPO-34 , H-MOR, H-X, H-Y, H-SAPO-5, H-SAPO-11, [39] ITQ-13 [40], ITQ-2 [41], MCM-36 [42], but only HZSM-5 zeolite-based catalyst shows best performance. That is attributed to the molecular diameter of the main product C_6H_6 being almost the same as the channel size of the HZSM-5 zeolite, which have two interconnected channels of 0.53nm × 0.56nm and 0.51nm × 0.55nm. A MCM-22 zeolite was synthesized and applied to the title reaction, and also showed a better catalytic performance and a high coke-resistance. It possesses two independent multidimensional channel systems: two-dimensional 10-ring sinusoidal inter-layer channel system and inter-layer channel system containing 12-ring interlayer super-cages with inner free space of 0.71 × 0.71 × 1.82 nm. The better coking tolerance of HMCM-22-based catalysts may come from the channel structures of HMCM-22, the 12-ring super-cages of which could function as a coke trap to allow heavier coke deposition [43, 44]. Nevertheless, the two best zeolite -based catalysts, Mo/HZSM-5 and Mo/HMCM-22, still suffer rapid deactivation for serious coke deposition. Therefore, the effort on modification of the zeolite based-catalysts and exploration of new catalysts has continued.

1.3.2. Creation of mesopores in zeolites

The access of reactants to the active site and diffusion behavior of products to the gas phase strongly depend on the textural properties of zeolites. Their structures influence the catalytic performances and coking formation behaviors of the catalysts in the MTB reaction. Therefore, the HZSM-5 zeolite with mesopores should be synthesized and applied to the title reaction to overcome mass transfer limitations prevent coke deposition in its micropores.

Creating proper mesopores in HZSM-5, by etching its zeolite framework with with alkali solution [45] or by usage of nanosized carbon templates in its synthesis

[42, 46-48], could improve the mass transfer in zeolite crystals so that coke formation occurring there could be avoided. On the one hand, it was reported that a larger amount of coke deposits formed in the catalyst comprising intracrystalline mesopores, while it showed an improved performance in terms of deactivation rate and aromatics yield. The enhanced tolerance to coke accumulation on the zeolite-based catalyst was related to the intracrystalline mesopores that act as a trap for coke precursors and allow more coke to deposit due to the less spatial constraints [49]. In contrast, Liu [48] and Hu [15] reported that the coke formation rate on the catalysts that possessed mesopores were lower than that over referenced catalysts, which was connected to their improved catalytic stability. These authors speculated that the probability of coke forming in their catalysts were considerably decreased since the rate of aromatics products diffusing out of their zeolite crystals was remarkably improved due to the presence of mesopores. The discrepancies in coke content between these previous studies should be ascribed to the used zeolites of different mesoporous structures.

1.3.3. Modification of the acidity of zeolite

The Bronsted acidity of the zeolite promotes the harmful carbonaceous deposition on the zeolite surface in the methane dehydroaromatization reaction, and hence removal of a part of Bronsted acid sites of the zeolite would lead to an enhancement in the catalytic stability of Mo/HZSM-5. It was found that a small fraction of Bronsted acid sites was sufficient to accomplish the aromatization of the intermediates in methane aromatization reaction, while the presence of any superfluous free Bronsted acid sites could enhance the deposition of aromatic carbonaceous deposits on the catalysts. The presence of these superfluous Bronsted acid sites actually facilitates the holding of coke precursors for a longer time on the zeolite surface, and consequently promotes their polymerization reactions and increases the rate of the aromatic-type carbonaceous deposition. Removal of these unnecessary Bronsted acid sites leads to an efficient and effective suppression on the formation of aromatic-type of coke in the title reaction. The methods of acidity modification included the pre-treatment of zeolites with steam [50-52], N_2 [53], NH_4F [54], the post-treatment of the catalysts using steam [55, 56], hydrothermal

post-synthesis of zeolites [57-59] and the dealumination treatment using aqueous HNO_3 solution [60]. The resulted catalysts exhibited in general stronger coking-resistance with less coke forming, apparently due to the substantial loss of the Bronsted acid sites in their zeolites. It should be pointed out that the dealumination treatment not only modified the zeolite acidity but also influenced the Mo species dispersion in the zeolite, which resulted in a new balance between Mo species and Bronsted acid sites, and made the situation more complex in the modified catalyst.

1.3.4. Synthesis of new zeolites

Nanosized zeolites [61], zeolites with hierarchical structures [47, 62], and other new zeolites catalysts [63], derived from MCM-22 or ZSM-5 zeolite, such as Mo-IM-5 [64], Mo/TNU-9 [65], were synthesized and applied to the title reaction. Although these zeolite-based catalysts showed higher activities or higher benzene selectivities, they still have some drawbacks to be improved, such as they are catalytically less stable and they are difficult to be synthesized.

1.3.5. Doping of metal promoters

Noble metals are known as good catalysts for the activation of hydrogen and for the hydrogenation of carbonaceous species. Therefore, they are expected to help to remove the deposited coke via the methanation reaction $C + 2H_2 = CH_4$, and consequently to improve the catalyst stability. Adding a second metal to Mo/HZSM-5 seems to be a promising way to develop highly stable catalysts for the reaction. The amount of coke formed in Mo/HZSM-5 catalyst or its coke selectivity was reported to decrease when it was added with with a second metal such as Pt [66], Co [67], Ga [68], Zn [69], Ru [21, 70], Pt [71], Rh [71], Cr [72], Cu [73], La [74], Pd [75], Tr [75].

It was also found that the stabilities of the catalysts modified with Cu [76], Ni [77], or Fe [10, 78-80] were drastically improved. However, the spent were reported to have a larger amount of coke deposition. That could be attributed to the formation

of carbon nanotubes during the reaction process. The positive effect of metal-induced carbon nanotube formation on improving the catalyst stability was clarified by our group.

1.3.6. Surface silanation treatment

Owing to its bifuncational working mechanism, Mo/HZSM-5 catalyst can be deactivated by coke formation on its Mo sites and Bronsted acid sites in the zeolite channels. Note that the product distribution of the reaction is remarkably affected by the zeolite channels. Bulky aromatics and coke could form over the external surface of the zeolite crystals where spatial constraint does not exist. The selective elimination of acid sites on the external surface of the zeolite prior to loading of Mo species could reduce the amount of active Mo and free Bronsted acid sites, and consequently lower the risk of the zeolite channels being blocked by external coke in the recation. Iglesia et al [81] reported the surface silanation treatment, using bulky exotic silicon source for selectively covering and eliminating the external surface acid sites of the zeolite, could decrease the density of acid sites on the external surface of HZSM-5, and lead to a catalyst with a higher one-ring aromatics production activity and deactivating at a slower rate. Ichikawa et al [82] studied the effect of different types of silicon sources on the catalytic performance of the resultant catalyst, and found that all silica-modifed Mo/HZSM-5 catalysts showed an improved benzene selectivity and catalytic stability while their selectivity to the formation of naphthalene was largely reduced. Xu et al [83] confirmed that the silanation of HZSM-5 zeolite significantly suppressed the deposition of carbonaceous species on the surface of the catalyst, while it improved the activity and stability of the catalyst.

1.3.7. Addition of oxygen-containing gases

The MTB reaction is equilibrium-limited and has a low methane conversion when compared with other methane conversion processes, such as oxidative coupling of methane (OCM), methane reforming to syngas. [2] Its conversion is certainly decreased with increasing H_2 partial pressure in feed. On the other hand, adding a small amount of H_2 into methane feed was reported to be very effective in

suppressing coke formation on the catalyst, especially on its Bronsted acid sites during the reaction, and thus realizing a highly stable performance [84, 85]. Adding H_2 into methane feed improves the catalyst stability, but has little influence on the product selectivity [86]. Moreover, Mo K-edge Fourier transform spectra obtained for used Mo/HZSM-5 samples confirmed that the highly dispersed Mo_2C, which works as the active phase for activation of methane, has an excellent thermal stability in the hydrogen atmosphere at 1023-1273K [87]. Tan and co-workers [88] speculated that a much more stable performance can be realized at higher H_2 concentration because excessive dehydrogenation of the coke precursors to surface coke is hindered due to the equilibrium limitations. Iglesia and co-workers [89] suggested that H_2 can scavenge the reactive surface carbon and suppress C–C bond formation pathways. The positive effect of H_2 on suppression of coke deposition can also be proved by the results obtained from membranes reactors where continuous withdrawal of coproduced H_2 promoted the formation and deposition of low-H/C carbonaceous species in catalysts, especially at high temperatures [90].

Ichikawa et al [25] reported that addition of a small amount of CO or CO_2 (less than 3%) to the CH_4 feed enhanced the catalyst stability and suppressed coke formation on Mo or Re based HZSM-5 catalysts in the MTB reaction. These authors suggested a unique role of CO in the methane aromatization reaction as shown in Figure 1-1. CO may dissociate on the catalyst surface, mostly on the Mo sites, to form active species [C] and [O]. The active carbon species [C] is then hydrogenated to [CHx] fragments, followed by the oligomerization to form higher hydrocarbons such as benzene and naphthalene. The dissociated oxygen species [O] from CO may react with the surface inert carbon species to regenerate CO, resulting in the suppression of coke formation on the catalyst [91]. It was also demonstrated that added CO_2 was converted to CO by the reforming process ($CO_2+CH_4=2CO+2H_2$) or by the reverse Boudart reaction ($CO_2+C=2CO$), which similarly promotes the catalytic stability [25].

In the case of co-feeding CO/CO_2 into CH_4, the reaction of coke species with [O] dissociated from the added CO/CO_2 should be the dominant route to coke removal,

since that the kinetics rate of coke gasification by CO_2, as another reaction pathway to removing coke, is relatively slow. However, it should be pointed out that the active [O] in the system could cause oxidation of any low valence reactants, including active species MoC_x, to reduce the catalyst's activity. XPS studies confirmed that the oxidation of Mo by CO_2 results in the formation of Mo ions of various oxidation states [92]. Tan et al [88] reported that in the presence of CO_2, the molybdenum oxide in the catalyst packed at the reactor inlet remained uncarburized, whereas in the zone away from the reactor inlet the formation of Mo_2C was found. When the concentration of CO_2 or O_2 in feed was too high, the entire catalyst bed remained oxidized and the methane aromatization reaction no longer took place, suggesting excessively co-feeding CO/CO_2 into the methane feed will lead to more significant negative effect on reducing the catalyst activity than that on suppressing coke deposition. Iglesia's results [86] also showed that the oxidation of Mo_2C at an oxidative environment could become easier as temperature increases, since higher activation energies are required for CH_4) than for CO_2 activation. XPS study confirmed that the oxidation of Mo results in the formation of Mo ions of various oxidation states during the reaction between CO_2 and ZSM-5- and SiO_2-supported Mo_2C catalysts [89, 92]. In addition, adding CO or CO_2 to pure methane will make the separation and purification of the reaction products more difficult. Therefore, one should carefully control the addition amount and operational condition when the CO/CO_2 co-feeding method is used for suppressing coke deposition and improving the catalytic performance.

1.3.8. Reaction coupling

It is obvious from above discussion that there is difficulty of preventing active Mo species from oxidation by the oxygen derived from CO and CO_2 dissociation, when CO or CO_2 is added to the CH_4 feed to suppress the coke deposition and enhance the catalyst stability. To enhance the advantage of and avoid the disadvantage of addition of CO or CO_2, researchers tried to pile up two types of catalysts in one single reactor to realize the coupling of the methane reforming and MTB for improving the MTB catalyst's performance. Yao et al [93] found that With CO_2 addition in feed, over a Mo/Al_2O_3 and Mo/MCM-49 integrated catalyst bed and at 1023 K, the conversion of

methane decreased very slowly and kept high at 8.2 % after 34 h reaction, whereas it decreased rapidly to 3.5 % in 15 h when only the latter catalyst was packed. Meanwhile, the deposition rate of the coke associated with the Bronsted acid sites, which is mainly responsible for the deactivation, in the two catalysts-combined system was much lower than that occurring in the MTB reaction alone, showing a very slow deactivation pattern. These authors also reported a similar result for the coupling of methane steam reforming with the MTB for improving durability of Mo/MCM-49 Catalyst [94]. Such promotional effects suggested that CO and H_2 produced through the methane reforming in the inlet layer of the combined catalyst bed work to significantly reduce the coke formation over the MTB catalyst in the downstream. The wonderful enhancement in catalyst performance by the combination of oxidative coupling (OCM) and dehydroaromatization (MTB) [95-97] could be attributed to an in-situ formation of CO_2 and H_2O via the OCM reaction, which serve as scavengers for actively removing the coke formed during the MTB reaction via gasification of coke species ($CO_2 + C = 2CO$; and $H_2O + C = CO + H_2$). However, the nascent CO from the inlet layer could dissociate to the active [O] to oxidize active Mo species in the outlet layer of the catalyst bed to non-active Mo oxides or other Mo species. Namely, adding oxidative reactants into feed, while surely suppressing the coke deposition and improving the catalyst stability, may also cause a gradual reduction in the number of the active Mo sites, i.e., lower the catalyst activity itself.

1.4. Regeneration of coked catalyst

1.4.1. O_2 regeneration

To keep their catalytic activity and extend their catalytic lifetime, coked Mo/HZSM-5 catalysts need to be regenerated timingly. It is natural to consider their regeneration using an oxidative technology. Oxygen is usually employed as an oxidant for the regeneration of coked catalysts in many other processes. Some researchers have also tried to apply this method to the MTB catalyst. Ma and co-workers [98] found that adding a small amount of NO to air increased the coke removing rate so that the regeneration temperature could be lowered to 723 K.

However, the catalyst activity continued decreasing with increasing the regeneration cycle. For a 6Mo/MCM-22 catalyst Bai et al [99] repeated a 10 min in situ regeneration in a stream of 1 vol% O_2 at 993 K once the catalyst activity in the term of methane conversion decreased to 10.5 %, and found the catalyst activity decreased more quickly with increasing the reaction-regeneration cycle. It seems that the oxidative regeneration approach, due to its exothermal feature, is not suit for the regeneration of coked Mo-based catalysts. A plausible explanation for this is that cyclic regeneration with oxidants causes the oxidation of Mo species in the catalyst to Mo oxides and then their sublimation to the gas phase, which is directly connected to a decrease of the number of Mo sites in the catalyst and therefore to a decrease in its activity. [100].

1.4.2. H_2 regeneration

Based on the above discussion, we should recognize that the oxidation of active Mo species in the regeneration of coked Mo/HZSM-5 catalyst must be avoided. For this purpose, our laboratory [101] first reported an effective periodic CH_4–H_2 switching operation approach to regenerating coked Mo/HZSM-5 catalyst and maintaining the catalyst stability. Under cyclic CH_4-H_2 switching operation mode coke formed in durations of the catalyst exposed to a CH_4 flow is removed in the durations of its exposure to a H_2 flow, and therefore the accumulation of coke over the catalyst in the whole reaction period would be significantly suppressed. Tests in a single fluidized bed under fluidization operation mode also demonstrated the effectiveness of the CH_4-H_2 switching operation approach in stabilizing the catalyst stability. ^{27}Al MAS NMR and XRD confirmed that the HZSM-5 structure of the catalyst was quite thermally stable under reductive atmosphere [102]. For the applicability of this approach in practical processes, our group also visualized a circulating fluidized reactor system for continuous operation of the title catalytic reaction system with the catalyst's continuous regeneration. [103]. Simultaneously, we have also developed a binder-free, fluidizable Mo-based catalyst to enable the title reaction system to be operated in a circulating fluidized bed system [38]. In the near future, we will determine all operation parameters for this catalyst and realize a highly stable performance in our two-bed type of circulating fluidized bed reactor

system.

1.5. Motivation and objectives

Non-oxidative methane dehydroaromatization reaction (MTB) over Mo/HZSM-5 catalyst, as a promising route for direct conversion of methane resources into highly value-added chemicals, has received considerable recent attention. Although many meaningful and inspiring studies were reported in the past two decades, coking-caused catalyst deactivation problem remains still unsolved. To date, as introduced in the section 1.1, coke formation mechanism and coking sites still remain a controversial issue and there is no systematic research done on coking pathway and the deactivation mechanism. This thesis aims to clarity the coking pathways, coking locations, types of coke formed and coke formation behavior and find out which type of coke on the where of the Mo/HZSM-5 catalyst is responsible for its deactivation in the MTB reaction, meanwhile to clarify the catalytic role of Mo species in coke burning.

1.6. Dissertation organization

The achievements and unsolved problems in studying coke formation and catalyst deactivation in the non-oxidative methane dehydroaromatization were reviewed and the objectives of this thesis were described in the first chapter. The experimental details are described in the second chapter. To investigate the coking pathway, two serious tests are conducted and the results presented in the third and fourth chapters, respectively: tests on pursuing the catalytic performance and coke formation behavior over the over the lifetime of Mo/HZSM-5 catalyst in the third chapter, and those on investigating the effect of co-fed H_2 in CH_4 feed on the distribution of coke formed in a three-layer fixed bed of Mo/HZSM-5 in the fourth chapter. To reveal the coke deposited on the where of the catalyst responsible for the catalyst deactivation, coke accumulation behavior in cyclic CH_4-H_2 switching operation mode and coke removal behavior in pure H_2 are investigated in the fifth chapter. At last in the sixth chapter, MoO3-added carbon materials as reference samples are used to clarify the

catalytic role of Mo species on promoting coke burning in TPO process.

References

[1] A. Demirbas, Energy Conversion and Management 51 (2010) 1547–1561.

[2] D. Ma, Energy & Environmental Science 7 (2014) 2580-2591.

[3] X. Guo, G. Fang, G. Li, H. Ma, H. Fan, L. Yu, C. Ma, X. Wu, D. Deng, M. Wei, D. Tan, R. Si, S. Zhang, J. Li, L. Sun, Z. Tang, X. Pan, X. Bao, Science 344 (2014) 616-619.

[4] J.J. Spivey, G. Hutchings, Chemical Society Reviews 43 (2014) 792-803.

[5] J. Bedard, D.-Y. Hong, A. Bhan, RSC Adv. 4 (2014) 49446-49448.

[6] L.S. Wang, L.X. Tao, M.S. Xie, G.F. Xu, J.S. Huang, Y.D. Xu, Catalysis Letters 21 (1993) 35-41.

[7] W. Zhang, D. Ma, X. Han, X. Liu, X. Bao, X. Guo, X. Wang, Journal of Catalysis 188 (1999) 393-402.

[8] J. Bedard, D.-Y. Hong, A. Bhan, Journal of Catalysis 306 (2013) 58-67.

[9] A. Sarıoğlan, Ö.T. Savaşçı, A. Erdem-Şenatalar, A. Tuel, G. Sapaly, Y.B. Taârit, Journal of Catalysis 246 (2007) 35-39.

[10] Y. Xu, Y. Suzuki, Z.-G. Zhang, Applied Catalysis A: General 452 (2013) 105-116.

[11] H. Zheng, D. Ma, X.H. Bao, J.Z. Hu, J.H. Kwak, Y. Wang, C.H.F. Peden, Journal of the American Chemical Society 130 (2008) 3722-3723.

[12] Y. Xu, L. Lin, Applied Catalysis A: General 188 (1999) 53-67.

[13] S. Liu, L. Wang, R. Ohnishi, M. Ichikawa, Journal of Catalysis 181 (1999) 175-188.

[14] D. Ma, Y. Shu, M. Cheng, Y. Xu, X. Bao, Journal of Catalysis 194 (2000) 105-114.

[15] J. Hu, S. Wu, H. Liu, H. Ding, Z. Li, J. Guan, Q. Kan, RSC Advances 4 (2014) 26577.

[16] Y. Song, Y. Xu, Y. Suzuki, H. Nakagome, Z.-G. Zhang, Applied Catalysis A: General 482 (2014) 387-396.

[17] B.M. Weckhuysen, M.P. Rosynek, J.H. Lunsford, Catalysis Letters 52 (1998) 31-36.

[18] F. Larachi, H. Oudghiri-Hassani, M.C. Iliuta, B.P.A. Grandjean, P.H. McBreen, Catalysis Letters 84 (2002) 183-192.

[19] D. Ma, D. Wang, L. Su, Y. Shu, Y. Xu, X. Bao, Journal of Catalysis 208 (2002) 260-269.

[20] S.D. Yuan, J. Li, Z.X. Hao, Z.C. Feng, Q. Xin, P.L. Ying, C. Li, Catalysis Letters 63 (1999) 73-77.

[21] P.D. Sily, F.B. Noronha, F.B. Passos, Journal of Natural Gas Chemistry 15 (2006) 82-86.

[22] A. Hassan, A. Sayari, Applied Catalysis A: General 297 (2006) 159-164.

[23] H. Liu, T. Li, B. Tian, Y. Xu, Applied Catalysis A: General 213 (2001) 103-112.

[24] H. Liu, L. Su, H. Wang, W. Shen, X. Bao, Y. Xu, Applied Catalysis A: General 236 (2002) 263-280.

[25] R. Ohnishi, S.T. Liu, Q. Dong, L.S. Wang, M. Ichikawa, Journal of Catalysis 182 (1999) 92-103.

[26] D. Ma, Y.Y. Shu, W.P. Zhang, X.W. Han, Y.D. Xu, X.H. Bao, Angewandte Chemie International Edition 39 (2000) 2928-2931.

[27] B.S. Liu, L. Jiang, H. Sun, C.T. Au, Applied Surface Science 253 (2007) 5092-5100.

[28] H.T. Ma, R. Kojima, S. Kikuchi, M. Ichikawa, Journal of Natural Gas Chemistry 14 (2005) 129-139.

[29] E.V. Matus, I.Z. Ismagilov, O.B. Sukhova, V.I. Zaikovskii, L.T. Tsikoza, J.A. Moulijn, Industrial & Engineering Chemistry Research 46 (2007) 4063-4074.

[30] J. Shu, A. Adnot, B.P.A. Grandjean, Industrial & Engineering Chemistry Research 38 (1999) 3860-3867

[31] A.C.C. Rodrigues, J.L.F. Monteiro, Catalysis Letters 117 (2007) 166-170.

[32] D. Ma, Y.Y. Shu, X.W. Han, X.M. LIu, Y.D. Xu, X.H. Bao, The Journal of Physical Chemistry B 105 (2001) 1786-1793

[33] D.J. Wang, J.H. Lunsford, M.P. Rosynek, Topics in Catalysis 3 (1996) 289-297.

[34] J. Bai, S.L. Liu, S.J. Xie, L.Y. Xu, L.W. Lin, Catalysis Letters 90 (2003) 123-130.

[35] Y. Cui, Y. Xu, Y. Suzuki, Z.-G. Zhang, Catalysis Science & Technology 1 (2011) 823-829.

[36] Y. Xu, Y. Song, Y. Suzuki, Z.-G. Zhang, Catalysis Science & Technology 3 (2013) 2769.

[37] Y. Cui, Y. Xu, J. Lu, Y. Suzuki, Z.-G. Zhang, Applied Catalysis A: General 393 (2011) 348-358.

[38] Y. Xu, H. Ma, Y. Yamamoto, Y. Suzuki, Z. Zhang, Journal of Natural Gas Chemistry 21 (2012) 729-744.

[39] C.L. Zhang, S. Li, Y. Yuan, W.X. Zhang, T.H. Wu, L.W. Lin, Catalysis Letters 56 (1998).

[40] C. Xu, J.Q. Guan, S.J. Wu, M.J. Jia, T.H. Wu, Reaction Kinetics, Mechanisms and Catalysis 99 (2010) 193-199.

[41] A. Martınez, E. Peris, G. Sastre, Catalysis Today 107/108 (2005) 676-684.

[42] P. Wu, Q.B. Kan, D.Y. Wang, H.J. Xing, M.J. Jia, T.H. Wu, Catalysis Communications 6 (2005) 449-454.

[43] Y.Y. Shu, D. Ma, L.L. Su, L.Y. Xu, Y.D. Xu, X.H. Bao, Studies in Surface Science and Catalysis, Elsevier, 2001, pp. 27-32.

[44] Y.Y. Shu, D. Ma, L.Y. Xu, Y.D. Xu, X.H. Bao, Catalysis Letters 70 (2000) 67-73.

[45] L.L. Su, L. Liu, J.Q. Zhuang, H.X. Wang, Y.G. Li, W.J. Shen, Y.D. Xu, X.H. Bao, Catalysis Letters 91 (2003) 155-167.

[46] Y. Wu, L. Emdadi, Z. Wang, W. Fan, D. Liu, Applied Catalysis A: General 470 (2014) 344-354.

[47] N. Chu, J. Wang, Y. Zhang, J. Yang, J. Lu, D. Yin, Chemistry of Materials 22 (2010) 2757-2763.

[48] H. Liu, S. Yang, J. Hu, F. Shang, Z. Li, C. Xu, J. Guan, Q. Kan, Fuel Processing Technology 96 (2012) 195-202.

[49] A. Mart ńez, E. Peris, M. Derewinski, A. Burkat-Dulak, Catalysis Today 169 (2011) 75-84.

[50] Y. Lu, Z.S. Xu, Z.J. Tian, T. Zhang, L.W. Lin, Catalysis Letters 62 (1999) 215-220.

[51] Y. Lu, D. Ma, Z.S. Xu, Z.J. Tian, Chemical Communications (2001)

2048-2049.

[52] D. Ma, Y. Lu, L.L. Su, Z.S. Xu, Z.J. Tian, Y.D. Xu, L.W. Lin, X.H. Bao, The Journal of Physical Chemistry B 106 (2002) 8524-8530.

[53] X.F. Dong, Y.B. Song, W.M. Lin, Catalysis Communications 8 (2007) 539-542.

[54] Y.G. Li, X.M. Huang, X.M. LIu, W.J. Shen, Y.D. Xu, X.H. Bao, Catalysis Communications 8 (2007) 1567-1572.

[55] H.X. Wang, L.L. Su, J.Q. Zhuang, D.L. Tan, Y.D. Xu, X.H. Bao, The Journal of Physical Chemistry B 107 (2003) 12964-12972.

[56] H.X. Wang, G. Hu, H. Lei, Catalysis Letters 89 (2003) 75-79.

[57] Y.B. Song, C.Y. Sun, W.J. Shen, L.W. Lin, Catalysis Letters 109 (2006) 21-24.

[58] Y. Song, C. Sun, W. Shen, L. Lin, Applied Catalysis A: General 317 (2007) 266-274.

[59] C. Sun, S. Yao, W. Shen, L. Lin, Microporous and Mesoporous Materials 122 (2009) 48-54.

[60] Y.Y. Shu, R. Ohnishi, M. Ichikawa, Catalysis Letters 81 (2002) 9-17.

[61] X. Yin, N. Chu, J. Yang, J. Wang, Z. Li, Catalysis Communications 43 (2014) 218-222.

[62] N.B. Chu, J.H. Yang, C.Y. Li, J.Y. Cui, Q.Y. Zhao, X.Y. Yin, J.M. Lu, J.Q. Wang, Microporous and Mesoporous Materials 118 (2009) 169-175.

[63] N.B. Chu, J.H. Yang, J.Q. Wang, S.X. Yu, J.M. Lu, Y. Zhang, D.H. Yin, Catalysis Communications 11 (2010) 513-517.

[64] H. Liu, S. Wu, Y. Guo, F. Shang, X. Yu, Y. Ma, C. Xu, J. Guan, Q. Kan, Fuel 90 (2011) 1515-1521.

[65] H. Liu, S. Yang, S. Wu, F. Shang, X. Yu, C. Xu, J. Guan, Q. Kan, Energy 36 (2011) 1582-1589.

[66] L.Y. Chen, L.W. Lin, Z.S. Xu, T. Zhang, X.S. Li, Catalysis Letters 39 (1996) 169-172.

[67] S.T. Liu, Q. Dong, R. Ohnishi, M. Ichikawa, Chemical Communications (1997) 1455-1456.

[68] B. Liu, Y. Yang, A. Sayari, Applied Catalysis A: General 214 (2001) 95-102.

[69] Y.P. Zhang, D.J. Wang, J.H. Fei, X.M. Zheng, Reaction Kinetics and Catalysis Letters 74 (2001) 151-161.

[70] R. Kojima, S. Kikuchi, M. Ichikawa, Chemistry Letters 33 (2004) 1166-1167.

[71] R. Kojima, S. Kikuchi, H.T. Ma, J. Bai, M. Ichikawa, Catalysis Letters 110 (2006) 15-21.

[72] A.K. Aboul-Gheit, A.E. Awadallah, Journal of Natural Gas Chemistry 18 (2009) 71-77.

[73] S. Li, C. Zhang, Q. Kan, D. Wang, T. Wu, L. Lin, Applied Catalysis A: General 187 (1999) 199-206.

[74] A. Malinowski, R. Ohnishi, M. Ichikawa, Catalysis Letters 96 (2004) 141-146.

[75] A.K. Aboul-Gheit, A.E. Awadallah, S.M. El-Kossy, A.-L.H. Mahmoud, Journal of Natural Gas Chemistry 17 (2008) 337-343.

[76] S.T. Qi, B.L. Yang, Catalysis Today 98 (2004) 639-645.

[77] A.V. Vosmerikov, V.I. Zaikovskii, L.L. Korobitsyna, G.V. EChevskii, V.V. Kozlov, Kinetics and Catalysis 50 (2009) 725-733.

[78] Y. Xu, J. Wang, Y. Suzuki, Z.-G. Zhang, Applied Catalysis A: General 409-410 (2011) 181-193.

[79] Y. Xu, J. Wang, Y. Suzuki, Z.-G. Zhang, Catalysis Today 185 (2012) 41-46.

[80] V. Abdelsayed, D. Shekhawat, M.W. Smith, Fuel 139 (2015) 401-410.

[81] W.P. Ding, G.D. Meitzner, E. Iglesia, Journal of Catalysis 206 (2002) 14-22.

[82] S. Kikuchi, R. Kojima, H.T. Ma, J. Bai, M. Ichikawa, Journal of Catalysis 242 (2006) 349-356.

[83] H.M. Liu, Y. Li, W.J. Shen, X.H. Bao, Y.D. Xu, Catalysis Today 93/95 (2004) 65-73.

[84] H.T. Ma, R. Ohnishi, M. Ichikawa, Catalysis Letters 89 (2003) 143-146.

[85] H.T. Ma, R. Kojima, S. Kikuchi, M. Ichikawa, Catalysis Letters 104 (2005) 63-66.

[86] Z. Liu, M.A. Nutt, E. Iglesia, Catalysis Letters 81 (2002) 271-279.

[87] R. Ohnishi, R. Kojima, Y. Shu, H. Ma, M. Ichikawa, X. Xinhe Bao and Yide, Studies in Surface Science and Catalysis Volume 147 (2004) 553-558.

[88] P.L. Tan, K.W. Wong, C.T. Au, S.Y. Lai, Applied Catalysis A: General 253 (2003) 305-316.

[89] H.S. Lacheen, E. Iglesia, Journal of Catalysis 230 (2005) 173-185.

[90] M.C. Iliuta, I. Iliuta, B.P.A. Grandjean, F. Larachi, Industrial & Engineering

Chemistry Research 42 (2003) 3203-3209.

[91] S.T. Liu, Q. Dong, R. Ohnishi, M. Ichikawa, Chemical Communications (1998) 1217-1218.

[92] F. Solymosi, A. Oszk, T. Banssgi, P. Tolmacsov, The Journal of physical Chemistry B 106 (2002) 9613-9618.

[93] S.D. Yao, L.J. Gu, C.Y. Sun, J. Li, W.J. Shen, Industrial & Engineering Chemistry Research 48 (2009) 713-718.

[94] S.D. Yao, C.Y. Sun, J. Li, L.J. Gu, W.J. Shen, Chinese Journal of Catalysis 30 (2009) 1022-1028.

[95] Y.G. Li, L.L. Su, H.X. Wang, H.M. Liu, W.J. Shen, X.H. Bao, Y.D. Xu, Catalysis Letters 89 (2003) 275-279.

[96] P. Qiu, J.H. Lunsford, M.P. Rosynek, Catalysis Letters 48 (1997) 11-15.

[97] Y.G. Li, T.H. Wu, W.J. Shen, X.H. Bao, Y.D. Xu, Catalysis Letters 105 (2005) 77-82.

[98] H.T. Ma, R. Kouichiro, R. Ohnishi, M. Ichikawa, Applied Catalysis A: General 275 (2004) 183-187.

[99] J. Bai, S.J. Xie, S.L. Liu, L.Y. Xu, L.W. Lin, Chinese Journal of Catalysis 24 (2003) 805-806.

[100] K. Skutil, M. Taniewski, Fuel Processing Technology 87 (2006) 511-521.

[101] K. Honda, T. Yoshida, Z.-G. Zhang, Catalysis Communications 4 (2003) 21-26.

[102] Y. Xu, J. Lu, Y. Suzuki, Z.-G. Zhang, H. Ma, Y. Yamamoto, Chemical Engineering and Processing: Process Intensification 72 (2013) 90-102.

[103] Y. Xu, J. Lu, J. Wang, Y. Suzuki, Z.-G. Zhang, Chemical Engineering Journal 168 (2011) 390-402.

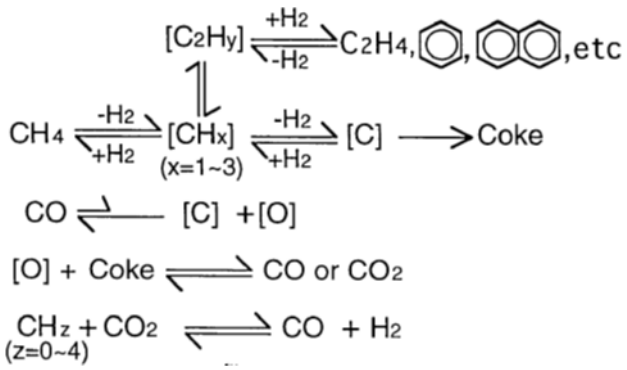

Fig. 1-1. Proposed mechanism for promotion of CO/CO_2 addition to methane feed to improve catalyst stability and reduce coke formation on Mo/HZSM-5 catalysts [91].

Chapter 2

Experimental

2.1. Catalyst preparation

2.1.1. Main chemicals and instruments for catalysts preparation

Tables 2-1 and 2-2 show the main chemistry reagents and instruments used for preparation of all test catalysts.

2.1.2. Catalyst preparation approaches

A series of 1, 2, 4, 6 and 8 wt% Mo-loaded HZSM-5 catalysts was prepared by a wet impregnation method, denoted as x/Mo/HZSM-5 (x=1, 2, 4, 6 and 8, respectively.). A commercial, highly crystalline 4 μm HZSM-5 zeolite (Si/Al ratio=40) was impregnated with a certain amount of ammonium heptamolybdate aqueous solution. The impregnated sample was dried at 393 K overnight and calcined in air at 773 K for 5 h. All the catalysts with different Mo-loadings were prepared by the same condition. Finally, the catalysts were pressed, crushed and sieved to particles in the range of 180-350 μm for use.

2.2. Catalyst characterization

The fresh and spent catalysts were characterized using various techniques including FT-IR, N_2 adsorption and desorption, XRD, FESEM, NH3-TPD, ^{27}Al-NMR, XPS, TG and TPO. The detailed procedures were described in the following:

2.2.1. FT-IR spectroscopy

FT-IR measurements were conducted using a NEXUS 670 FTIR spectrometer at room temperature. A tube type of glass IR cell equipped with a pair of CaF_2 windows was self-designed and made for the measurements. For each measurement a self-supported wafer of 20mg/cm^2 was made by pressing the samples and then

carefully transferred into the IR cell for pretreatment. The pretreatment was performed in a separate glass vacuum system. After connected to the system, the cell was vacuumed to 10^{-3} Pa, heated up to 773 K and kept there for 1 h for removing adsorbed water from the wafer. After natural cooling of the vacuumed cell to 373 K, the sample was exposed to the pyridine vapor of 2.0 Pa at 373 K for 0.5 h and vacuum-treated at 423K for 1 h for FT-IR measurement. IR spectra were recorded in the range from 4000 to 400 cm^{-1}.

2.2.2. N_2 adsorption and desorption isotherm

N_2 adsorption and desorption experiments of fresh and spent catalysts were carried out at 77 K using a BELSORP-max equipment (Bel. Japan Inc.). Prior to the adsorption measurements, all samples were vacuum-degassed at 623 K for 5 h to remove adsorbed moisture from their surfaces. Specific micropore surface areas of the samples as well as their micropore volumes were analyzed by BET method and t-plot method.

2.2.3. X-ray diffraction

X-ray diffraction (XRD) patterns of the zeolite and Mo/HZSM-5 catalysts were recorded on a Rigaku RU-300 X-ray diffractometer, using Cu Kα radiation, over a 2θ range of 5-60 °. The scanning rate was set at 0.02 °/min.

2.2.4. Scanning Electron Microscope

Scanning Electron Microscope (SEM) observations of all spent samples were conducted using a FESEM (Hitachi S-4300) with the maximum magnification of 100000×.

2.2.5. NH_3 adsorption/temperature programmed desorption

NH_3 adsorption/temperature programmed desorption (NH_3-TPD) technique was applied to evaluate the acidities of the HZSM-5 and Mo/HZSM-5 catalysts. The measurements were conducted in an auto-controlled flow reactor system (TPD-1-ATSP1, Bel., Japan). 50 mg of the zeolite or prepared catalyst was used for each measurement. The sample was first treated in a He stream at 773 K for 1 h and

cooled down to 403 K. Subsequently at the temperature ammonia was introduced into the reactor up to 40 Torr by pulse technique. After 30 min of adsorption at the pressure and another 30 min of evacuation, the sample was heated again in a He stream to 873 K at a rate of 10 K/min to obtain its NH_3-TPD pattern. The effluent gas was analyzed with a Q-MASS (ULVAC RG-201). The signal m/e = 17 was used for the detection of NH_3.

2.2.6. ^{27}Al NMR spectra

The ^{27}Al NMR spectra of the fresh catalyst and spent samples were measured on a Varian Infinity Plus 400NMR spectrometer at 200 MHz with a pulse duration of 2 μs and are cycling delay of 5 s.

2.2.7. X-ray photoelectron spectroscopy

The XPS measurements of some spent samples were conducted in a PHI Versa Probe instrument using Al Kα primary radiation (15 kV, 25 W). The radiation source probed a 100 μm diameter spot on the powdered samples. The Si 2p line at 103.4 eV was taken as a reference for binding energy calibration.

2.2.8. Thermal gravimetric analysis

The coke contents of spent samples recovered after the different periods of reaction were quantified using a TG/DTA analyzer (EXSTAR TG/DTA 6200, Seiko Instruments Inc.). About 10 mg of a spent sample was used for each measurement. After loaded to a TG cell, the sample was kept in a dry air stream for 30 min to ensure that the measurement starts with a stable base. Then it was heated to 393 K and held there for 30 min to have an accurate measurement of the weight loss originated from vaporization of physically adsorbed water. Subsequently it was further heated to 873 K at a rate of 10 K/min and kept there for 30 min to obtain the TG profile of the sample. The weight loss recorded in the temperature region of 673-873 K was used to estimate the coke amount. Some preliminary tests were conducted for the sample recovered after reaction to confirm good reproducibility of the TG measurements in this procedure.

2.2.9. Temperature programmed oxidation

Also in the same TPD apparatus, burning behavior of the coke in the spent samples was characterized using temperature programmed oxidation (TPO) technique. An auto-controlled TPD apparatus (TPD-1-ATSP1, Bel. Japan) was employed for the purpose and 30 mg of a spent catalyst sample was used for each measurement. The sample was heated from room temperature to 1103 K at a rate of 10 K/min in a 50 mL/min flow of a gas mixture composed of 10 vol% O2 and 90 vol% He. The mass spectra of the gases evolved during the TPO were monitored by a Q-MASS spectrometer (ULVAC RG-201).The signals at m/e = 28, 44 and 18 were used for the detections of CO, CO2 and H2O, respectively.

2.3. Catalyst activity evaluation

2.3.1. Apparatus

Fig. 2-1 shows the schematic diagram of the experimental set-up. It consisted mainly of a gas supply system (1, 2), a fixed bed reactor of 8mm in inner diameter (3), a temperature control system (4) and a data analysis and acquisition system (5, 6,7). All catalytic tests were carried out at 1073 K under atmospheric pressure. The bed temperature was monitored and controlled with a K-type thermal couple. The effluent from the reactor was sampled at pre-designed intervals into 2 loops of 100 and 500 μL on an on-line 10-port sampling valve. Under continuous mode the sampling intervals were 8 min, while each sampling was performed at 2 min after a switching from H_2 to CH_4 under cyclic CH_4-H_2 switching operation. The effluent line and sampling valve were held at 503 K to prevent the condensation of condensable products. This system enables the on-line analysis of the effluent product gas using two gas chromatographs: Shimadzu GC-14A/TCD with a MS-5A packed column for separation of CH_4 and Ar at 333 K and GC-14B/FID with a Chemipak PH packed column for that of aromatics at 453 K.

In order to excluding the effect of product back mixing, an up-flow, integral fixed bed quartz reactor (8 mm i.d.) was used for activity evaluation of the catalyst. As shown in Fig. 2-2, the reactor has a U-shape and a mounted filter in its bottom part

to support the catalyst bed. In the 3rd and 6th chapters the catalyst bed was packed into one single layer bed. To investigate the coking behavior and coke distribution the catalyst beds, used in 4th and 5th chapters were packed into three layers and each of them had the same height of about 2.5 mm (created by the packing of 100 mg catalyst sample). For convenience, these layers are refereed hereinafter to as the bottom, middle and top ones, respectively (Fig. 2-2). In addition to packing a certain amount of quartz wool between any two catalyst layers for their separation, quartz wool was also packed at the upper end of each layer. The quartz packed on the top layer was to prevent the catalyst from being flowed out of the reactor during the test. Pressed over the quartz wool was then an inner inserted quarts tube with a flat, sealed bottom end and the upper end capable to be connected to the top end of the reactor body in a manner of ball joint connection. This inner inserted tube was designed to have an outside diameter of about 6 mm, just 2 mm smaller than the insider diameter of the reactor itself. It functioned to eliminate the dead space in the upper part of the reactor and at the same time to be a detachable seal. This design made it much easy the routine work to pack fresh catalyst samples into different layers and collect the spent ones from the different layers of the bed. The reaction temperature was controlled and monitored by a K-type of thermal couple. It was inserted in a small pocket mounted on the outside wall of the reactor and with its sealed bottom end at a position locating at about 6 mm over the filter. While this ensured that the temperature at exactly the same position of the outer wall of the reactor was monitored in each test, special attention was also paid to the position-setting of the reactor itself to ensure that the catalyst bed was set every time into the same heating zone of a vertical golden furnace around its central vertical axis and therefore the identical bed-temperature distributions were reached in all tests. All these contributed to increasing test reproducibility.

2.3.2. Experimental procedure

In this study, two types of operation modes were used for gas feeding: continuous feeding mode and cyclic CH_4-H_2 switching model. Fig. 2-3 shows the schematic of heating procedure for continuous operation mode. After packed into the reactor to form a catalyst bed, the sample was heated in a H_2 stream to 923 K and then kept

there in a CH_4 stream for pre-set minutes for pre-carburizing its MoO_3 to active Mo_2C. Subsequently it was heated in a H_2 stream to 1073 K and maintained at the temperature for 5 min. Finally, the H_2 stream was switched to a feed gas to start the reaction. Fig. 2-4 shows the schematic of heating procedure for cyclic operation mode. After the reactor was heated to 1073 K following the procedure for the continuous operation mode, the first switching operation on a 4-port valve from H_2 to CH_4 was performed to start the reaction. The cyclic operation was repeated every 10 min, 5 min for flowing CH_4 and another 5 min for H_2. The details will be described in each related chapter.

2.3.3. Methodology

10% Ar contained in the feed CH4 was used as internal standard to estimate the volume flow rate of the reactor outlet (F_{out}, mL/s, Eq. (2-1)), and then CH4 conversion (Conv./%, Eq. (2-2)), it should be pointed out that the internal reference method was also used in the tests with H_2-co-fed in the chapter 6. The rates of formation of benzene and naphthalene (R_i, μmol-C/g/s) and their selectivities were estimated according to Eqs. (2-3) and (2-4), respectively.

$$F^{out} \times x_{\mathrm{Ar}}^{out} = F^{in} \times x_{\mathrm{Ar}}^{in} \qquad \text{Eq. (2-1)}$$

$$Conv. = \frac{F^{in} \times x_{\mathrm{CH_4}}^{in} - F^{out} \times x_{\mathrm{CH_4}}^{out}}{F^{in} \times x_{\mathrm{CH_4}}^{in}} \times 100\% = \left(1 - \frac{x_{\mathrm{CH_4}}^{out} \times x_{\mathrm{Ar}}^{in}}{x_{\mathrm{CH_4}}^{in} \times x_{\mathrm{Ar}}^{out}}\right) \times 100\% \qquad \text{Eq. (2-2)}$$

$$R_i = f_i \times A_i \times n_i \times \frac{F^{\mathrm{out}}}{\mathrm{V_{loop}}} \times \frac{\mathrm{T_{loop}}}{\mathrm{T_0}} \times \frac{1}{m_{\mathrm{cat}}} \qquad \text{Eq. (2-3)}$$

$$S_i = \frac{R_i \times m_{\mathrm{cat}} \times 0.0224}{F^{\mathrm{in}} \times x_{\mathrm{CH_4}}^{\mathrm{in}} \times Conv.} \times 100\% \qquad \text{Eq. (2-4)}$$

where f_i (μmol/GC peak area) represents a calibration factor for the aromatic product i (benzene or napthalene) and was determined using the external calibration technique; A_i refers to the GC peak area measured for the product i in a gas sample; n_i the carbon number in one molecule of the product i (6 for benzene and 10 for naphthalene); V_{loop} (mL) the volume of the sampling loop used; and T_{loop} (K) the

loop temperature; T_0 (K) room temperature and m_{cat} (g) the weight of catalyst sample. Coke selectivities at different reaction times were estimated from the corresponding carbon mass balances.

Table 2-1. Main chemicals used for the catalyst preparation.

Chemical		Supplier
HZSM-5	SiO_2/AL_2O_3=40	Tosoh Company
$(NH_4)_6MoO_{24}\cdot 4H_2O$	>99.0%	Kanto Chemical Co., Inc.

Table 2-2. Main instruments used for the catalyst preparation.

Chemical	Model	Supplier
Muffle furnace	TMF-2200	Tokyo Rikakikai Co., Ltd.
Rotary evaporator	RE600	Yamato
Drying oven	Snow-450	As one Corporation
Magnetic stirrer	CHPS-250D	As One Corporation
Tablet press machine	TB-70H	テックジャム株式会社
Electronic balance	ER-182A	研精工業株式会社

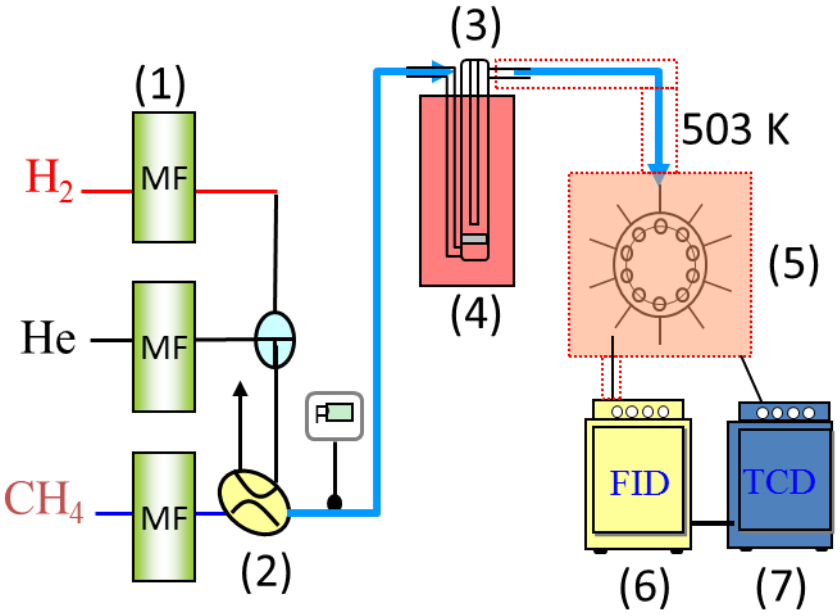

Fig. 2-1. Schematic diagram of experimental set-up. (1) Mass flow controller, (2) 4-port valve, (3) reactor, (4) furnace, (5) 10-port valve, (6) GC/FID, (7) GC/TCD.

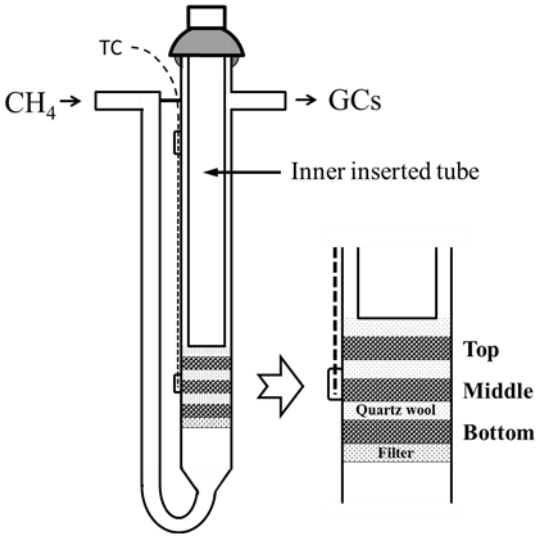

Fig. 2-2. Schematic diagram of the three layers fixed bed reactor.

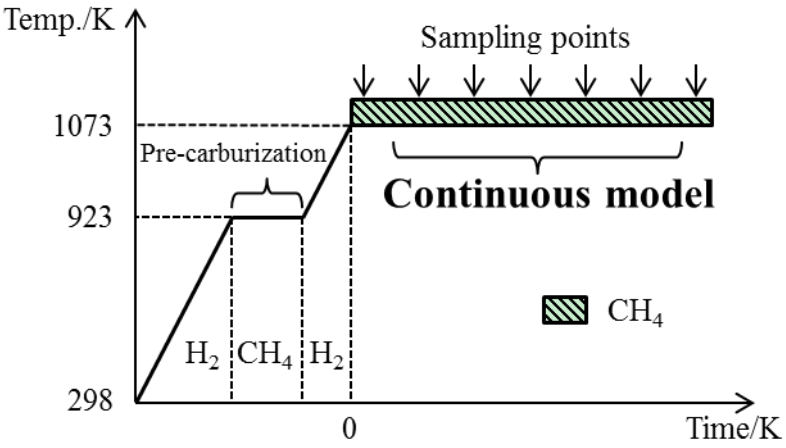

Fig. 2-3. Schematic diagram of the heating procedure for continuous operation mode.

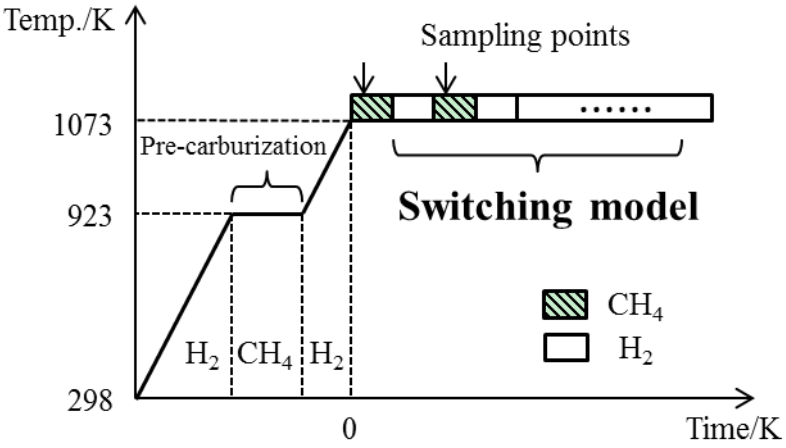

Fig. 2-4. Schematic diagram of the heating procedure for switching operation mode.

Chapter 3

The lifetime performance of Mo/HZSM-5: the pathway of coke formation in the last stage of catalyst deactivation

3.1. Introduction

Coking-caused deactivation of Mo/HZSM-5 catalyst in the non-oxidative methane dehydroaromatization reaction is considered the main problem to be overcome for its industrial application [1,2]. Over years concerted efforts have been made to tackle this problem and more than 150 papers have been published, but most of them focused on developing highly coking-resistant catalysts [3-6], in-situ coke removal technologies [2,7-9], and catalyst regeneration ones [10-13]. A few of them attempted to make a better understanding of the characteristics of coke in coked catalysts and to identify the types of coke and their locations in catalysts [14-18], but very surprisingly, none was found to aim to explore and clarify the coking pathways. Two possible coking pathways, pyrolysis of CH_x (x=1~3) and polycondensation of formed aromatics, were proposed in previous papers [2,19,20], but no experimental evidence was given.

Pyrolysis of CH_4 to coke indeed occurs over Mo/HZSM-5 catalysts at temperatures ≥923 K, but it seems to proceed mainly in the carburization of the loaded MoO_3 to Mo_2C and/or at the very initial stage of the methane dehydroaromatization reaction over the fresh or reduced Mo_2C surface [21,22]. During the period of stable benzene formation, the surface of Mo_2C in Mo/HZSM-5 is considered to be coke-modified and provide active sites for activation of CH_4 and formation of the reaction intermediate C_2H_4 [21-25]. Highly dispersive Mo_2C exhibits metal-like catalytic behaviors, but when its surface is covered by excess carbon it must behave more likely as a carbon material, becoming inactive for CH_4 pyrolysis. Namely, there are reasons for one to exclude the possibility of catalytic CH_4 pyrolysis dominating the coking process throughout the lifetime of any Mo/HZSM-5 catalyst. Note that HZSM-5 itself is incapable of catalyzing the pyrolysis of CH_4 at 1073 K [26], and further presume that

the speculative intermediates CH_x (x=1-3) do not desorb or desorb at a negligibly small rate from the Mo_2C surface into the gas phase in the reaction. The dominating contribution of free radical chain reactions to coke deposition [27] in the stable benzene formation period can be excluded as well.

Polycondensation of formed aromatics over the Bronsted acid sites in Mo/HZSM-5 can also lead to serious coke formation and catalyst deactivation, but this type of coking reactions is supposed to mainly take place on the external surfaces of zeolite crystals and at the channel mouths. The channels of HZSM-5 zeolite are almost identical in size to the kinetic diameters of benzene and naphthalene molecules, and therefore spatially confine conversion of these aromatic products to larger molecules and further to coke inside themselves [28]. If the polycondensation of formed aromatics is the main contributor to the external surface coke accumulation and leads eventually to the full deactivation of Mo/HZSM-5 catalyst by partial blocking of channel mouths, the coke formation rate must be decreasing with the decrease in benzene formation rate with time until the catalyst loses its all benzene formation activity. The fact, however, as shown below, is that the average coke formation rate increases in the last stage of catalyst deactivation, in which the catalyst's benzene formation activity decreases rapidly and finally falls nearly to zero.

Thermodynamically, thermal oligomerization and/or cracking of C_2H_4 to coke is more favorable than both CH_4 pyrolysis and polycondensation of benzene at the reaction temperatures of 923-1073 K. Thus, the previous experimental observation that the rate of formation of C_2H_4 is always increasing with the decrease of benzene formation rate with time on stream [20,22,29], suggests that C_2H_4 could be a source compound of coke formation. Note the kinetic diameters of both CH_4 and C_2H_4 (~3.9Å) are much smaller than that of benzene (about 6.0Å) and coke deposition in the catalyst will have less influence on the diffusion of CH_4 into and that of C_2H_4 out of its zeolite channels than on the formation of benzene inside the channels. Therefore, the C_2H_4 formation rate could continue increasing after the catalyst enters its last deactivation stage and its benzene formation activity is significantly inhibited for narrowing of the zeolite channels and/or partial blocking of the channel mouths by

coke. If this is the case and most of C_2H_4 molecules formed inside the channels in this period go to oligomerize and/or crack to coke, the coke formation rate in the last stage of reaction will not decrease; on the contrary, it might increase. Consequently, an unordinary time-dependence of catalyst coke content, which has a more steep upward slope in the region of high coke contents, not in that of low ones, might be obtained for a Mo/HZSM-5 catalyst when its deactivation is pursued over its lifetime.

Investigations on the time-dependence of the content of coke in spent Mo/HZSM-5 catalysts have been reported in three previous studies [13, 16, 30], but all catalyst activity tests were stopped in the relatively stable benzene formation period and no data was given to show that the average coke formation rate in the last stage of catalyst deactivation increases, remains unchanged or decreases. Note that the formation of C_2H_4 takes place in the title reaction not only in the last stage of catalyst deactivation but also in the period in which its benzene formation activity is relatively stable. In other words, if we are able to demonstrate that it is thermal and/or catalytic oligomerization and/or cracking of C_2H_4 to dominate the coke formation in the last stage of catalyst deactivation, we might get a clue to exploration of the coke sources that dominate the coking process throughout the whole period of the reaction.

Therefore, the aim of this study is to experimentally demonstrate that the coke formation rate in the last stage of deactivation of Mo/HZSM-5 does become higher, not lower, and consequently provide strong evidence that C_2H_4 is the main source of coke formation in the last period of the reaction in which the catalyst's selectivity to benzene is significantly inhibited by coke deposition and finally decreases nearly to zero. For achieving this aim, it is essential to obtain the lifetime-dependence of the amount of coke accumulated in Mo/HZSM-5 catalyst. Therefore, a set of activity evaluation tests lasting for different periods of time was designed and conducted over a microcrystal-based, 6wt%Mo/HZSM-5 catalyst at 1073 K and a space velocity of 5000 mL/g/h to collect coked samples with different coke contents. To increase the reliability of the resultant coke content data, all tests were conducted in a three layers fixed-bed mode so that three coked samples could be obtained from every single test under exactly the same condition. The time-dependences of both lifetime performance

and coking behavior of the catalyst obtained strongly suggested that the coke formation originated from C_2H_4 dominates the coking process in its last deactivation stage. Additionally, identification of types of the coke in some of the spent samples by XPS analysis and in all of them using TPO technique with considering the accessibility of O_2 into the coked zeolite channels were conducted in this work to identify the locations where coke formation takes place and at which of them coke accumulates to severely inhibit the catalyst's benzene formation activity.

3.2. Experimental

3.2.1. Catalyst preparation

A 6wt%Mo/HZSM-5 catalyst was prepared by a wet impregnation method. A commercial HZSM-5 zeolite with a Si/Al ratio of 20 (TOSOH Co., Japan) was impregnated with an aqueous solution of ammonium heptamolybdate, followed by evaporating the water, drying at 393 K overnight and calcining in air at 773 K for 5 h. The resulting sample was then pressed, crushed and sieved to collect a fraction of 350–500 μm for use.

3.2.2. Catalyst characterization

The test catalyst was characterized using various techniques including FESEM, XRD, BET, ^{27}Al-NMR, NH_3-TPD and FT-IR. The detailed procedures were described in previous papers [13, 31, 32].

3.2.3. Reactor

An up-flow, integral fixed bed quartz reactor (8 mm i.d.) was used for activity evaluation of the catalyst. As shown in Figure 3-1, the reactor has a U-shape and a mounted filter in its bottom part to support the catalyst bed. The catalyst bed was composed in all tests of three layers and each had the same height of about 2.5 cm (created by the packing of 100 mg catalyst sample). For convenience, these layers are refereed hereinafter as to the bottom, middle and top ones, respectively (Figure 3-1). In addition to packing a certain amount of quartz wool between any two catalyst layers for their separation, some quartz wool was also packed at the upper end of the

top layer to prevent the catalyst from being flowed out of the reactor during the test. Pressed over the quartz wool was then an inner inserted quarts tube with a flat, sealed bottom end and the upper end capable to be connected to the top end of the reactor body in a manner of ball joint connection. This inner inserted tube was designed to have an outside diameter of about 6 mm, just 2 mm smaller than the insider diameter of the reactor itself. It functioned to eliminate the dead space in the upper part of the reactor and at the same time to be a detachable seal. This design made it much easy the routine work to pack fresh catalyst samples into three different layers and collect the spent ones from the different layers of the bed. The reaction temperature was controlled and monitored by a K-type of thermal couple. It was inserted in a small pocket mounted on the outside wall of the reactor and with its sealed bottom end at a position falling in a horizontal cross section through the middle catalyst layer (about 6 mm over the filter). While this ensured that the temperature at exactly the same position of the outer wall of the reactor was monitored in each test, special attention was also paid to the position-setting of the reactor itself to ensure that the catalyst bed was set every time into the same heating zone of a vertical golden furnace around its central vertical axis and therefore the identical bed-temperature distributions were reached in all tests. All these contributed to increasing test reproducibility.

3.2.4. Activity evaluation

All activity evaluation tests were conducted at a condition of atmospheric pressure, 1073 K and a space velocity of 5000 mL/g/h (corresponding to a superficial velocity of 3 cm/s). Totally 300 mg of a catalyst sample was used for each test. After packed into the reactor to form a catalyst bed of three layers (100 mg catalyst in each layer), the sample was heated in a H_2 stream to 923 K and then kept there in a CH_4 stream for 20 min for pre-carburizing its MoO_3 to active Mo_2C. Subsequently it was heated in a H_2 stream to 1073 K and maintained at the temperature for 5 min. Finally, the H_2 stream was switched to a feed gas mixture of 10vol%Ar/CH_4 to start the reaction. The reaction lasted for a period of 10, 20, 60, 100 or 160 min, and then the furnace was turned off and the catalyst sample was naturally cooled in the CH_4 flow down to room temperature for its recovery. To measure the time dependence of the catalyst activity over the reaction period the reacted stream was analyzed at certain intervals with two

on-line gas chromatographs：Shimadzu GC-14A/TCD with a MS-5A packed column for separation of CH_4 and Ar at 333 K and GC-14B/FID with a Chemipak PH packed column for that of aromatics at 453 K. CH_4 conversion was determined using an internal calibration method, while the rates of formation of aromatics and their selectivities were estimated using an external calibration technique. The detailed sampling procedure, analysis condition and data analysis method were described in previous papers [32-33].

3.2.5. Coke characterization

The coke contents of spent samples recovered after the different periods of reaction were quantified using a TG/DTA analyzer (EXSTAR TG/DTA 6200, Seiko Instruments Inc.). About 10 mg of a spent sample was used for each measurement. After loaded to a TG cell, the sample was kept in a dry air stream for 30 min to ensure that the measurement starts with a stable base. Then it was heated to 393 K and held there for 30 min to have an accurate measurement of the weight loss originated from vaporization of physically adsorbed water. Subsequently it was further heated to 873 K at a rate of 10 K/min and kept there for 30 min to obtain the TG profile of the sample. Some preliminary tests were conducted for the sample recovered after the longest period of reaction (160 min) to confirm good reproducibility of the TG measurements in this procedure.

Burning behavior of the coke in the spent samples was characterized using TPO technique. An auto-controlled TPD apparatus (TPD-1-ATSP1, Bel. Japan) was employed for the purpose and 30 mg of a spent catalyst sample was used for each measurement. The sample was heated from room temperature to 1103 K at a rate of 10 K/min in a 50 mL/min flow of a gas mixture composed of 10vol% O_2 and 90vol% He. The mass spectra of the gases evolved during the TPO were monitored by a Q-MASS spectrometer (ULVAC RG-201). The signals at m/e = 28, 44 and 18 were used for the detections of CO, CO_2 and H_2O, respectively.

The XPS measurements of some spent samples were conducted in a PHI Versa

Probe instrument using Al Kα primary radiation (15kV, 25W). The radiation source probed a 100 μm diameter spot on the powdered samples. The Si 2p line at 103.4 eV was taken as a reference for binding energy calibration.

3.3. Results and discussion

3.3.1. Catalyst characterization

While FESEM observation revealed that the used zeolite crystals had flattened hexagonal prismatic shapes and sizes of micro scale, XRD measurement confirmed its high crystallinity [32]. Besides, BET measurements showed that the BET surface and micropore volume of the zeolite were 400 m^2/g and 0.173 cm^3/g, and those of the 6%Mo/HZSM-5 catalyst were 310 m^2/g and 0.134 cm^3/g, respectively; and ^{27}Al MAS NMR measurement showed that the test catalyst contained a tiny amount of extraframework aluminium but no $Al_2(MoO_4)_3$ [31]. Furthermore, as shown by the NH_3-TPD profiles in Figure 3-2 and the FT-IR spectra of chemisorbed pyridine in Figure 3-3, most of Bronsted acid sites in the zeolite disappeared after the 6wt%Mo loading, strongly suggesting Mo migration and anchoring onto the Bronsted acid sites inside the zeolite channels in the calcination stage of catalyst preparation [34-38]. Note that the amount of highly dispersed Mo sites might be more crucial for maximizing the catalyst performance of Mo/HZSM-5 in the title reaction than that of Mo-unoccupied Bronsted acid sites [1,21], the test catalyst is expected to be highly active and to provide a typical deactivation profile of Mo/HZSM-5 catalysts used in the title reaction.

3.3.2. Activity evaluation

Figure 3-4 shows the time-dependences of the performance of the test catalyst over time frames of 10, 20, 40, 100, 130 and 160 min, respectively. As described above in the Experimental section 3.2, ending the tests at the different times is to obtain the spent samples with different coke contents, that is, a time-dependence of the catalyst coke content over the lifetime of the catalyst. Thanks to the careful setting of the reactor at a fixed position in the furnace and the precise controlling of the reaction temperature, the well duplicated data were acquired at each measure point in these

"actually repeated" tests and therefore ensure acquirement of the well-defined spent samples.

It is clear from Figure 3-4, particularly 3-4(c) and 3-4(d), that the test catalyst underwent three stages of deactivation over its lifetime: the most rapid decrease in the CH_4 conversion activity in the very initial stage of the reaction (~10 min), followed by a linearly slow deactivation in the period of 10-100 min and then an accelerated deactivation period in the last 60 min. Under periodic CH_4-H_2 (reaction-regeneration) switch operation modes, such a three-staged deactivation feature becomes more obvious for Mo/HZSM-5 catalyst [39].

In the very initial stage of the reaction, not the conversion of CH_4 to benzene but the fast carburization to Mo_2C of the remaining MoO_3 ($MoO_3 + CH_4 \rightarrow Mo_2C, H_2, CO, H_2O$) [40] and rapid conversion to Mo_2C of the reduced surface Mo ($Mo + CH_4 = Mo_2C + H_2$) [33] occur and dominate the conversion of CH_4. As a result, the rapidly decreasing CH_4 conversion (Figure 3-4(a)) and outlet H_2 concentration (Figure 3-4(c)) are observed with the fast increases in C_2H_4, benzene and naphthalene formation rates (Figure 3-4(b)). The title reaction is well recognized to proceed via a bifunctional mechanism: CH_4 is first activated on Mo_2C sites to form the C_2H_4 intermediate and then the oligomerization and cyclization of C_2H_4 on Bronsted acid sites follows to form benzene as well as naphthalene [1, 20, 40]. Therefore, at the very initial point of this "Mo_2C-forming" period (first sampling point), both benzene and naphthalene formation rates are very low, then rapidly increase and finally reach their maximum values with the completion of the full activation of Mo species at about 10 min. In this period, as shown below and also in three previous papers [13, 16, 30], the coke formation rate is very high, and rapid coke accumulation over Mo sites might be the main contributor. In the subsequent period (the second stage of deactivation), while the benzene and naphthalene formation rates keep monotonously decreasing and that of C_2H_4 monotonously increasing, the selectivity to benzene shows little variation with time (65-75 %). Similar observations were also reported in previous papers [20,22,29]. All these suggest that in this stage coke continuously accumulates over the

catalyst to cause it to slowly lose its benzene formation activity but its selectivity to benzene remains in essence uninfluenced. This can be understood in terms of coke formation capacity [33]. Mo/HZSM-5 catalyst, due to its high microporosity, has a considerably high capacity for coke deposition, and therefore any amount of coke accumulation, if it is not over a critical level, would have little effect on its aromatic formation selectivity. In this connection, the observation that Mo/MCM-22 catalyst exhibits a more stable activity than Mo/HZSM-5 [40, 41] may be explained by the fact that MCM-22 has not only 10-ring channels but also 12-ring pockets to give it a larger coking capacity than HZSM-5.

For the test catalyst, coke accumulation seems to reach its critical level at about 100 min. Evidence for this is that in the period beyond this time point the decrease of benzene selectivity is much more rapid than that observed in the second stage (Figure 3-4(d)). The primary reason for this is that the benzene formation rate itself started at this time point to decrease more rapidly and then fell along the curve of a steeper slope, as indicated by the dashed line in Figure 3-4(b). Note that the zeolite channels are essential for aromatics formation in the title reaction and the channel openings are almost identical in size to the kinetic diameter of benzene molecules. Thus, the most plausible explanation for the sudden appearance of this turning point for benzene formation (benzene selectivity) is that most of zeolite channels and/or their openings, due to coke accumulation, became very crucial in size by the time point for benzene diffusion, and any little more coke deposition could lead to a large reduction in benzene formation. If this is the case and such coke accumulation occurs mainly at the channel mouths and/or channel cross-sections not so distant from the channel mouths, continuously monitoring the behaviors of formation of the intermediate C_2H_4 and coke in the subsequent period (the last stage of deactivation) might provide clues to a better understanding of the catalytic role of Mo sites deep inside the zeolite channels and an exploration of coking pathways in the period. Note that benzene molecules have a kinetic diameter of about 6.0 Å, while those of CH_4 and C_2H_4 are 3.4 and 3.9 Å, respectively. Namely, over a certain time frame beyond the critical time point the zeolite channels might remain still large enough for CH_4 to enter into and for C_2H_4 to diffuse out of them. Further note that over the same time frame most of Mo sites

inside the channels might remain still active for CH_4 activation [42, 43]. Thus, it is expected that the activation of CH_4 over Mo sites inside the channels to form C_2H_4 will continue to take place in the last stage of deactivation. In this period, however, benzene is hardly allowed to diffuse out of the channels, and therefore its formation will be largely limited or completely inhibited. Namely, in the last stage of catalyst deactivation C_2H_4 keeps forming inside the zeolite channels whereas its conversion to benzene there is severely or fully inhibited. Probably for this reason the C_2H_4 formation rate did not exhibit an accelerated decrease in the last deactivation period beyond the critical time point (100 min), but continues its slow increasing, reaches a maximum at about 120 min and then turns to decrease (Figure 3-4(b)). For Mo sites on the external surfaces of individual zeolite crystals, if there are any still active in this period, they must function to catalyze the conversion of CH_4 to C_2H_4 just as those Mo sites inside the channels. The contribution to the total C_2H_4 formation rate, however, is believed to be negligibly small since the external surface area of the used microsized zeolite is very small (less than 4 m^2/g vs. the total BET surface area of 400 m^2/g) and most of the loaded Mo was confirmed to migrate into the Bronsted acid sites inside the zeolite channels in the calcination step of catalyst preparation (Figures 3-2 and 3-3).

Continuous increase in C_2H_4 formation rate with the decrease in benzene formation rate with time on stream was also observed in previous tests [21, 22], but all these tests were stopped in the relatively stable benzene formation period (the second stage of deactivation). There are also a few papers [44-46] that report the phenomenon of three-staged benzene formation over Mo/HZSM-5 catalyst in the title reaction, but no data on the corresponding C_2H_4 species and coke formation rate was given in them. To our best knowledge, the lifetime catalytic behaviors of a Mo/HZSM-5 catalyst including its C_2H_4 and coke formation behaviors are presented for the first time in this study. One might imagine that the selectivity to the intermediate C_2H_4 and that to coke both could behave in a way opposite to the selectivity to benzene, increasing with time in the last stage of catalyst deactivation (Figure 3-4 (c) and 3-4(d)). The monotonous decrease in CH_4 conversion over the same period (Figure 3-4(a)), however, gives one little confidence to predict a continuous increase in C_2H_4

formation rate itself (up to 120 min). Further, it is worth noting here that the selectivity to coke in the same period increased with time more rapidly than the selectivity to C_2H_4, and finally reached its maximum of about 50 % at 160 min (the end of the longest test), in comparison with 32 % selectivity to C_2H_4. These facts together suggest that the coke formation in this stage occurs mainly inside the zeolite channels and C_2H_4 could be the main source, which is completely missed in the literature [2, 19, 20].

3.3.3. Quantification of the coke deposit

Figure 3-5(a)-(f) show the TG profiles of the spent samples recovered from the top, middle and bottom layers of the catalyst beds experiencing the different reaction times, respectively. All profiles were measured under the same temperature-programmed heating mode given in Figure 3-5(c) and 3-5(f). The highest temperature and the holding time at the temperature were programmed to be 873 K and 30 min, respectively. At this condition the weight loss caused by MoO_3 sublimation was confirmed using the fresh catalyst to be negligible. It was also confirmed by visual observation that coke in all spent samples was burnt off completely at the programmed temperature condition.

It is clear from Figure 3-5 that all spent samples exhibit a very similar weight variation with time in the linear heating period of 303-873 K and subsequent holding period (30 min): a small decrease followed by a similar degree of increase and then a large decrease with a short period of tailing. While the first small weight loss in the region up to 393 K can be reasonably attributed to the desorption of residual adsorbed water, the weight gain in the subsequent region to 673 K was confirmed with commercially available Mo_2C to originate from the oxidation of Mo in reduced state in the sample into oxidative Mo compounds such as MoO_3. Thus, the second large weight loss starting at around 673 K was used to estimate the coke content of the sample, and the obtained results are summarized in Figure 3-6. For each sample the oxidation of coke to CO_2 gas, might also occur in the weight-increasing region to produce an error in the estimated coke content, but, as will be seen from the TPO profiles of all spent samples being given below, it was not over 10 %.

It is clear from Figure 3-6 that the contents of coke accumulated in the different layers of the catalyst bed in each test are not identical. The coke content shows an obviously decreasing tendency along the bed from the bottom to the top layer for the samples recovered after the reaction over the periods of up to 130 min, but for the samples recovered after 160 min of reaction (the longest test) it reached almost an identical level. While confirming the high reliability of TG measurement, these observations also suggest the following two conclusions. First, coke formation in an integral fixed bed occurs non-uniformly. Second, the amount of coke accumulated in any Mo/HZSM-5 catalyst irrespective to its position in a bed remains essentially fixed over its lifetime. While both observations are explainable by the variation of the gas phase composition along the bed, the detailed explanation will be omitted in this paper since it is out of the focus of the work.

Pursuing the lifetime-dependence of the coking behavior of the catalyst yet led us to another new finding: for all three layers of the catalyst, irrespective to their positions in the bed, their average coke formation rates in the last stage of deactivation become higher, not lower, than that recorded in the second stage of deactivation. For example, while the amount of coke accumulated in the bottom catalyst increased from 3.7 to 6.7 wt% over the period of 40-100 min to give an average coke formation rate of 0.075 wt%/min, it increased in the last 60 min of the reaction (the period of 100-160 min) from 6.7 to 11.6 wt%, which indicates a higher rate of 0.123 wt%/min. Note that in most of catalytic systems coke formation rate is decreasing with catalyst deactivation, particularly in the last deactivation stage. The present observation is very unordinary and entirely out of our anticipation based on the variation of the monotonously decreasing CH_4 conversion over the period (Figure 3-4(a)). Since it was reached with the samples from the three different layers of catalyst beds, its reliability should be undoubtable. Nevertheless, I performed a similar set of tests with another nanocrystal-based 6%Mo/HZSM-5 catalyst and measured the coke contents in the collected spent samples to make further confirmation. The result showed that at 1073 K and a space velocity of 21,080 mL/g/h the average coke formation rate recorded over a time frame of 55 min in the last

deactivation stage of the catalyst, during which benzene selectivity decreased from 44 to 12 %, was about 0.145 wt%/min, whereas that over the previous 55 min in the slow deactivation stage was about 0.073 wt%/min. Namely, the average coke formation rate can truly become higher as Mo/HZSM-5 catalyst enters its last deactivation stage. If this is a universal phenomenon for the title catalytic system, confirming the types of coke accumulated preferentially in the last stage of deactivation might provide a clue to understanding the coking sources in the period as well as that throughout the whole period of the reaction.

3.3.4. Characterization of the coke deposit

The characterization of the coke deposit in the spent samples was first conducted using TPO technique to distinguish the coke on the external surface of zeolite crystals and that inside the zeolite channels. Figures 3-7 and 3-8 show the results obtained.

As shown by the dash lines in Figure 3-7, all TPO profiles can be well deconvoluted into four fitting peaks denoted as I, II, III, and V. The appearance of the latter three eye-distinguishable peaks can also be confirmed in a typical DTA profile given in Figure 3-9, where three obvious exothermic peaks are observed at 755, 774 and 820 K, respectively. Similar TPO patterns with obvious three-peak features were also reported in previous papers [44,47]. With the increase in reaction time on stream all four TPO peaks in Figure 3-7 shift to higher temperatures, and finally after 160 min of the reaction their peak temperatures reach 760, 810, 860 and 920 K, respectively. For the first peak the oxidation of Mo_2C with CO_x releasing might be considered to be responsible for, but the theoretical maximum carbon loss via this reaction is about 0.37 wt% for the test catalyst, much smaller than the coke contents of 0.93-1.36 wt% estimated from the area of peak I for the samples experiencing 100, 130 and 160 min of the reaction. Additionally, in a previous work Ding et al [25] have reported that C in Mo_2C in a Mo/HZSM-5 catalyst burns off at a very low temperature of about 573 K, and its burning peak was quite sharp and observable only for a sample experiencing a very short time (tens of seconds) of carburization treatment and with a very limited coke content. Thus, the CO_x evolution assigned here to peak I in Figure 3-7 has to be ascribed to slow oxidation of the most reactive carbon deposits

on the external surface of the catalyst, which is often observed in the TPO of carbon materials [48].

To reveal the origins of peaks II, III and IV, types of coke deposits in the spent samples were identified by XPS analysis. As exemplified in Figure 3-10, for the samples recovered after 100 and 160 min of tests, only one main peak at 284.5 eV with a shoulder at 286.5eV was observed in the C 1s region. Compared to the C 1s spectrum of a commercial graphite sample given in the same figure, the main peak can undoubtedly be attributed to graphitic-like C. On the other hand, for the shoulder, since it appeared on the higher binding energy side of the main peak, and matches the binding energies C-C and C-H bonds in the literature [17,49], it is attributed here to resulting from the aromatic type of C.

Note that XPS analysis is surface-sensitive and provides information only on surface carbon deposits. Any conclusion from the present observation must only be applicable to the coke deposits on the external surface of catalyst. Thus, the graphitic-like C detected at 284.5 eV is considered to be the dominant type of coke on the external surface of zeolite crystals in the present cases. Graphitic-like C forms not only on the zeolite surface and at the channel mouths but also on top of Mo sites dispersed there [18]. By fitting their XPS spectra in the C 1s region, Larachi et al [17] reported that graphitic-like C (at 284.2eV) was the most prominent carbon species formed over a 0.5wt%Ru-3wt%Mo/HZSM-5 catalyst at a low temperature of 973 K. For a 2wt% Mo/HZSM-5 catalyst exposed for 13 h to methane at the same low temperature, 973 K. Weckhuysen et al [14] also identified the formation of graphitic-like C by angle-resolved XPS analysis. Note that theoretically O_2 molecules in the TPO will first approach the external surface of zeolite crystals and react with the coke there and then diffuse into the zeolite channels. Thus, peak II in the TPO profiles of Figure 3-7 is naturally considered to be the consequence of burning of the surface graphitic-like C.

Compared with graphite-like C, the aromatic type of coke has a higher H/C ratio, and its oxidation must be companied with formation of more water steam. Namely,

the profiles of mass number m/z = 18 recorded simultaneously in the TPO measurements can be helpful in confirming the formation of the aromatic type of coke and pursuing its burning behavior [16]. As shown by the thick solid lines in Figure 3-8, the formation of water steam in the TPO becomes obvious for the samples experiencing 40 min and longer periods of reaction, and in all these cases the signal intensity of m/z = 18 increases with temperature in a low temperature range, reaches the maximum at 800-850 K, and then falls to nearly zero at about 920 K. For the samples recovered after 100, 130 and 160 min of reaction and having the higher coke contents of 5.3, 8.3 and 11.3 wt%, the formation of water steam peaks at around 800, 820 and 860 K, all being well consistent with the peak temperatures of CO_x evolution peak III in Figure 3-7 (for readers' convenience CO_x evolution patterns were also re-plotted by thin dashed lines in Figure 3-8). This strongly suggests that the aromatic type of coke detected by XPS at 286.5eV is the origin of the peak III. If we assume that this type of coke formed mainly inside the zeolite channels, then we can explain why it is observed as a shoulder, not a strong peak, in the XPS/C 1s spectra, and also why its burning occurs at a higher temperature after burning off of the less reactive surface graphitic-like C. For the favorable formation of this type of coke inside the channels, it may be understood because deep polycondensation of formed aromatics to graphitic-like C is spatially limited in the channels and most of coke has to stay in a less polycondensed form. Experimental evidence for this can also be found in the literature. For a spent 6wt%Mo/HZSM-5 catalyst, which showed two TPO peaks at about 770 and 860 K, Liu et al [15] reported that heating it in H_2 up to 1013 K (H_2-TPR treatment) enabled most of its coke that burned off at the high temperature 860 K in the TPO to be removed, whereas it had little effect on removal of the coke burnt off at the low temperature of 770 K. This experimental observation suggests that the type of coke burning at 860 K is actually more reactive to H_2 than the type of coke that burned off at 770 K. Thus, the only plausible explanation for this reactivity-burning temperature inconstant TPO behavior is that the H_2-removalble coke in their sample located inside the zeolite channels and its accessibility to O_2 in the TPO was severely hampered by the coke deposits on the external surfaces of the zeolite crystals and/or at the channel mouths. Namely, the aromatic type of coke inside the zeolite channels could indeed start its burning in the TPO, due to mass

transport limitations, at a higher temperature than less reactive graphitic-like C formed on the external surfaces of zeolite crystals.

Note that peaks II, III and IV are eye-distinguishable for the samples after 100, 130 and 160 min of reaction, whereas only two types of coke were detected by XPS analysis. Presume that intracrystalline diffusion limitations do exist in the TPO. Thus, according to the above discussion on the accessibility of O_2 to the coke in the catalyst one may easily figure out that burning of the coke deep inside the zeolite channels must come last to give peak IV. The used zeolite crystals are microsized (~2 μm in thickness) and physically allow this type of coke to form. For a spent 6wt%Mo/HMCM-22, Ma et al [40] argued two types of aromatic cokes formed on two different Bronsted acid sites. Additionally, Ding et al [25] also claimed that carbon deposits inside the zeolite channels could give two TPO peaks, depending upon their distances to Mo sites. Note that Mo component was impregnated first on the external surface of zeolite crystals and then migrated in the calcination step into the Bronsted sites inside the channels [33-37]. It means that, if there are any Bronsted acid sites remaining Mo-unoccupied after a sufficient Mo loading, they should be those residing deep inside the channels. Further note that for the test catalyst there remained indeed approximately 10% of the total Mo-unoccupied Bronsted acid sites (Figure 3-3). Therefore, here the peak IV is attributed to the burning of carbon deposits on the free Bronsted acid sites deep inside the channels. Considering the spatial restriction effect of the zeolite channels, this type of coke might hardly form via polycondensation of formed aromatics.

3.3.5. Coke source

While Figure 3-6 suggests that the net increases of the amounts of coke accumulated in the bottom, middle and top catalyst layers over the last 60 min of reaction (the last stage of deactivation) reached about 4.9, 5.6 and 6.0 wt%, respectively, the corresponding TPO profiles and their curve-fitting results in Figure 3-7 reveal how the relative amounts of the different types of coke vary throughout the period. For the spent samples recovered from the top layers of catalyst beds, distributing their total coke amounts among the four deconvoluted peaks and then

graphing the resulting data led to a bar graph, Figure 3-11 (for the samples from the middle and bottom layers similar bar graphs were obtained). It is clear from the figure that the absolute amounts of all types of coke keep increasing in the last 60 min of reaction, and that the aromatic type of coke and the graphite-like C make the two largest contributions of about 56 % and 24 % to the total increase, respectively. Note that over the same period the benzene formation rate decreased by 92 % from 3.6 to 0.3 μmol-C/g/s, and the benzene selectivity decreased by 69 % from 64 to 20 %. If polycondensation of formed benzene and naphthalene molecules were the main route to the coke formation of the graphite-like C on the external surface of zeolite crystals in this period, its average coke formation rate would be lower than that recorded over the same 60 min time frame in the previous deactivation stage. The fact, however, as shown in Figure 3-11, is that it increased and became larger (from 0.019 to 0.023 wt%/min). For the aromatic type of coke, there is difficulty in excluding the possibility of an accelerated aromatics polycondensation inside the zeolite channels to increase its average formation rate, but in that case the questions must be answered of why the C_2H_4 formation rate keeps still increasing even after the catalyst enters its last deactivation stage and its average in the whole last stage becomes obviously higher than that in the second stage (Figure 3-4). It seems to us more reasonable to consider an increased intracrystalline diffusion resistance in the last stage to lower the CH_4 diffusion rate and consequently the benzene formation rate inside the channels than to imagine occurrence of an accelerated polyaromatization of formed benzene there.

In addition to polycondensation of formed aromatics on the Bronsted acid sites, thermal and/or catalytic oligomerization and/or cracking of C_2H_4, schemed as Route ③ in Figure 3-12, can also cause serious coke formation and catalyst deactivation in the title reaction. Note again that the C_2H_4 formation rate kept increasing after the benzene selectivity turned to a sharper decrease at about 100 min to indicate the start of the last deactivation stage, and reached its maximum value at a delayed point of time of 120 min (Figure 3-4(b)). Further presume, as did above, that in this period Mo sites inside the zeolite channels remain still accessible to CH_4 and also active for its activation and the formation of C_2H_4. Then a conclusion could be reached that it

must be the coking reactions of C_2H_4 (say, its oligomerization and/or cracking) inside the channels to cause the large increase in the coke content of the spent sample after 130 or 160 min of reaction (as shown by TG and TPO results). This is understandable because most of the Mo in the test catalyst is highly dispersed on the Bronsted acid sites inside the zeolite channels (suggested by Figures 3-2 and 3-3) and its much larger internal than external surface area provides much more active sites inside the channels for coke deposition. As suggested by the NH_3 TPD patterns of two typical spent samples in Fig. 3-2, a considerable number of Lewis acid sites as well as a small number of Bronsted acid sites did remain coke-uncovered after the test catalyst lost most of its benzene formation activity in the 160 min reaction. Thus rather than its thermal reactions acid-catalyzed conversion of C_2H_4 to coke is believed to play a key role in the formation of aromatic type of coke over the last stage of catalyst deactivation. At the same time, due to its short thermal history this type of coke might have little chance to convert to the graphitic-like C with a lower H/C ratio; which gives a reasonable explanation of why the intensity of the peak III in the TPO profiles increased most rapidly in the last stage of deactivation and the corresponding coke made the primary contribution (about 56 %) to the total increase in the catalyst coke content. Further note that carbon deposits accumulated over nanozeolite-based Mo/HZSM-5 catalysts always produce TPO profiles composed of only one intense peak with a negligibly small shoulder in the high temperature side [31,32,39]. Thus this aromatic type of coke might form at the cross-sections of the channels slightly distant from their mouths and therefore burned off at a relatively high temperature. In this connection, with little O_2 transfer limitations the coke at the channel mouths and the near-surface channel coke could burn simultaneously with burning of the coke on the external surface of crystals to lead to a gradually increasing evolution of steam water in the region of the peak II (Figure 3-8).

The graphite-like C on the external surface of zeolite crystals made the second largest contribution (about 24 %) to the total increase in the amount of coke accumulated in the last deactivation stage. Although the average formation rate of this type of coke in the period is not as large as that of the aromatic type of coke, it did increase from about 0.019 wt%/min over the second deactivation period to 0.023

wt%/min in the last deactivation stage. For this the secondary coking reactions of formed C_2H_4 should be responsible as well. An improvement in the coking activity of the catalyst in either pyrolysis of CH_4 or polycondensation of aromatics could lead to an increase in the average formation rate of the graphite-like C in the last deactivation stage, but occurrence of such an improvement seems very unlike and unreasonable. In fact, CH_4 conversion itself had fell to its lowest levels in the last stage of deactivation, suggesting that the CH_4 pyrolysis activity of the catalyst was significantly decreased in the first two deactivation stages, not improved at all. With its zeolite crystals as well as Mo sites covered by coke, the catalyst in this stage can only be expected to provide an active surface for thermal conversion of CH_4 and all reaction products to coke. Thus, the possibility that polycondensation of the formed aromatics dominates the formation of graphite-like C on the external surface of zeolite crystals in the last deactivation stage can be excluded, since the concentrations of both benzene and naphthalene had decreased to their lowest levels in the period and the rate of their conversion to coke should go to decrease, not to increase. Thermodynamically, C_2H_4 is more reactive than benzene and naphthalene, and therefore its secondary coking reactions would most likely take place to accelerate the formation of this type of coke and increase its average formation rate in the period.

Thus, two additional activity tests were designed and carried out to make further confirmation. One was conducted with 200 mg of the catalyst alone and packed in one layer, and the other in a two layers mode and with 200 mg of the catalyst packed in the inlet layer and simultaneously 200 mg of a highly pure silica (Fuji Silysia, CARiACT Q-30 with a BET surface area of 120 m^2/g, and a uniform pore diameter of 30 nm) in the outlet layer. The reaction temperature and CH_4 feed rate used in these two tests were exactly the same as those used in all other tests. As shown in Figure 3-13, doubling the height of the bed with the Mo-unloaded pure silica did not cause any decrease in either benzene or naphthalene formation rate over the test period, while the outlet C_2H_4 rate was obviously decreased and that H_2 rate obviously increased at all measured points. Further, TG measurement of the spent SiO_2 sample confirmed that about 3.2 wt% of coke accumulated in it. All these thus suggest that the conversion of C_2H_4 to coke is kinetically more favorable than those of benzene

and naphthalene under the test condition, and also that the secondary coking reactions of C_2H_4 do occur over the highly pure SiO_2 whereas those of benzene and naphthalene might not. If the highly pure SiO_2 in this test just functions to provide an active surface for thermal conversion of C_2H_4 to coke, the external surface-coked zeolite crystals in any catalyst particles in the three layers operation mode are expected to do the same and promote the thermal conversion of C_2H_4 to the graphite-like C on the external surface of zeolite crystals in the last deactivation stage. Thus, the increased average C_2H_4 concentration in the period surely leads to an increase in its average conversion rate to coke, namely an increase in the average graphite-like C formation rate.

3.4. Further discussion

If we assume that the continuous increase in C_2H_4 rate in the second stage of catalyst deactivation and the initial 20 min of the last deactivation stage (Figure 3-4(b)) is resulted from a gradual decrease with time in the C_2H_4-to-benzene conversion activity of the catalyst (Route ② in Figure 3-12) due to the coking-caused channel mouth narrowing, not from a continuous increase with time in the C_2H_4 formation activity of Mo sites, it will be easily imaginable that C_2H_4, as the reaction intermediate, might form at a much higher rate over the period than what was actually measured. In fact, thermodynamic calculation of CH_4-C_2H_4-H_2 system using the actually measured outlet H_2 concentration data indicated that the observed outlet C_2H_4 concentration attained almost its equilibrium values at all measured time points in the period of 20-100 min. If this is the case, there always exists a sufficient amount of C_2H_4 in the system in the period available for its cyclization to benzene (Route ② in Figure 3-12) and simultaneously its oligomerization and/or cracking to coke (Route ③ in Figure 3-12). Namely, the formation of coke originating from C_2H_4, in competing with its conversion to benzene, could be a main contributor to the slow deactivation of catalyst in the second stage as well. Since in this stage benzene forms still at relatively high rates and its selectivity remains quite stable, most of the C_2H_4 formed on the Mo sites inside the zeolite channels is believed to be consumed in

benzene formation. Thus it might be concluded that, if the formation of coke does originate mainly from C_2H_4 in this period, it must proceed mainly on the external surfaces of zeolite crystals and at the channel mouths. Probably for this reason the average coke formation rate observed in the second deactivation stage was lower than that recorded in the last stage (Figure 3-6). Also probably for the same reason, for all spent samples recovered after 20, 40 and 100 min of reaction the type of coke suggested by peak II and on the external surface of the zeolite crystals was the most abundant fraction among all types of coke and attained 48-55 % of their total in quantity.

3.5. Conclusions

Pursuing the catalytic performance of the 6%Mo/HZSM-5 over its lifetime confirmed its three stages deactivation characteristics. While the benzene selectivity of the catalyst shows a very rapid decrease in the last deactivation stage due to channel narrowing and/or partial block of channel mouths by coke, its C_2H_4 formation rate exhibits reversely a continuous increase throughout a wide region, which covers the whole second deactivation stage and part of the third stage. Simultaneously quantification of the amounts of coke accumulated in the catalyst over different lengths of reaction time revealed an unordinary phenomenon that the average coke formation rate in the last deactivation stage becomes obviously higher, not lower, than that observed throughout the second stage. These two observations together suggest that the secondary conversion of C_2H_4 is the main source of coke formation in the last deactivation stage. Further, the detailed analysis of all TPO results with considering the accessibility of O_2 to the zeolite channels led to a conclusion that the coke burning during the TPO takes an order that is determined by coke's location in the spent catalyst: the graphite-like C on the external surface of zeolite crystals and at channel mouths coke burns first, followed by the aromatic type of coke inside the zeolite channels, and then the type of coke on the free Bronsted acid sites deep inside the channels. Moreover, the peak deconvolution of the TPO patterns and distribution of the total coke contents among the different types of coke revealed that the aromatic type of coke inside the channels makes a primary contribution of 56 % to the total

coke formed in the last stage of catalyst deactivation; this further suggests that the coking reactions in the last deactivation stage occurs mainly inside the zeolite channels and C_2H_4 must be involved. C_2H_4 forms throughout the whole reaction period and therefore its secondary coking reactions could also dominate the coking process in the second stage of catalyst deactivation as well.

References

[1] Y.D. Xu, L.W. Lin, Appl. Catal. A 188 (1999) 53-67.

[2] R. Ohnishi, S. Liu, Q. Dong, L.S. Wang, M. Ichikawa, J. Catal. 182 (1999) 92-103.

[3] C.L. Zhang, S. Li, Y. Yuan, W.X. Zhang, T.H. Wu, L.W. Lin, Catal. Lett. 56 (1998) 207-213.

[4] W.P. Ding, G.D. Meitzner, E. Iglesia, J. Catal. 206 (2002) 14-22.

[5] F. Solymosi, A. Oszkó, T. Bánsági, P. Tolmacsov, J. Phys. Chem. B 106 (2002) 8524-8530.

[6] S. Burns, J.S.J. Hargreaves, P. Pal, K.M. Parida, S. Parija, Catal. Today 114 (2006) 383-387.

[7] H.T. Ma, R. Kojima, S. Kikuchi, M. Ichikawa, Catal. Lett. 104 (2005) 63-66.

[8] H.T. Ma, R. Ohnishi, M. Ichikawa, Catal. Lett. 89 (2003) 143-146.

[9] P.L. Tan, Y.L. Leung, S.Y. Lai, C.T. Au, Catal. Lett. 78 (2002) 251-258.

[10] H.T. Ma, R. Kojima, R. Ohnishi, M. Ichikawa, Appl. Catal. A 275 (2004) 183-187.

[11] K. Honda, T. Yoshida, Z.-G. Zhang, Catal. Commun. 4 (2003) 21-26.

[12] Y.Y. Shu, H.T. Ma, R. Ohnishi, M. Ichikawa, Chem. Commun., (2003) 86-87.

[13] Y.B. Xu, J.Y. Lu, J.D. Wang, Y. Suzuki, Z.-G. Zhang, Chem. Eng. J. 168 (2011) 390-402.

[14] B.M. Weckhuysen, M.P. Rosynek, J.H. Lunsford, Catal. Lett. 52 (1998) 31-36.

[15] H.M. Liu, T.Li, B.L. Tian, Y.D. Xu, Appl. Catal. A 213 (2001) 103-112.

[16] D. Ma, D.Z. Wang, L.L. Su, Y.Y. Shu, Y.D. Xu, X.H. Bao, J. Catal. 208 (2002) 260-269.

[17] F. Larachi, H. Oudghiri-Hassani, M.C. Iliuta, B.P.A. Grandjean, P.H. McBreen, Catal. Lett. 84 (2002) 183-192.
[18] E.V. Matus, I.Z. Ismagilov, O.B. Sukhova, V.I. Zaikovskii, L.T. Tsikoza, Z.R. Ismagilov, Ind. Eng. Chem. Res. 46 (2007) 4063-4074.
[19] L. Li, R. W. Borry, E. Iglesia, Chem. Eng. Sci. 57 (2002) 4595-4604.
[20] S.T. Liu, L.S. Wang, R. Ohnishi, M. Ichikawa, J. Catal. 181 (1999) 175-188.
[21] D.J. Wang, J.H. Lunsford, M.P. Rosynek, Top. Catal. 3 (1996) 289-297.
[22] F. Solymosi, J. Cserényi, A. Szöke, T. Bánsági, A. Oszkó, J. Catal. 165 (1997) 150-161.
[23] Y. Chen, L.W. Lin, Z.S. Xu, X.S. Li, T. Zhang, J. Catal. 157 (1995) 190-200.
[24] D.J. Wang, J.H. Lunsford, M.P. Rosynek, J. Catal. 169 (1997) 347-358.
[25] W.P. Ding, S.Z. Li, G.D. Meitzner, E. Iglesia, J. Phys. Chem. B, 105 (2001) 506-513.
[26] Y.D. Xu, S.T. Liu, L.S. Wang, M.S. Xie, X.X. Guo, Catal. Lett. 30 (1995) 135-149.
[27] M.H. Back, R.A. Back, in: L.F. Albright, B.L. Crynes, W.H. Corcoran (Eds.), Pyrolysis: Theory and Industrial Practice, Academic Press London, 1983, pp. 1-4.
[28] Y.H. Kim, R.W. Borry, E. Iglesia, Micropor. Mesopor. Mater. 35-36 (2000) 495-509.
[29] F. Solymosi, A. Szöke, J. Cserényi, Catal. Lett. 39 (1996) 157-161.
[30] J. Bai, S.L. Liu, S.J. Xie, L.Y. Xu, L.W. Lin, Catal. Lett. 90 (2003) 123-130.
[31] Y.B. Cui, Y.B. Xu, J.Y. Lu, Y. Suzuki, Z.-G. Zhang, Appl. Catal. A 393 (2011) 348-358.
[32] Y.B. Cui, Y.B. Xu, Y. Suzuki, Z.-G. Zhang, Catal. Sci.Technol. 1 (2011) 823-829.
[33] Y.B. Xu, J.D. Wang, Y. Suzuki, Z.-G. Zhang, Appl. Catal. A 409-410 (2011) 181-193.
[34] Y.D. Xu, Y.Y. Shu, S.T. Liu, J.S. Huang, X.X. Guo, Catal. Lett. 35 (1995) 233-243.
[35] D. Ma, W.P. Zhang, Y.Y. Shu, X.M. Liu, Y.D. Xu, X.H. Bao, Catal. Lett. 66 (2000) 155-160.
[36] R.W. Borry, Y.H. Kim, A. Huffsmith, J.A. Reimer, E. Iglesia, J. Phys. Chem. B 103 (1999) 5787-5796.

[37] J.P. Tessonnier, B. Louis, S. Walspurger, J. Sommer, M.J. Ledoux, P.H. Cuong, J. Phys. Chem. B 110 (2006) 10390-10395.
[38] J.P. Tessonnier, B. Louis, M.J. Ledoux, P.H. Cuong, Catal. Commun. 8 (2007) 1787-1792.
[39] Y.B. Xu, Y. Suzuki, Z.-G. Zhang, Appl. Catal. A 452 (2013) 105-116.
[40] D. Ma, Y.Y. Shu, M.J. Cheng, Y.D. Xu, X.H. Bao, J. Catal. 194 (2000) 105-114
[41] Y.Y. Shu, D. Ma, L.Y. Xu, Y.D. Xu, X.H. Bao, Catal. Lett. 70 (2000) 67-73.
[42] K. Honda, X. Chen Z.-G. Zhang, Catal. Commun. 5 (2004) 557-561.
[43] P.L. Tan, Y.L. Leung, S.Y. Lai, C.T. Au, Catal. Lett. 78 (2002) 251-258.
[44] H.T. Ma, R. Kojima, S. Kikuchi, M. Ichikawa, J. Nat. Gas Chem. 14 (2005) 129-139.
[45] C.Y. Sun, S.D. Yao, W.J. Shen, L.W. Li, Catal. Lett. 122 (2008) 84-90.
[46] Y.G. Li, T.H. Wu, W.J. Shen, X.H. Bao, Y.D. Xu, Catal. Lett. 105 (2005) 77-82.
[47] H.M. Liu, X.H. Bao, Y.D. Xu, J. Catal. 239 (2006) 441-450.
[48] F.R. Reinoso, in: H. Marsh, E.A. Heintz, F.R. Reinoso (Eds.), Introduction to Carbon Technologies, University of Alicante Secretariado de Publicaciones Spain, 1997, pp. 57.
[49] B.S. Liu, L. Jiang, H. Sun, C.T. Au, Appl. Surf. Sci. 253 (2007) 5092-5100.

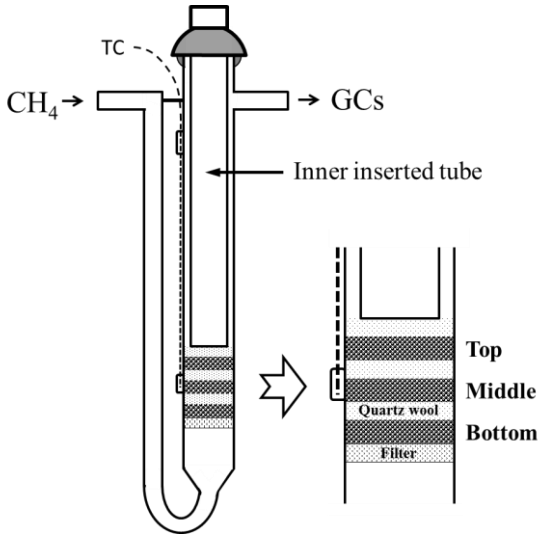

Fig. 3-1. Schematic diagram of the three layers fixed bed reactor.

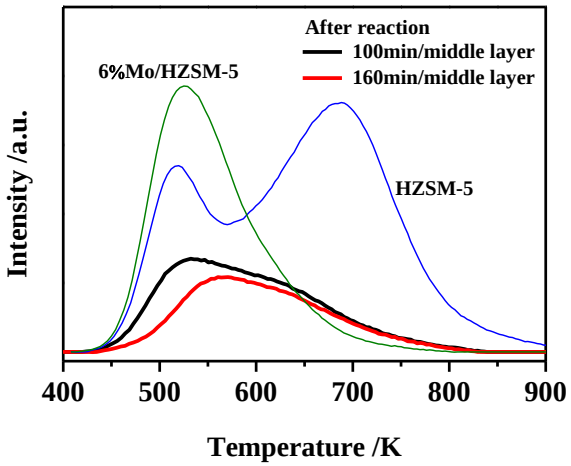

Fig. 3-2. NH_3-TPD profiles of HZSM-5 and 6%Mo/HZSM-5 samples.

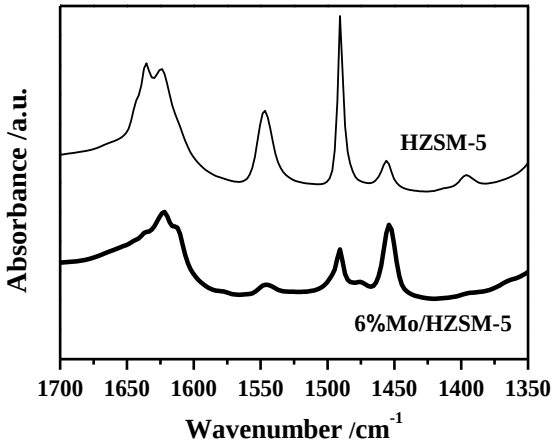

Fig. 3-3. FT-IR spectra of pyridine-chemisorbed HZSM-5 and 6%Mo/HZSM-5 samples**.**

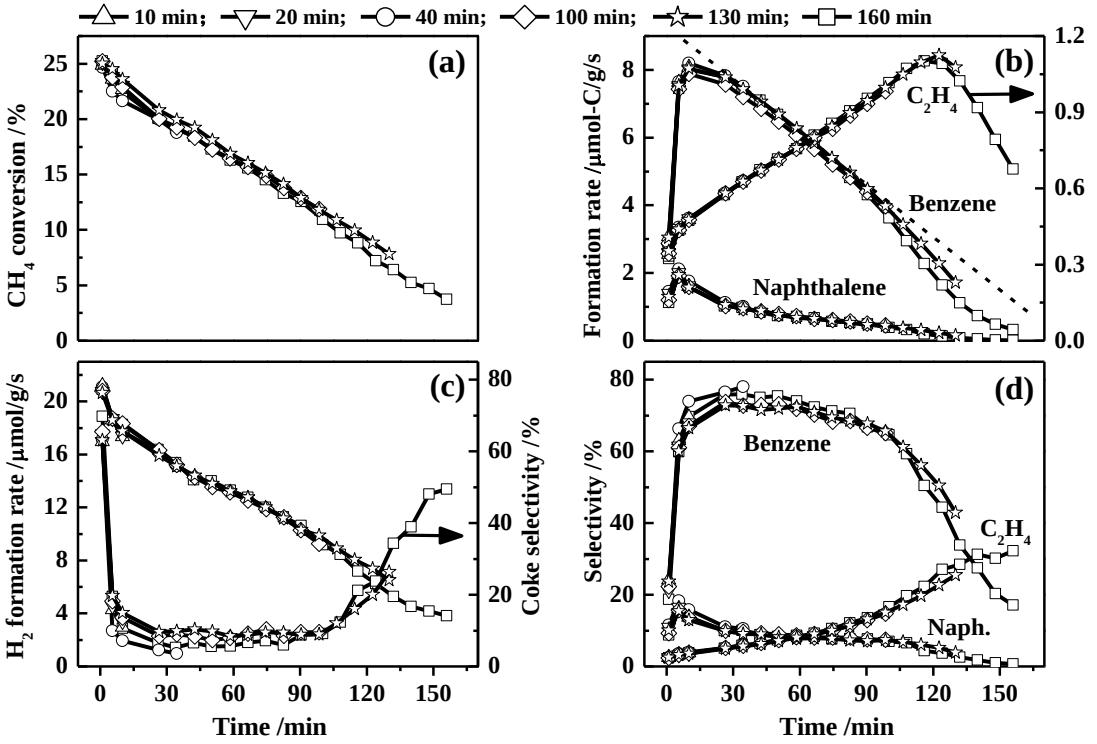

Fig. 3-4. Time-dependences of catalytic performance of 6%Mo/HZSM-5 over different lengths of reaction time at 1073 K and 5,000 mL/g/h in continuous CH_4 feed mode.

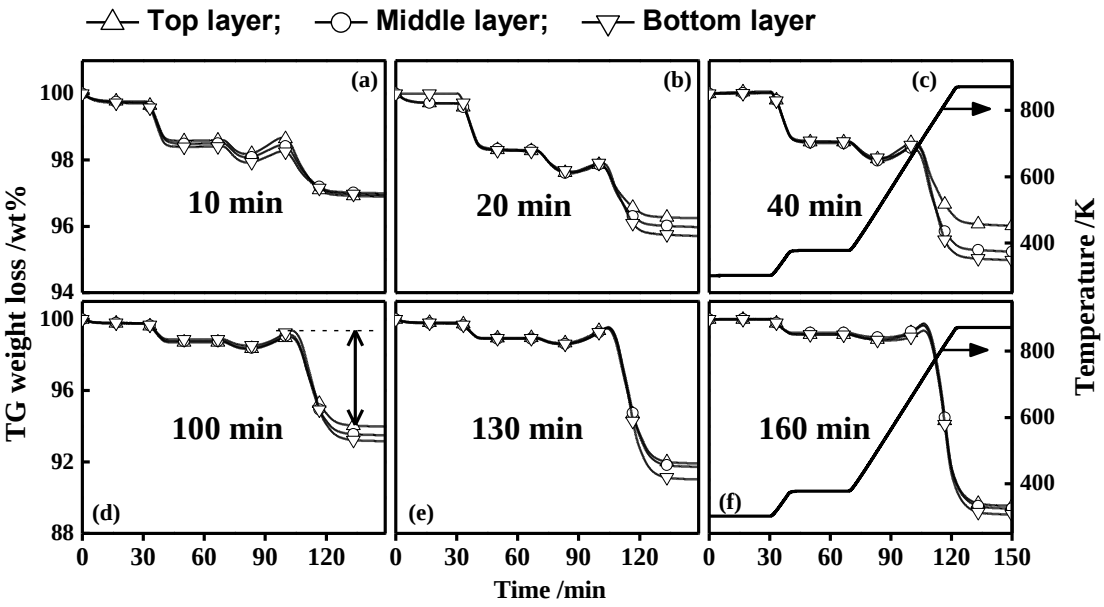

Fig. 3-5. TG profiles of the spent catalyst samples recovered after the reaction tests over different lengths of time.

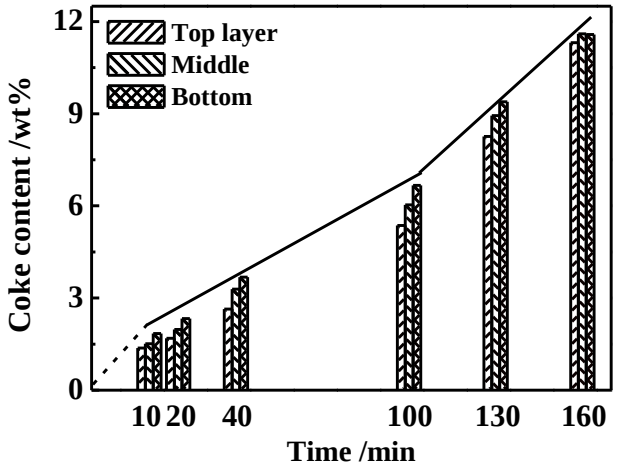

Fig. 3-6. Variations with reaction time of the amounts of coke accumulated in three catalyst layers.

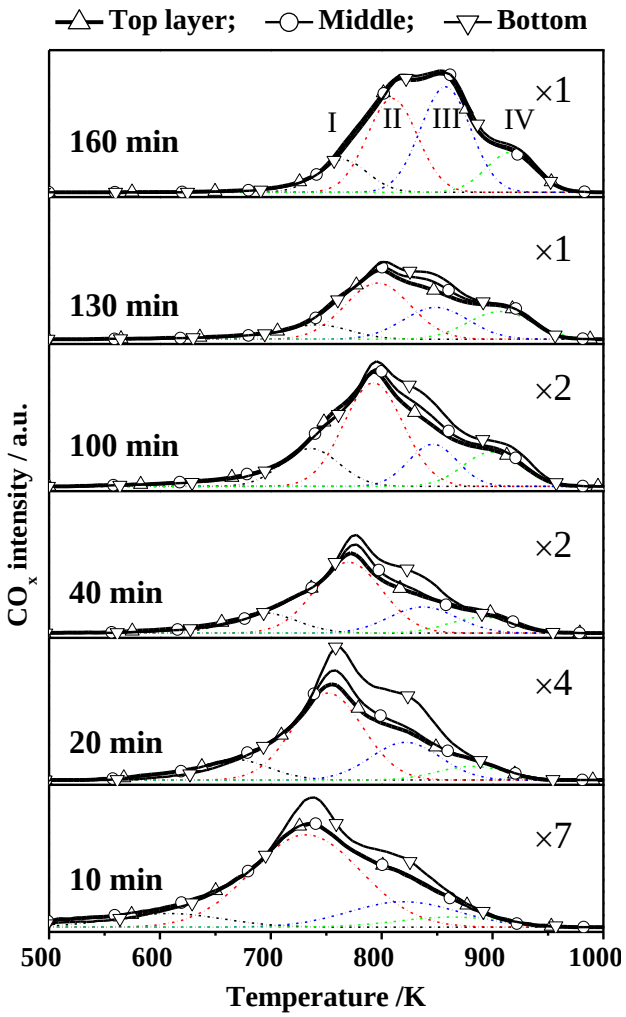

Fig. 3-7. TPO CO_x-profiles of the spent samples recovered from the different catalyst layers after the reaction tests over different lengths of time.

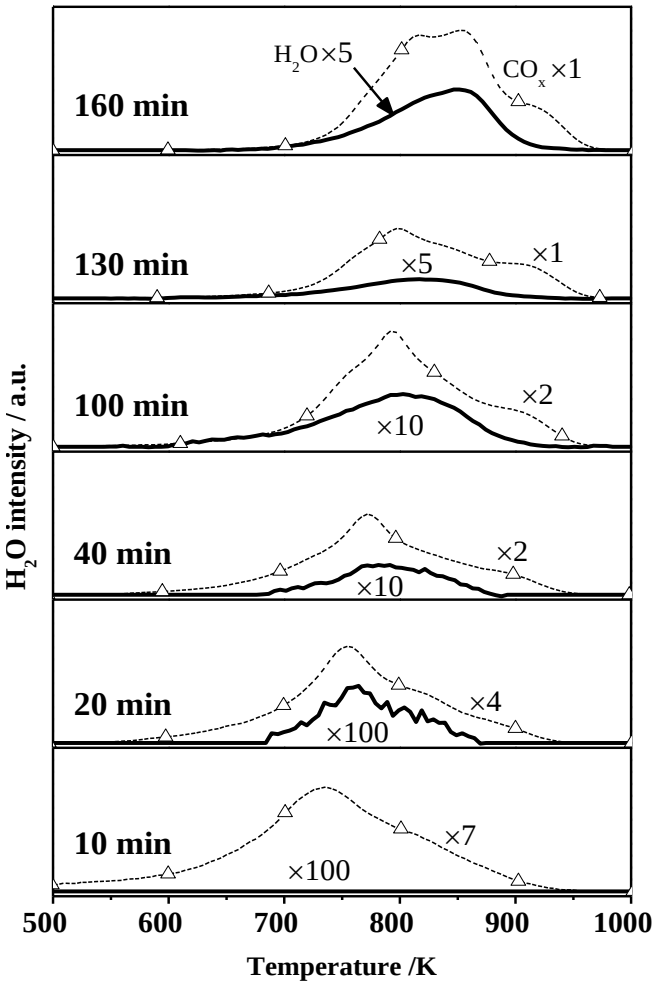

Fig. 3-8. H_2O profiles recorded simultaneously in the TPO measurements of the spent samples specified in Figure 3-7.

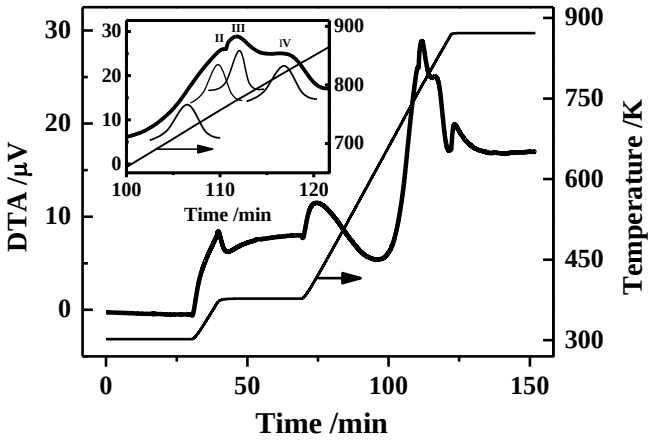

Fig. 3-9. DTA profile of the spent sample recovered from the top catalyst layer after 160 min of reaction.

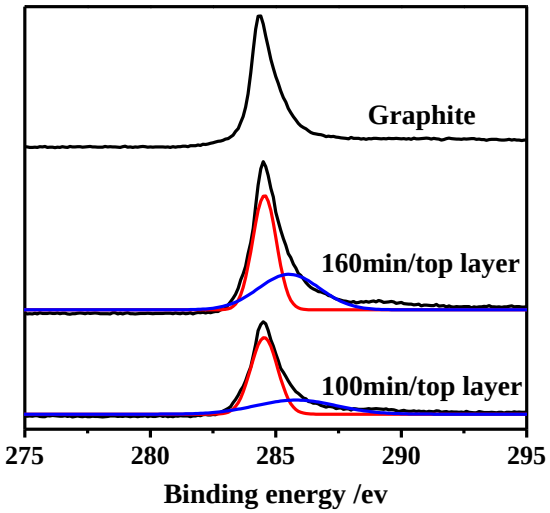

Fig. 3-10. XPS spectra in C 1s region of the spent samples recovered from the top catalyst layers after 100 and 160 min of reaction.

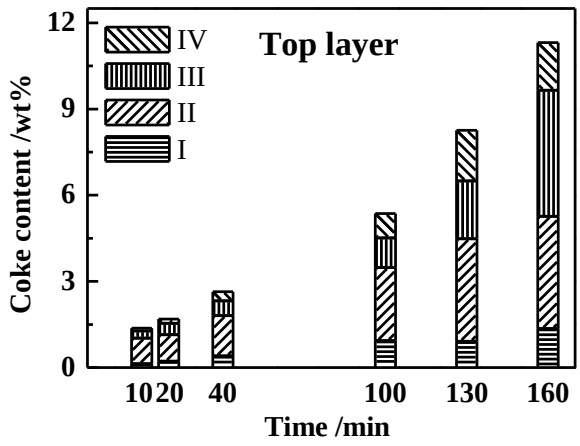

Fig. 3-11. Variation with reaction time of distribution of different types of coke accumulated in the top catalyst layer.

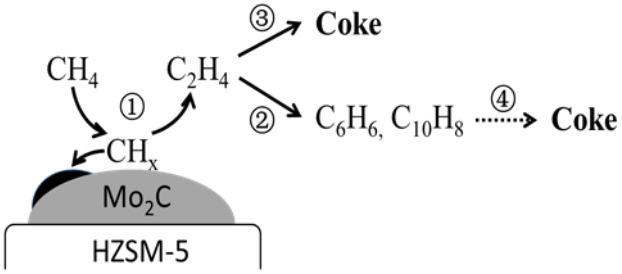

Fig. 3-12. Schematic diagram of coking pathways.

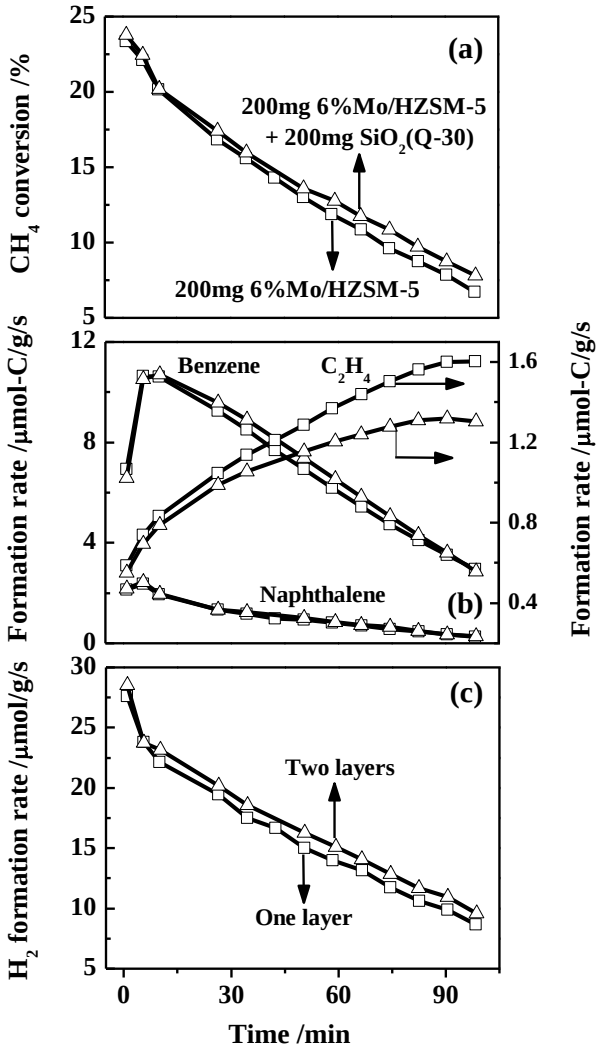

Fig. 3-13. Verification of coking reactions of the nascent C_2H_4 occurring on a highly pure silica (Q-30) at the reaction condition. 200 mg of Q-30 was packed in the outlet layer of bed to provide active sites for coking of both C_2H_4 and aromatics from the inlet catalyst layer.

Chapter 4

Effect of co-fed H_2 on the distribution of coke formed: the pathway of coke formation in the stable benzene formation stage

4.1. Introduction

Mo/HZSM-5 is the most promising catalyst for the non-oxidative methane dehydroaromatization reaction [1-4]. However it suffers rapid deactivation due to serious coke formation under practically required severe conditions. [5-8] Various approaches were attempted to tackle this problem, which include promotion of mass transfer by using the zeolite with mesoporous/microporous hierarchical structures [9-10], optimization of the Si/Al ratio of the zeolites [11-13], silane modification of the zeolite surface [14,15], modification of the active metal composition [16-18], and addition of CO_2, CO or H_2 into CH_4 feed [19-24]. However, no satisfactory solution has been found yet. Obviously formulating a highly active Mo/HZSM-5 catalyst together with strong resistance to coke formation requires a full understanding of the coking pathway and factors that control the coke formation rate.

Three coking pathways, catalytic pyrolysis of methane, oligomerization and /or cracking of the intermediates (mainly C_2H_4), and polycondensation of formed aromatics, have been proposed in previous studies for coke formation in the title reaction. [20,25] However, to our best knowledge, no other study than one of ours tended to reveal the dominant pathway [26]. While no approach capable of providing direct evidence for distinguishing these proposed coking routes has been reported yet, quantifying the suppressive effect of H_2 on coke formation via each route might provide insight into the main coke formation-controlling factor. In fact, adding H_2 into CH_4 feed has been experimentally demonstrated to be very effective in suppressing the overall coke formation rate over Mo/HZSM-5 catalysts, and consequently stabilizing their activities. [21-24] Thus, the nascent hydrogen formed

in the inlet layer of an integral catalyst bed is expected to function to suppress coke formation in the rest of the bed [27-29], particularly in its outlet layer where the H_2 concentration in the gas phase always reaches its highest level. As a result, non-uniform coke distribution could form in any integral catalyst bed. In such a case, measurement of the coke contents accumulated in the different catalyst layers of the bed is then expected to provide direct evidence for evaluating the effect of nascent hydrogen on the coking behavior of the catalyst and individual coking routes (mainly C_2H_4 cracking and equilibrium-limited polycondensation of aromatics). Further pursuing the maximum suppressive effect of co-fed H_2 on coke formation via varying its concentration over a wide range is expected to lead to valuable data for confirming if the formation of all types of coke is uniformly suppressed by H_2 addition, that is, if there exists any coking route that is less or little influenced by H_2. Moreover, quantitative analysis of the correlations among the average coke formation rate, the outlet H_2 concentration and the concentrations of hydrocarbon products (possible coke sources) for the different catalyst layers of the bed is expected to give insight into the dominant factors that control coke formation. All these, when clarified, will surely provide new clues to a better understanding of the coke formation pathways in the title reaction.

In a previous paper we have demonstrated that non-uniform coke distribution does form along a three-layer fixed bed of Mo/HZSM-5 in 10%Ar/CH_4 at 1073 K[26]. In the same study, by pursuing both benzene and C_2H_4 selectivities over the catalyst lifetime and simultaneously quantifying the coke accumulated in the different layers of the bed over different reaction periods, we have also successfully revealed that the reaction intermediate C_2H_4 is the dominant source of coke formation at the last stage of catalyst deactivation, where benzene formation selectivity shows a rapid decrease from about 65% to 18%. Note that the formation of C_2H_4 in the title reaction occurs throughout all stages of catalyst deactivation. The coking reactions of C_2H_4 could also dominate coke formation at the stage where benzene selectivity is stable at 60-70%.

This work systematically investigated, for the first time, the distribution of coke,

formed in a three-layer Mo/HZSM-5 bed over its stable benzene-forming period at 1073 K and variable H_2 concentration, using TG and TPO techniques. The H_2 concentration was varied from 0 % to 30 % by volume to obtain the maximum suppressive effect on coke formation. The results show that while non-uniform coke formation still occurs, the distribution is narrowed at high H_2 concentrations, however it is less effective in suppressing coke formation on the outlet layer of the bed. Results also show that it is non equilibrium-limited C_2H_4 pyrolysis dominating coke formation in the period. Experimental support and detailed discussion on these findings are given below.

4.2. Experimental

4.2.1. Catalyst preparation and characterization

A microzeolite-based 6%Mo/HZSM-5 catalyst was prepared by a conventional wet impregnation method. The obtained catalyst powder was pressed, crushed, and sieved to 250-500 μm for use. The zeolite and catalyst were characterized using various techniques including XRD, BET, NH_3-TPD, FTIR and NMR and the detail procedures and results were given in previous papers.[30-32]

4.2.2. Activity evaluation test

All activity evaluation tests were carried out in an upstream fixed bed quartz reactor at atmospheric pressure and 1073 K for 40 min. 300 mg of catalyst was used in each test. As shown in Fig. 4-1, it was packed to form a bed of three layers, with 100 mg of catalyst in each layer. The catalyst sample was heated in a H_2 flow of 25 ml/min to 923 K. CH_4 was then introduced at a rate of 18 ml/min for 20 min to pre-carburize MoO_3 to active Mo_2C. Subsequently it was heated under H_2 to 1073 K, held there for 5 min and subjected to a gas mixture of H_2 and Ar/CH_4 to start the reaction. The feed rate of the Ar/CH_4 make-up gas was controlled using a mass flow controller and its rate was fixed at 25 ml/min for all tests. The feed rate of H_2 was controlled by another mass flow controller from 1.3 to 10.7 ml/min to realize a H_2 concentration of 0 to 30 % in feed. The reaction was performed over a period of either 40 or 5 min. The 5 min reaction tests were designed to monitor coke formation

at the initial fast deactivation stage. The 40 min reactions allowed for sampling at pre-designed intervals and on-line analysis using two GCs. The detail procedure was given in a previous paper[19]. At the end of the reaction the catalyst sample was cooled under the reaction atmosphere to room temperature for its recovery.

Prior to starting the reaction at the temperature 1073 K, the catalyst was heat-treated in H_2 two times, before and after the carburization at 923 K. The purpose of the first H_2 treatment below 923 K was to reduce the surface layer of MoO_3 in the catalyst sample to a lower valence state and prevent its migration and re-dispersion. On the other hand, the aim of the second H_2 treatment in the heating from 923 to 1073 K was to remove most of the coke formed during the carburization and assure that the starting catalyst sample in every experiment has an identical low coke content, i.e, an identical initial activity. In such way experimental errors were minimized and the standard deviation of the error between repeated activity evaluation tests in terms of CH_4 conversion (at 10 and 35 min) was confirmed to be within ±3%. [26]

Additionally, a fixed CH_4 space velocity of 4500 mL/g/h with variable H_2 concentration was realized in the present tests by adding a variable amount of H_2 (1.3 to 10.7 ml/min) in the 10%Ar/CH_4 feed stream of 25 ml/min. In this way while the feed with variable CH_4 concentration is likely to well simulate the reacted gas through a real catalyst bed and the resultant conclusions could be of more practical interest, the dilution effect of H_2 addition needs to be considered. For this a preliminary test was conducted in 30%He/Ar/CH_4 to make confirmation and the result is given in the Results and Discussion section.

Moreover, note that 10%Ar in feed was used as an internal standard for estimation of CH_4 conversion, not for adjustment of CH_4 concentration. For convenience the mixture 10%Ar/CH_4 is referred to as Ar/CH_4 whereas any H_2-added feed mixture as x%H_2/Ar/CH_4 (x = 0, 5, 10, 15, 20, 25 or 30).

4.2.3. Coke characterization

The coke content in all spent catalyst samples was quantified using a TG/DTA analyzer (EXSTAR TG/DTA 6200, Seiko Instruments Inc.). About 10 mg of a spent sample was used for each measurement. The sample was loaded into a TG cell, and purged with dry air for 30 min to ensure a stable base. Then it was heated in an air stream to 393 K and held there for 30 min to measure the weight loss from vaporization of adsorbed water. Subsequently it was heated in the same air stream further to 873 K at a rate of 10 K/min and kept there for 30 min to obtain the TG profile of the sample. The weight loss in the region of 673-873 K was used to estimate the coke content.

The burning behaviour of coke in all spent samples was pursued using TPO technique. An auto-controlled TPD apparatus (TPD-1-ATSP1, Bel. Japan) was employed for the purpose and 30 mg of a spent catalyst sample was used for each measurement. The sample was heated from room temperature to 1103 K at a rate of 10 K/min in a gas mixture of 10 % O_2/He (50 mL/min). The mass spectra of the gases evolved during the TPO were monitored by a Q-MASS spectrometer (ULVAC RG-201). The signals at m/e = 28, 44 and 18 were used for the detection of CO, CO_2 and H_2O, respectively.

4.3. Results and discussion

4.3.1. Suppressing effect of co-fed H2 on catalyst performance and coke formation

Fig. 4-2 shows the performance of the catalyst tested in x% H_2-added CH_4 feeds (x = 0, 5, 10, 15, 20, 25 or 30). In terms of CH_4 conversion as well as outlet H_2 concentration, the catalyst in Ar/CH_4 shows a two-stage activity-decreasing feature: the rapid decrease over the first 5 min followed by a slow decrease in the period thereafter. Not surprisingly, this deactivation pattern duplicated our previous work with similar Mo/HZSM-5 catalysts [19,26], and confirmed that a 5 min activation at 1073 K is needed for our pre-carburized catalyst to attain its maximum benzene formation activity. In this activation period pyrolysis of CH_4 on the H_2-reduced Mo surface and carburization of the residual MoO_3 to form active Mo_2C are believed to dominate the coking process. Since these two reactions are irreversible, their kinetics

are little influenced by H_2 at low partial pressures (<30 %) and therefore rapid coke formation and deactivation could occur at all H_2 feed rates. Consequently, as shown below, the content of coke formed in this period accounts for proximately 40-45 % of the total amount of coke over the whole 40 min reaction period. Probably for the proceeding of these irreversible coking reactions the CH_4 conversions higher than equilibrium were observed at the first two sampling points (1 and 5 min) in all cases.

In the second stage of deactivation over the last 35 min the catalyst exhibits a slower deactivation rate in Ar/CH_4. Both benzene and naphthalene formation rates keep decreasing whereas that of C_2H_4 keeps increasing, strongly suggesting that conversion of the intermediate C_2H_4 to the aromatics is increasingly inhibited due to accumulative coke deposition in this period. [2,11,33] Note that the zeolite channels are certainly involved in the formation of aromatics in the title reaction. [34-37] This slow deactivation must result from coke accumulation at the channel mouths and/or inside the channels. [38-42]

Comparison of all the time-dependent curves in Fig. 4-2 suggests that the addition of H_2 is particularly effective in improving the catalyst stability over the slow deactivation period (the last 35 min). Due to equilibrium limitations all CH_4 conversions and the formation rates of C_2H_4, benzene and naphthalene in this period show stepwise decreases with stepwise increasing H_2 concentration. Nevertheless, as shown in Table 4-1, the benzene selectivities reached at 35 min fell in a very narrow range of 69.8-72.3%. For naphthalene its selectivities fell also in a small range of 7.4-10.6%. As a result, coke selectivity estimated from carbon balance varied in a range of 7.5 to 12.0%. At the high H_2 concentrations of 25 and 30%, while coke selectivity showed a slight decrease (from 9.8 to 7.5%) with the increasing of H_2 concentration, benzene selectivity still remained the same at 71.3-72.0% and naphthalene at a slightly lower range of 7.5-8.5%. All these strongly suggest that co-feeding H_2, while surely inhibiting coke accumulation in the slow deactivation period, causes little essential change in the selectivity of the catalyst to aromatics. The selectivity to C_2H_4, on the other hand, increased stepwise from 5.0 to 12.2% with stepwise increasing H_2 concentration from 5 to 30 %. It is well recognized the

title reaction proceeds via a two-step mechanism: activation of CH_4 to C_2 species (mainly C_2H_4) over Mo sites and cyclization of these C_2 intermediates to aromatics inside the zeolite channels. [2,43-46] Namely, the net C_2H_4 formation rate is governed by the two steps' rate ratio.

According to Iglesia and co-workers [47,48] and Bhan and collaborators[24,29], both steps are reversible and inhibited by increased H_2 partial pressures. However, as one can derived from the equations, $2\ CH_4 \leftrightarrow C_2H_4 + 2\ H_2$ and $C_2H_4 \leftrightarrow 1/3\ C_6H_6 + 1/2\ H_2$, the dependences of the two steps to H_2 partial pressures are respectively represented by the terms of $1/p^2$ and $p^{0.5}$, and are not identical. That is, varying H_2 partial pressure might lead to an increase or a decrease in C_2H_4 selectivity. Thus, equilibrium calculation was made for a mixture of $H_2/CH_4/C_2H_4/C_6H_6$/He to make confirmation. The result showed that C_2H_4 selectivity increases with increasing H_2 partial pressure, providing theoretical support for the stepwise increases of C_2H_4 selectivity at increased H_2 concentrations in Fig. 4-2. Additionally, reduced C_2H_4 formation rates at increased H_2 concentrations lower the probability of a required number of C_2H_4 molecules simultaneously sticking into a same benzene synthesis site inside the zeolite channels, and consequently could contribute to lowering benzene formation rate and increasing C_2H_4 selectivity.

Addition of 5% H_2 is sufficient to remain the stable benzene formation in the last 35 min (Fig. 4-2), but its suppressive effect on coke formation is very limited. This can be understood from the relatively high coke contents of the corresponding spent samples. As determined by TG measurement and shown in Fig. 4-3, the coke content from the different catalyst layers keeps decreasing with increasing H_2 concentration up to 30%. While this confirms that raising H_2 concentration does increase its effect on suppression of total coke accumulation over all three catalyst layers, the most obvious effect is observed in suppressing the coke formation in the inlet layer. Then, the minimum inlet H_2 concentration required for a complete suppression of coke formation in the inlet layer can be extrapolated to be about 39%. Since this extrapolated prediction is based on the total amounts of coke accumulated over the whole reaction period (40 min), a correction is needed to find the true minimum inlet

H_2 concentration required to stop coke formation during the stable benzene formation period (the last 35 min). Actually, this was made by subtracting the amount of coke formed in all inlet layers during the first 5 min at all feed compositions (Fig. 4-4) from the corresponding coke contents in Fig. 4-3; and it led to a slight decrease in the slope of the fitting line in Fig. 4-3. Consequently a slightly larger x-intercept (about 40 %) was obtained. In the same way the minimum inlet H_2 concentrations needed for stopping coke formation over the middle and outlet layers of the bed were estimated to be about 44 % and 46 %, respectively. Obviously the minimum inlet H_2 concentrations needed for stopping the coke formation over the three different layers of the bed are increasing from inlet to outlet. This phenomenon might be understood because the variation of the gas phase composition (mainly H_2 concentration) throughout the bed causes a gradual change in the dominant coking route along the bed. For example, in case both oligomerization and cracking of the intermediate C_2H_4 proceed simultaneously to form coke over the whole bed, the rate of the former reaction over its outlet layer is expected to be suppressed by an increased H_2 partial pressure due to equilibrium limitations whereas that of the latter reaction would not. As a result the contribution of C_2H_4 cracking to coke formation in the outlet layer is expected to increase.

Thus, to consolidate the basis for extending and deepening the above discussion, two additional tests were performed to confirm that non-uniform coke formation does occur in any integral catalyst bed and increasing the H_2 concentration in feed does narrow the distribution. The first test was carried out over a catalyst bed of an increased height (five layers packed with 500 mg of catalyst) in Ar/CH_4 for 40 min, and Fig. 4-5 shows the coke contents of the resultant spent samples. Again a similar wide coke distribution was obtained with the highest coke content at the inlet catalyst layer and the lowest in the outlet layer. The second test was carried out over a three-layer bed in30%$He/Ar/CH_4$. As compared in Fig. 4-3, the 40 min reaction led again to a non-uniform coke formation with 3.8 wt% coke in the inlet layer, 3.1 wt % in the middle, and 2.6 wt% in the outlet. It is almost identical to the distribution formed in Ar/CH_4 but entirely different from that in 30%$H_2/Ar/CH_4$. This fact thus strongly confirms that it is not the dilution effect of H_2 but its coke-suppressing

effect causing the leveling off of coke distribution at higher H_2 concentrations in Fig. 4-3. Namely, occurrence of non-uniform coke formation is an inherent characteristics of any integral Mo/HZSM-5 bed and is only influenced by H_2 partial pressure in feed.

Now there should be little doubt about the formation of non-uniform coke distribution and the distribution-narrowing effect of H_2 addition. Careful comparison of the coke distributions in Figs. 4-3 and 4-4 at all given feed compositions then indicates that the distribution formed in the initial 5 min is further widened over the last 35 min in the feed streams containing lower than 20 % of H_2. This implies that the non-uniform coke formation continues over the stable benzene formation period in these cases and therefore quantifying and correlating the effects of H_2 concentration on both aromatics and coke formation over the different catalyst layers in the period might lead to valuable information for identifying the dominant coking pathway. Data analysis showing that not aromatic products but C_2H_4 be the dominant coke source and detailed discussion will be given in the Section 3.3.

In addition to reducing the total amount of coke and narrowing the coke distribution, co-feeding H_2 might also affect the formation behaviors of different types of coke in each catalyst layer. Therefore, TPO measurements were performed for all spent samples and Fig. 4-6 compares the resultant TPO profiles. All TPO profiles were deconvoluted into four peaks, among which two eye-distinguishable ones repeatedly centered at temperatures 770-790 K and 830-850 K, respectively. Similar TPO patterns were also reported in previous papers.[49-52] According to these papers these two peaks at 770-790 K and 830-850 K, which are denoted as lower- and higher-temperature peaks in this work, are attributed to the burning of graphite-like C on the external surface of zeolite crystals and aromatic-type of coke inside the zeolite channels, respectively. For the peak at 890-910 K and the CO_x evolution in the low temperature region of ~700 K, their origins could be ascribed to the coke on free Bronsted acid sites deep inside the zeolite channels and the most reactive surface carbon deposits, respectively. [26] The amounts of these two types of coke became negligibly small at high H_2 concentrations, denying their dominant

formation at the test conditions. Therefore, the focus here is laid on the former two types of coke.

Confirmation of the formation of graphite-like C on the zeolite surface was conducted by XPS and Raman analyses of typical spent samples. The C 1s XPS spectra exemplified in Fig. 4-7 and Raman spectra in Fig. 4-8 do provide evidence for its formation. On the other hand, identification of the aromatic-type was adjudged from the evolution of water steam during the TPO. Fig. 4-9 presents a typical evolution pattern of steam water together with those of CO_2 and CO. While the intensity of the higher-temperature CO_x peak is obviously weaker than that of the lower-temperature one, the intensity of the corresponding H_2O-peak is even stronger in the higher- than lower-temperature region, confirming that the type of coke burning in the higher-temperature region must be richer in H and of aromatic-type. [21,53-56]

Comparison of the TPO patterns between the inlet layer samples, middle layer or outlet layer ones at all feed compositions suggests that adding H_2 into CH_4 is particularly effective in suppressing the formation of aromatic type of coke inside the zeolite channels in the inlet catalyst layer. An increased H_2 partial pressure functions to slowdown the diffusion rate of reaction-formed H_2 from the zeolite channels and makes the reaction environment inside the channels more favorable for coke removal than its deposition, thus leading to suppressed coke deposition there. Comparatively, the coke that burned and gave the lower temperature CO_x peaks during the TPO (Fig. 4-6) forms on the external surface of zeolite crystals, easily grows to graphite-like C [14,15,26], and therefore is more difficult to be methanated by H_2.

4.3.2. Mechanism of the suppressive effect of H_2

Adding H_2 into CH_4 feed could have the following two effects, both contributing to lowering the overall coke formation rate. First the backward rates of all reversible coke formation reactions, say, oligomerization of the intermediate C_2H_4 and polycondensation of formed aromatics, will be promoted. Very recently Bhan and

co-workers [24,29] have shown "that dehydroaromatization of CH_4 is governed by thermadynamic reversibility so that an increase in H_2 partial pressure causes a decrease in the net benzene formation rate but does not affect the forward synthesis rate". Second, the rate of the coke-removing reaction $2H_2 + C = CH_4$ will be increased. Occurrence of this reaction in pure H_2 has been well demonstrated in periodic CH_4-H_2 switching operation mode. [7,30] This reaction is likely at any coking sites as long as the local environment allows, for example, there are sufficient H atoms available. If this is true, lower coke content in the outlet catalyst layer rather than in the inlet layer might be considered a consequence of the methanation there being enhanced due to an increased H_2 partial pressure.

Thus, a feed-switching test was specially designed to prove coke can really be removed via methanation. Another three-layer catalyst bed at 1073 K was first fed with Ar/CH_4 for 40 min and then $25\%H_2/Ar/CH_4$ for another 40 min for a total of 80 min. Fig. 4-10 presents the time dependence of catalytic performance of the whole catalyst bed. The performances over the first 40 min and last 40 min essentially duplicated the results of the two 40 min tests conducted separately in the streams of Ar/CH_4 and $25\%H_2/Ar/CH_4$ (Fig. 4-2). However, the amount of coke accumulated in each layer of the bed over the whole 80 min reaction period did not match the simple sum of the coke from the spent samples of the two separate tests. In fact the amount of coke became much smaller (about 3.80 wt% in the inlet layer, 2.87% in the middle and 2.77% in the outlet), even slightly smaller than the amount of coke accumulated in the Ar/CH_4-fed, 40 min reaction alone. If we presume that the amount of coke accumulated in the first 40 min of this feed-switching test is identical to that formed in the separate Ar/CH_4-fed 40 min test just as the performance does, then the small coke content observed for the sample from the feed-switching test suggests that a considerable part of the coke formed in the first half of the test was removed via methanation in the last half. Therefore, increasing H_2 partial pressure does promote the removal of coke that had formed in a lower H_2 concentration. Further presume that the forward coking reactions continue in the last half of the test producing about 1.5 % additional coke, which is equal to the coke formed in the separate 40 min test in $25\%H_2/Ar/CH_4$ (Fig. 4-2), then the actual

beneficial effect caused by the feed-switching in the present case would be more significant than estimated from the measured coke contents. In case that similar enhanced methanation occurs in the outlet layer in the test cases, the coke content accumulated there is expected to be much lower than that in the inlet layer. In fact, however, the coke content from the outlet layer samples accounts for 69-100% of that in the inlet layers (Fig. 4-3). This, in combination with the TPO patterns of the samples subjected to higher H_2 concentrations in Fig. 4-6, seems to suggest that the coking reactions occurring in the outlet layer of the bed are less-suppressed by H_2 and tend to produce more graphite-like C. Detailed data analysis and further discussion are given below.

4.3.3. Dominant coke source

As shown in Fig. 4-11, there are three possible routes, by which coke forms during the stable benzene formation period in the title reaction. [20,25,26] While the rates of all three are theoretically suppressed by increasing the H_2 concentration, the rates of Routes ② and ③ might be closely related to the C_2H_4 and aromatics concentrations of the system, respectively. Thus, the correlations between the average formation rates of C_2H_4, aromatics and coke, in the stable aromatics formation period (the last 35 min of reaction), were assessed to attempt to identify the dominant coking pathway or coke source.

As shown in Fig. 4-12, the average C_2H_4 formation rate shows independent variation with regard to the average coke formation rate. However, two linear relationships appear between the average aromatics and coke formation rates, one where H_2 concentrations range from 0 to 15 % and again where H_2 concentrations range from 20 to 30 %. The simultaneous decreases in both average aromatics and coke formation rates with the increase of the H_2 concentration suggest two possibilities: (1) the proportional coke formation along with aromatics formation and (2) the proportional involvement of formed aromatics in coke formation. For the first case the competitive conversion of the intermediate C_2H_4 to coke (Route②) can be considered the main pathway; and thus a linear relationship between the C_2H_4

formation rate and the average coke formation rate is expected. However, when the intrinsic formation rate of C_2H_4 is high and its concentration in the gas phase remains always in equilibrium, its overall production rate will remain constant and be kept independent of the rate of its conversion to coke. For the second case, the reversible polycondensation of formed aromatics might dominate the coking process, and therefore the overall production rate of aromatics and the rate of their secondary conversion to coke are expected to decrease simultaneously with the increase in the H_2 partial pressure. However, the steeper slope, covering the high H_2 concentration region of 20-30 % suggests that coke formation would not stop even if aromatics formation is fully suppressed at a higher inlet H_2 partial pressure. Additionally, the least coke is always observed to accumulate in the outlet catalyst layers where the aromatics concentrations reach their maxima. These facts together deny the dominant role of Route ③ in coke formation at least in the cases where the H_2 concentration of feed falls in a high range of 20-30 %. Thus high outlet H_2 concentrations (>20%) shown in Fig. 4-2 might fully exclude formed aromatics being the dominant coke source, at least for the outlet layer at all feed compositions.

This conclusion was supported by the results of another two set tests over 100 and 200 mg of catalyst, respectively. The purpose of these tests was to quantify the aromatics productivity of each catalyst layer (the total amount of aromatics produced over the layer in the last 35 min) and its correlation with the corresponding average coke formation rate and consequently to provide further evidence to exclude the dominant role of Route ③ in coke formation at high H_2 concentration. Fig. 4-13 compares the resultant time-dependences of CH_4 conversion and C_2H_4 and aromatics formation rates, and Fig. 4-14 shows the coke contents of the corresponding spent samples. For comparison the date obtained from the earlier 300 mg three-layer bed was also plotted (dotted lines).

Integration of all benzene and naphthalene curves in Fig. 4-13 leads to the aromatics productivities listed in Table 4-2. If we assume that the 100 mg bed simulates the inlet layer and the 200 mg bed represents the first two layers (inlet and

middle layers) of the three-layer catalyst bed, then with the aromatics productivities of these two beds we can estimate the contribution of each catalyst layer of the three-layer bed to its overall aromatics productivity (the total amount of aromatics produced over 300 mg catalyst) in either Ar/CH_4 or $10\%H_2/Ar/CH_4$ stream. As listed in Table 4-2, while the contributions made by the inlet catalyst layers with Ar/CH_4 and $10\%H_2/Ar/CH_4$ reach 61 and 66 % respectively, those of the corresponding outlet layers are only about 8 and 7 %. This non-uniform nature may be considered inherent to any integral fixed catalyst bed, but here without doubt it is because the aromatics formation reaction approached the equilibrium along the bed height and little space was left for further formation of aromatics over the outlet catalyst layer in either feed stream. In $30\%He/Ar/CH_4$, as compared in the same table, 100 mg catalyst in one layer bed accounted for 48% of the aromatic productivity of a three-layer bed, further confirming the non-uniform nature of integral Mo/HZSM-5 beds and strengthening the present discussion.

Although an assumption was made for the above analysis, it is actually quite reasonable judged from the distribution of coke formed in the spent samples. As shown in Fig. 4-14, in the Ar/CH_4 feed the coke contents accumulated over the two layers of the 200 mg catalyst-packed bed duplicated those over the inlet and middle layers of the 300 mg catalyst-packed bed; and in $10\%H_2/Ar/CH_4$ the coke content formed over 100 mg catalyst bed correlated well to those over the inlet layers of the 200 mg and 300 mg catalyst-packed beds. Therefore the ratio of the coke content to aromatics productivity for each catalyst layer was estimated and adapted to quantify the variation in the coke formation activity per unit aromatics productivity along the bed height. As summarized in Table 4-3, in either Ar/CH_4 or $10\%H_2/Ar/CH_4$ the smallest ratio was obtained for the inlet catalyst layer, the largest for the outlet and a number in between for the middle. Namely, in either feed the highest coke formation rate per unit aromatics productivity occurs not over the inlet catalyst layer where up to 61-66 % of the total aromatics is formed (Fig. 4-13), but over the outlet layer that contributes the least to the overall aromatics productivity over 300 mg catalyst. This denies again occurrence of any linear relationship between the coke formation and aromatics productivity over the three-layer bed and excludes the dominant role of

polycondensation of formed aromatics in coke formation in the bed, particularly in its outlet catalyst layer. Furthermore, the present observation, in addition to the TG results in Fig. 4-3 as well as TPO results in Fig. 4-6, also suggests that the coke formation over the outlet catalyst layer is less influenced by the partial pressure of H_2, which strengthens the greater importance of non-equilibrium controlled coking processes, say, via Route ②, than equilibrium controlled ones in the title reaction.

Experimental confirmation that benzene is not cracking and/or polycondensing to coke at high H_2 concentration was also made in this work. This was done by performing another two additional tests over HZSM-5 itself at 1073 K in the streams of Benzene/N_2 and 20%H_2/Benzene/N_2, respectively. In the absence of H_2 the cracking and polycondesation of benzene did take place over HZSM-5 which led to serious coke formation (about 3 wt% of coke was formed over 200 mg of HZSM-5 in a 120 min reaction), but such coking process was fully inhibited when 20 % H_2 was added into the feed. This observation, in addition to all above observations, forced us to believe that coke formed in the outlet catalyst layers in most of the present cases and the whole catalyst bed in the streams of 20, 25 and 30 % H_2 came from sources other than benzene.

Thus, cracking of C_2H_4 (Route ②) has to be considered the dominant coking pathway to explain the presently observed non-uniform coke formation, while no experimental evidence has yet been found to support the occurrence of free radical chain reactions (Route ①) at the test conditions. Actually a piece of experimental evidence for this has been shown in Fig 4-13. At all sampling time points the C_2H_4 formation rates did not increase, but showed stepwise decreases as the bed height was increased from one layer to two and further to three layers. This stepwise decrease is opposite to both the stepwise increases in aromatics formation rate and bed height. Here again we reasonably assume that the C_2H_4 formation rates realized over one- and two-layer beds in either Ar/CH_4 or 10%H_2/Ar/CH_4 stream (Fig. 4-13) can well simulate the C_2H_4 rates formed over the inlet layer and the first two layers (inlet and middle layers) of the three-layer catalyst bed at the same feed composition.

Then, the stepwise decrease in C_2H_4 rate observed with the increase of the bed height in either stream strongly suggests the occurrence of the secondary conversion of C_2H_4 in the upper two layers of the bed. Note that the outlet catalyst layer in both Ar/CH_4 and $10\%H_2/Ar/CH_4$ streams makes little contribution (about 7-8 %) and that middle layer provides a less than 31 % contribution to the overall aromatics productivity of 300 mg catalyst. Most of the C_2H_4 consumed in these two layers is believed to convert to coke, not to aromatics. Thus the difference of the areas under the C_2H_4 rate curves indicated by □ and ○ in Fig. 4-13 and that between the curves by ○ and ▽ were estimated by numerical integration to obtain the maximum amount of coke that could form via the secondary cracking of C_2H_4 in the middle and outlet layers of the bed. The obtained results showed that approximately 0.96 and 0.60 mg of coke could form over the last 35 min in the middle layer and outlet layer in Ar/CH_4, and 0.72 and 0.36 mg in $10\%H_2/Ar/CH_4$, respectively. Then comparison of these numbers with the corresponding total coke contents in Figs. 4-3 and 4-4 revealed that the maximum amounts of coke formed via such secondary cracking of C_2H_4 in the middle and outlet layers are proximately 50 and 37 % of the total coke in Ar/CH_4, and 51 and 30 % in $10\%H_2/Ar/CH_4$, respectively. This thus suggests that cracking of the C_2H_4 from a lower catalyst layer can contribute only in part to the total coke formation in the neighboring upper layer.

Thus, a question arises of how the unaccounted for coke found in the two upper catalyst layers forms in the feeds of the different H_2 concentrations. One plausible answer to the question is that, in parallel to the secondary cracking of C_2H_4, the cracking of the "nascent C_2H_4" on its way out of the channels of any individual zeolite crystal and further out of the mesopores into the gas phase also takes place in any individual catalyst particle in the reaction. [26] Here the "nascent C_2H_4" refers to all those C_2H_4 molecules that once formed and existed inside the zeolite channels and is imaginarily distinguished from the C_2H_4 from other catalyst particles in a lower layer or the gas phase. As suggested in previous papers [2,45-48], the title catalytic reaction proceeds via the two-step mechanism: CH_4 activation over Mo sites to the intermediates C_2 species followed by their cyclization to aromatics inside

the zeolite channels. In the event that the second reaction step is rate-controlling [11,57], not the first, the C_2H_4 concentration of the system should always reach and remain constant at equilibrium, and consequently there should be sufficient "nascent C_2H_4" available inside any zeolite channel to maintain constant cracking there to coke. Therefore, an estimate of C_2H_4 availability, namely the reaction approach to equilibrium, η, was conducted for the reaction $CH_4 \rightarrow 1/2C_2H_4 + H_2$ for all input cases to make confirmation.

Concretely it was calculated from Eq. (4-2), derived from Eq. (4-1), using the measured outlet pressures (concentrations) and the equilibrium constant determined from thermodynamic values at 1073 K (Keq = 0.0193). Fig. 4-15a shows the results obtained for all three-layer beds and Fig. 4-15b exhibits those for one- and two-layer beds. In all but one case, η remains essentially constant over the last 35 min of reaction time and falls in a range of 0.98-1.09. This confirms that C_2H_4 did reach its equilibrium values in the middle layer of three-layer bed (300 mg) to make a constant "nascent C_2H_4" cracking rate possible (Fig. 4-12). Similarly estimations were also made for aromatics products (the reactions $1/2C_2H_4 \rightarrow 1/6C_6H_6 + H_2$ and $1/2C_2H_4 \rightarrow 1/10C_{10}H_8 + 3/5H_2$) and led to a η of 0.65-0.80 for benzene and a η of 0.50-0.70 for naphthalene, which confirms that aromatization of the intermediates C_2 species could indeed be a slower step than its formation via activation of CH_4 over Mo_2C sites. [11]

$$CH_4 \overset{K_{eq}}{\longleftrightarrow} \frac{1}{2} C_2H_4 + H_2 \qquad \text{Eq. (4-1)}$$

$$\eta = \frac{P_{C_2H_4}^{\frac{1}{2}} * P_{H_2}}{P_{CH_4} * K_{eq}} \qquad \text{Eq. (4-2)}$$

The only case where the C_2H_4 approach to equilibrium, η, shows a monotonous decrease with respect to time on stream occurred in the one layer catalyst bed in Ar/CH_4 (● in Fig. 4-15b). In this case coke formation occurred at a higher rate, as evidenced by the rapid drop in benzene formation in Fig. 4-13 (indicated by □) and

also by the largest coke content measured in Fig. 4-14. For this its higher outlet C_2H_4 and low H_2 concentrations (Fig. 4-13) must be responsible. If this is true, then coke formation at the inlet catalyst layers in the present cases can also be explained by C_2H_4 cracking. In fact, the formation rate of coke over Mo/HZSM-5 has experimentally proved to increase with the increase of the outlet C_2H_4 concentration in its last deactivation stage, during which the benzene formation rate and selectivity decrease very rapidly to very low levels. [26]

Finally, another two tests fed with C_2H_4-containing gas mixtures were conducted in a three-layer bed at 1073 K for 40 min to confirm that the presence of C_2H_4 does accelerate coke formation. Fig. 4-16 shows the resultant coke distributions. The 40 min reaction in 2%C_2H_4/N_2 led to a coke accumulation of 7.2 wt% in the inlet layer, much higher than the coke content of 4.1 % accumulated in 10%Ar/CH_4 (Fig. 4-3). This confirms that the pyrolysis of C_2H_4 does proceed over the test catalyst at a higher rate than that of CH_4. However, in the co-presence of 15%H_2 and 75%CH_4 (in the mixture of H_2 and 2%C_2H_4/10%Ar/CH_4) the dehydroaromatization of C_2H_4 might take priority over its pyrolysis, and therefore the lower coke contents (2.0-2.5 wt%, Fig. 4-16) were formed in the three different layers of the bed. Nevertheless, when compared to the case fed with 15%H_2/Ar/CH_4, the coke contents in the three layers were still increased by 18 % for the inlet, 19 % for the middle and 28% for the outlet, respectively.

In addition to C_2H_4 pyrolysis, free radical chain reactions (Route ① in Fig. 4-11) could also make a contribution to the total coke formation. However it is obvious that designing experiments able to prove the formation and existence of CH_x radicals at reaction conditions remains a big challenge.

4.4. Conclusions

1) The distribution of coke formed in the three-layer Mo/HZSM-5 bed in the non-oxidative methane dehydroaromatization is non-uniform and the coke content in its three layers decreases from its inlet to outlet layer. For this the H_2 concentration

gradient along the bed has proved to be responsible.

2) While narrowing the coke distribution, increasing the H_2 concentration in feed is more effective in suppressing the formation of aromatic type of coke inside the zeolite channels than in reducing the accumulation of graphite-like C on the external surfaces of individual zeolite crystals. An increased H_2 concentration has proved to promote the removal of coke that had formed in a stream of a lower H_2 content, which implies occurrence of the instantaneous removal of "nascent" coke via methanation in any upper layer of the bed, particularly in its outlet layer.

3). All experiment data obtained denies the dominant role of polycondensation and/or cracking of the formed aromatics in coke formation in the title reaction. While the concentrations of aromatic products always reach their maxima at the outlet of the three-layer catalyst bed, the amount of coke formed over the outlet catalyst layer is always the least. This excludes the possibility of the formed aromatics being the main coke sources there. Further, quantitatively correlating the average aromatics and coke formation rates over the stable reaction period (the last 35 min) with H_2 concentration in feed led to an analytical conclusion that also denies the significance of the formed aromatics as coke sources. Moreover, the results obtained over one- and two-layer catalyst beds revealed that the contributions of the different layers of the three-layer bed to its total aromatics production are not identical, the inlet layer contributing the most (~66 %) while the outlet the least (less than 8 %). Thus the average coke formation rate per unit aromatics productivity was estimated for the three layers of the bed and it follows an order of the outlet layer >> the middle >> the inlet. This denies again the dominant role of the secondary reactions of the formed aromatics in coke formation.

4) Increasing the bed height from one layer to two and further to three layers resulted in an obviously stepwise decrease in the outlet C_2H_4 concentration. This indicates the occurrence of the secondary conversion of C_2H_4 in any upper layer of a multi-layer catalyst bed. Comparison of the C_2H_4 concentration decrements throughout the upper two layers with their contributions to the total aromatics

formation further revealed that most of the C_2H_4 molecules consumed in these two layers were converted to coke, not aromatics. Additionally, equilibrium calculation indicated that the outlet C_2H_4 concentration reached its equilibrium levels in all but one case, whereas those of the aromatic products did not. This implies that there was always sufficient C_2H_4 inside any catalyst particles to ensure its constant cracking there. Hence the intermediate C_2H_4 is considered the main coke source at the test condition.

References

[1] L.S. Wang, L.X. Tao, M.S. Xie, G.F. Xu, Catal. Lett. 21 (1993) 35.

[2] F. Solymosi, J. Cserényi, A. Szöke, T. Bánsági, A. Oszkó, J. Catal. 165 (1997) 150.

[3] J.J. Spivey, G. Hutchings, Chem. Soc. Rev. 43 (2014) 792.

[4] P. Tang, Q.J. Zhu, Z.X. Wu, D. Ma, Energy Environ. Sci. 7 (2014) 2580.

[5] B. Cook, D. Mousko, W. Hoelderich, R. Zennaro, Appl. Catal., A: Gen. 365 (2009) 34.

[6] M.C. Iliuta, F. Larachi, B.P.A. Grandjean, I. Iliuta, Ind. Eng. Chem. Res. 41 (2002) 2371.

[7] K. Honda, T. Yoshida, Z-G Zhang, Catal. Commun. 4 (2003) 21-26.

[8] M.P. Gimeno, J. Soler, J. Herguido, M. Menéndez, Ind. Eng. Chem. Res. 49 (2010) 996.

[9] Y.Q. Wu, L. Emdadi, S.C. Oh, M. Sakbodin, D.X. Liu, J. Catal. 323 (2015) 100.

[10] J. Hu, S.J. Wu, H. Liu, H. Ding, ZF. Li, J.Q. Guan, Q.B. Kan, RSC Adv. 4 (2014) 26577.

[11] S.T. Liu, L.S. Wang, R. Ohnishi, M. Ichikawa, J. Catal. 181 (1999) 175.

[12] J.P. Tessonnier, B. Louis, S. Rigolet, M.J. Ledoux, C.P. Huu, Appl. Catal., A: Gen. 336 (2008) 79.

[13] A. Sarioğlan, A.E. Senatalar, Ö.T. Savaşçi, Y.B. Taârit, J. Catal. 226 (2004) 210.

[14] W.P. Ding, G.D. Meitzner, E. Iglesia, J. Catal. 206 (2002) 14.

[15] C.H.L. Tempelman, V.O. Rodrigues, E.R.H. Eck, P.C.M. Magusin, E.J. Hensen, Micropor. Mesopor. Mat. 203 (2015) 259.

[16] V. Abdelsayed, D. Shekhawat, M.W. Smith, Fuel 139 (2015) 401.

[17] T.E. Tshabalala, N.J. Coville, M.S. Scurrell, Appl. Catal., A: Gen. 485 (2014) 238.

[18] S. Burns, J.S.J. Hargreaves, P.Pal, K.M. Parida, S. Parija, J. Mol. Catal., A-Chem. 245 (2006) 141.

[19] Y.B. Xu, J.D. Wang, Y. Suzuki, Z.-G. Zhang, Appl. Catal., A: Gen. 409-410 (2011)181.

[20] R. Ohnishi, S.T. Liu, Q. Dong, L.S. Wang, M. Ichikawa, J. Catal. 182 (1999) 92.

[21] H.T. Ma, R. Ohnishi, M. Ichikawa, Catal. Lett. 89 (2003) 143.

[22] H.T. Ma, R. Kojima, S. Kikuchi, M. Ichikawa, Catal. Lett. 104 (2005) 63.

[23] Z. Liu, M.A. Nutt, E. Iglesia, Catal. Lett. 81 (2002) 271.

[24] J. Bedard, D.Y. Hong, A. Bhan, J. Catal. 306 (2013) 58.

[25] E.V. Matus, I.Z. Ismagilov, O.B. Sukhova, V.I. Zaikovskii, L.T. Tsikoza, Z.R. Ismagilov, Ind. Eng. Chem. Res. 46 (2007) 4063.

[26] Y. Song, Y.B. Xu, Y. Suzuki, H. Nakagome, Z.-G. Zhang, Appl. Catal., A: Gen. 482 (2014) 387.

[27] P.L. Tan, K.W. Wong, C.T. Au, S.Y. Lai, Appl. Catal., A: Gen. 253 (2003) 305.

[28] T. Osawa, I. Nakano, O. Takayasu, Catal. Lett. 83 (2003) 57.

[29] J. Bedard, D.Y. Hong, A. Bhan, Phys.Chem. Chem. Phys. 15 (2013) 12173.

[30] Y.B. Xu, J.Y. Lu, J.D. Wang, Y. Suzuki, Z.-G. Zhang, Chem. Eng. J. 168 (2011) 390.

[31] Y.B. Cui, Y.B. Xu, J.Y. Lu, Y. Suzuki, Z.-G. Zhang, Appl. Catal., A: Gen. 393 (2011) 348.

[32] Y.B. Cui, Y.B. Xu, Y. Suzuki, Z.-G. Zhang, Catal. Sci. Technol. 1 (2011) 823.

[33] F. Solymosi, A. Szöke, J. Cserényi, Catal. Lett. 39 (1996) 157.

[34] D. Ma, Y.Y. Shu, M. Cheng, Y.D. Xu, X.H. Bao. J. Catal. 194 (2000) 105.

[35] P.L. Tan, Y.L. Leung, S.Y. Lai, C.T. Au, Appl. Catal., A: Gen. 228 (2002) 115.

[36] A. Sarioğlan, Ö.T. Savaşçi, A.E. Senatalar, V.T. Ha, G. Sapaly, Y.B. Taârit, Catal. Lett. 118 (2008) 123.

[37] J.Z. Zhang, M.A. Long, R.F. Howe, Catal. Today 44 (1998) 293.

[38] J. Bai, S.L. Liu, S.J. Xie, L.Y. Xu, L.W. Lin, Catal. Lett. 90 (2003) 123.

[39] P. Wu, Q.B. Kan, D.Y. Wang, H.J. Xing, M.J. Jia, T.H. Wu, Catal. Commun. 6

(2005) 449.

[40] A. Smiešková, P. Hudec, N. Kumar, T. Salmi, D.Y. Murzin, V. Jorík, Appl. Catal., A: Gen. 377 (2010) 83.

[41] S. Müller, Y. Liu, M. Vishnuvarthan, X.Y. Sun, A.C. Veen, G.L. Haller, M.S. Sanchez, J.A. Lercher, J. Catal. 325 (2015) 48.

[42] F.L. Bleken, K. Barbera, F. Bonino, U. Olsbye, K.P. Lillerud, S. Bordiga, P. Beato, T.V.W. Janssens, S. Svelle, J. Catal. 307 (2013) 62.

[43] D. Ma, Y.Y. Shu, X.H. Bao, Y.D. Xu, J. Catal. 189 (2000) 314.

[44] J. Shu, A. Adnot, B.P.A. Grandjean, Ind. Eng. Chem. Res. 38 (1999) 3860.

[45] B.M. Weckhuysen, D.J. Wang, M.P. Rosynek, J.H. Lunsford, J. Catal. 175 (1998) 338.

[46] W. Liu, Y.D. Xu, J. Catal. 185 (1999) 386.

[47] L. Li, R.W. Borry, E. Iglesia, Chem. Eng. Sci. 56 (2001) 1869.

[48] H.S. Lacheen, E. Iglesia, J. Catal. 230 (2005) 173.

[49] W.P. Ding, S.Z. Li, G.D. Meitzner, E. Iglesia, J. Phys. Chem. B 105 (2001) 506.

[50] H.T. Ma, R. Kojima, S. Kikuchi, M. Ichikawa, J. Nat. Gas Chem. 14 (2005) 129.

[51] H.M. Liu, X.H. Bao, YD. Xu, J. Catal. 239 (2006) 441.

[52] S.D. Yao, L.J. Gu, C.Y. Sun, J. Li, W.J. Shen, Ind. Eng. Chem. Res. 48 (2009) 713.

[53] F. Larachi, H. Oudghiri-Hassani, M.C. Iliuta, B.P.A. Grandjean, P.H. McBreen, Catal. Lett. 84 (2002) 183.

[54] B.M. Weckhuysen, M.P. Rosynek, J.H. Lunsford, Catal. Lett. 52 (1998) 31.

[55] H.M. Liu, T. Li, B.L. Tian, Y.D. Xu, Appl. Catal., A: Gen. 213 (2001) 103.

[56] D. Ma, D.Z. Wang, L.L. Su, Y.Y. Shu, Y.D. Xu, X.H. Bao, J. Catal. 208 (2002) 260.

[57] L.Y. Chen, L.W. Lin, Z.S. Xu, X.S. Li, T. Zhang, J. Catal. 157 (1995) 190.

Table 4-1. CH_4 conversion, product formation rate and selectivity for methane dehydroaromatization reaction in the feeds of different H_2 concentrations at 35 min sampling time.

H_2 (%)	CH_4 Conversion (%)	Rate (μmol-C/g/s)				Selectivity (% C)				
		C_2H_4	C_6H_6	C_7H_8	$C_{10}H_8$	C_2H_4	C_6H_6	C_7H_8	$C_{10}H_8$	Coke
0	17.6	0.55	6.28	0.26	0.94	5.6	69.8	2.8	10.6	11.2
5	16.8	0.48	6.11	0.22	0.86	5.0	71.4	2.5	10.1	11.0
10	14.5	0.43	5.36	0.18	0.75	5.3	72.3	2.3	9.7	10.4
15	12.2	0.42	4.42	0.13	0.56	6.3	70.9	2.1	8.7	12.0
20	9.2	0.40	3.56	0.09	0.44	7.4	71.7	2.1	8.5	10.3
25	7.4	0.37	2.74	0.09	0.31	8.9	72.0	1.9	7.4	9.8
30	4.8	0.32	1.72	0.04	0.19	12.2	71.3	1.5	7.5	7.5

Table 4-2. Aromatics productivities of the beds of 100, 200 and 300 mg catalyst over the last 35 min reaction period.

Feed composition	Catalyst in bed (mg)	Aromatics productivity (mmol-C)				C^a (%)
		C_6H_6	C_7H_8	$C_{10}H_8$	Total	
0%H_2/Ar/CH_4	100	2.64	0.09	0.42	3.15	61
	200	3.94	0.14	0.65	4.73	92
	300	4.20	0.16	0.80	5.16	100
10%H_2/Ar/CH_4	100	2.24	0.07	0.25	2.56	66
	200	3.07	0.10	0.44	3.61	93
	300	3.24	0.12	0.54	3.90	100
30%He/Ar/CH_4	100	2.40	0.09	0.41	2.90	48
	300	4.92	0.15	0.91	5.98	100

[a] Contribution to the productivity over 300 mg-catalyst.

Table 4-3. Coke content per unit aromatics productivity estimated for each catalyst layer over the last 35 min reaction period (wt%/mmol-C).

	Feed composition	
	0%H_2/Ar/CH_4	10%H_2/Ar/CH_4
Outlet layer	3.73	3.96
Middle layer	1.22	1.34

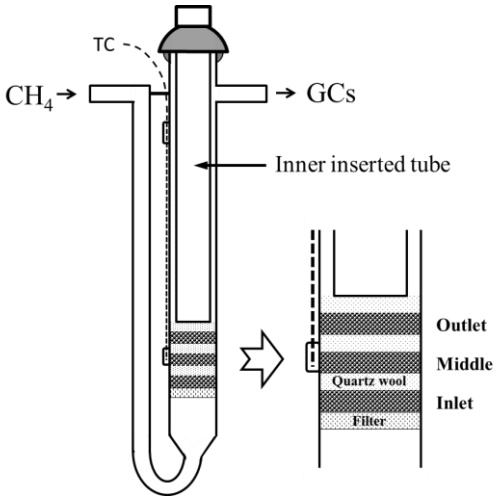

Fig. 4-1. Schematic diagram of the three-layer fixed bed reactor.

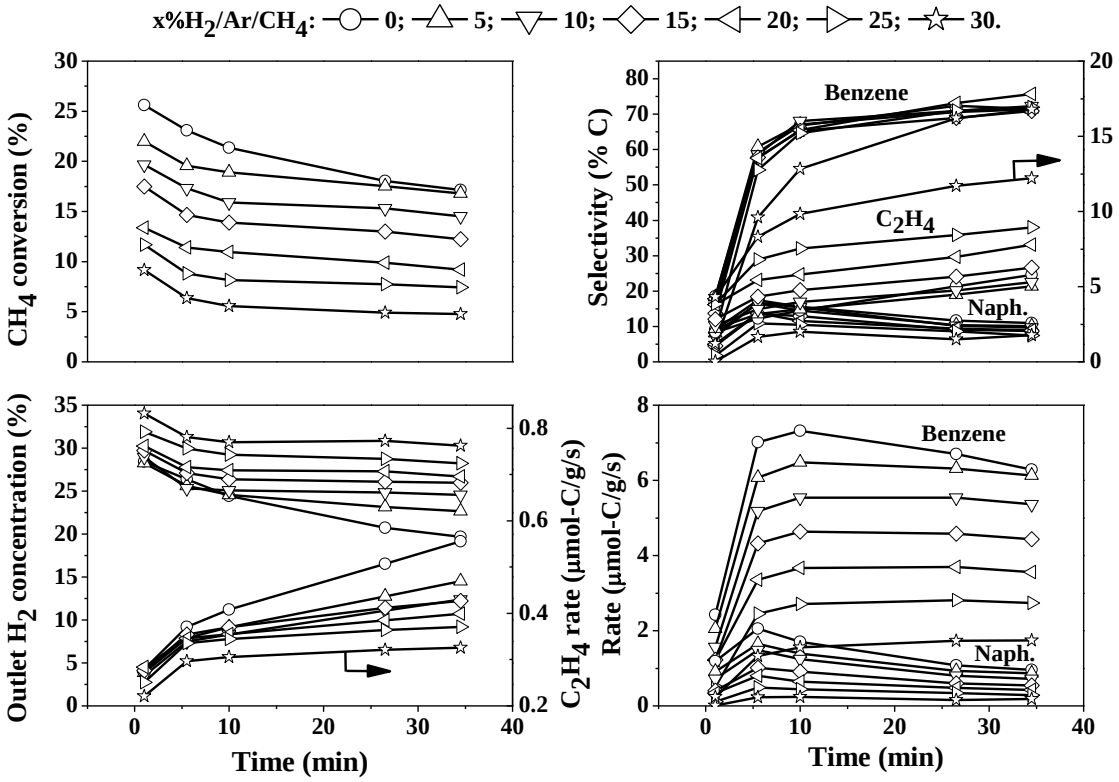

Fig. 4-2. Time-dependences of catalytic performance of 6%Mo/HZSM-5 observed over the tests of 40 min in the feeds of x % H_2 (x = 0, 5, 10, 15, 20, 25 or 30) at 1073 K and CH_4 space velocity 4,500 ml/g/h.

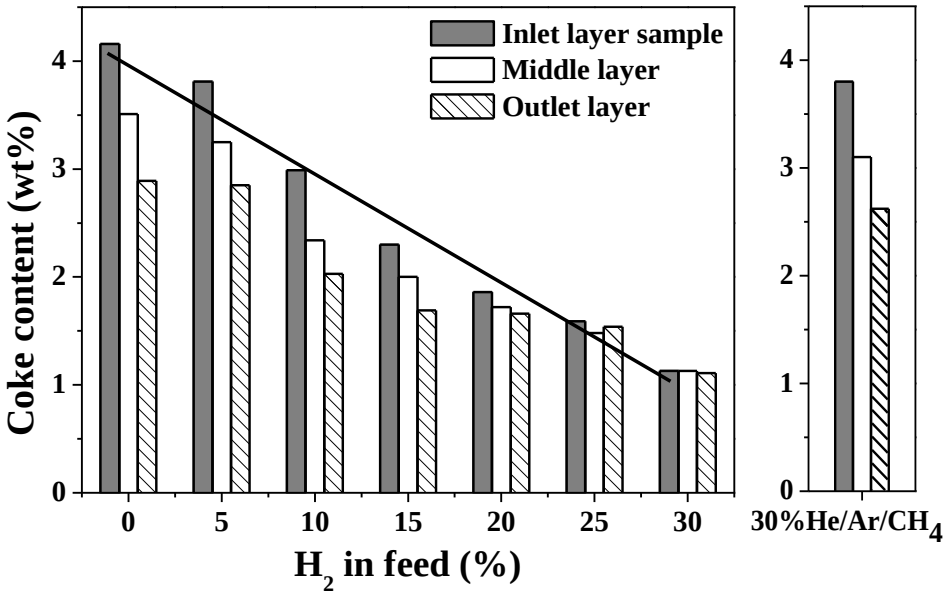

Fig. 4-3. Coke contents accumulated in the different catalyst layers over the tests of 40 min in the feeds of different H_2 concentrations.

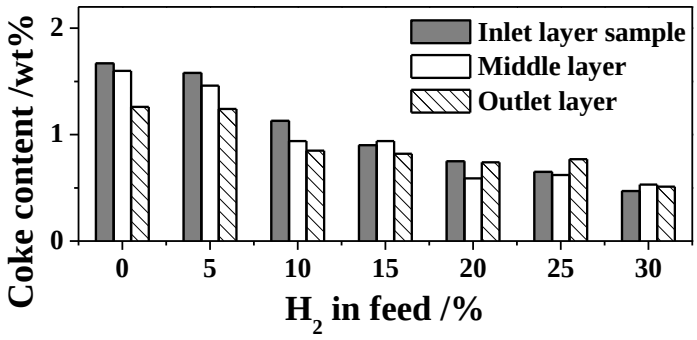

Fig. 4-4. Coke contents accumulated in the different catalyst layers over the tests of 5 min in the feeds of different H2 concentrations.

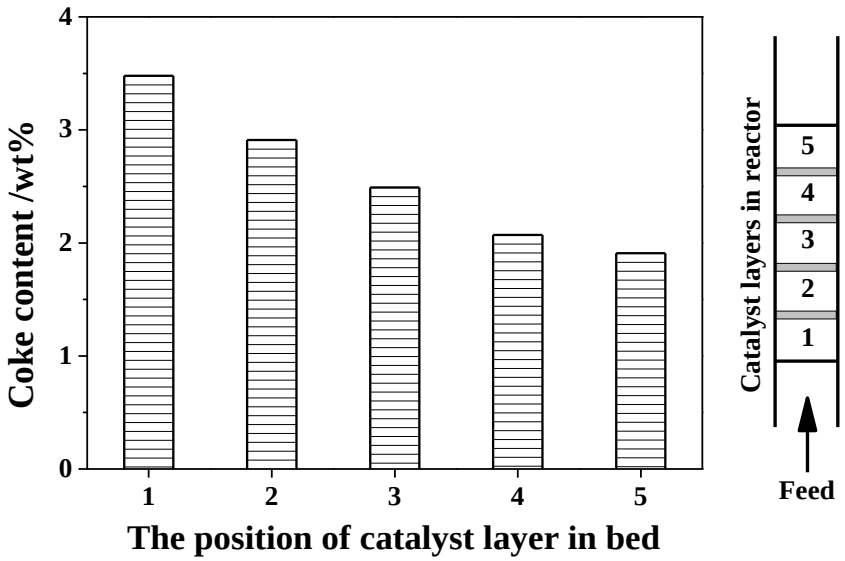

Fig. 4-5. Coke contents accumulated in the different layers of a five-layer bed over the test of 40 min in the feed of 10%Ar/CH_4 at 1073 K.

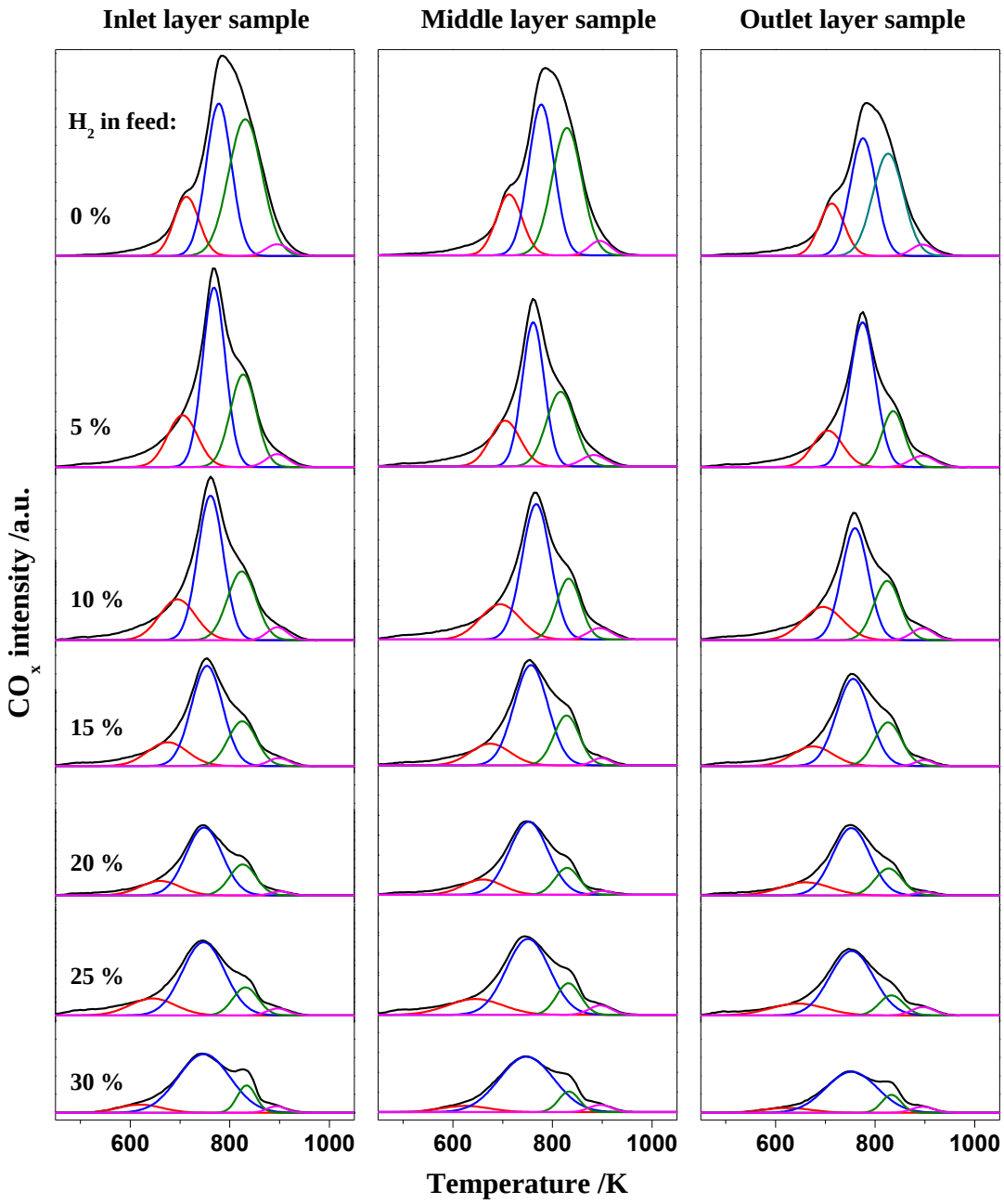

Fig. 4-6. TPO profiles of the spent samples recovered after the tests described in Fig. 4-2.

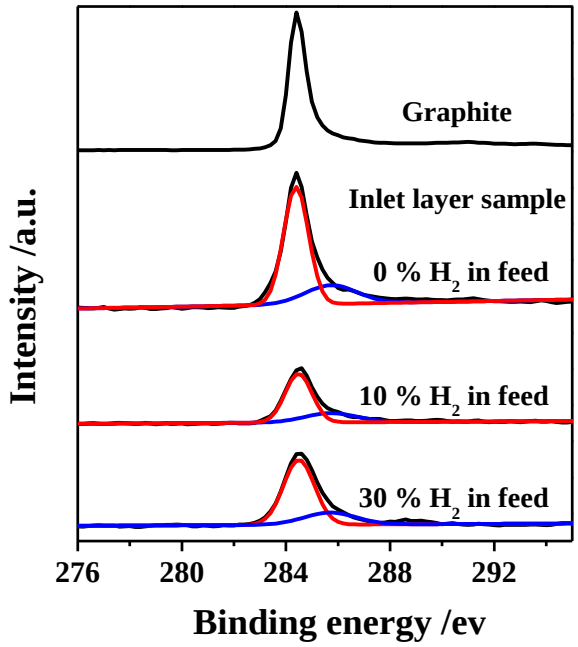

Fig. 4-7. XPS spectra in C 1s region of the spent samples recovered after the tests of 40 min in the feeds of different H_2 concentrations at 1073 K.

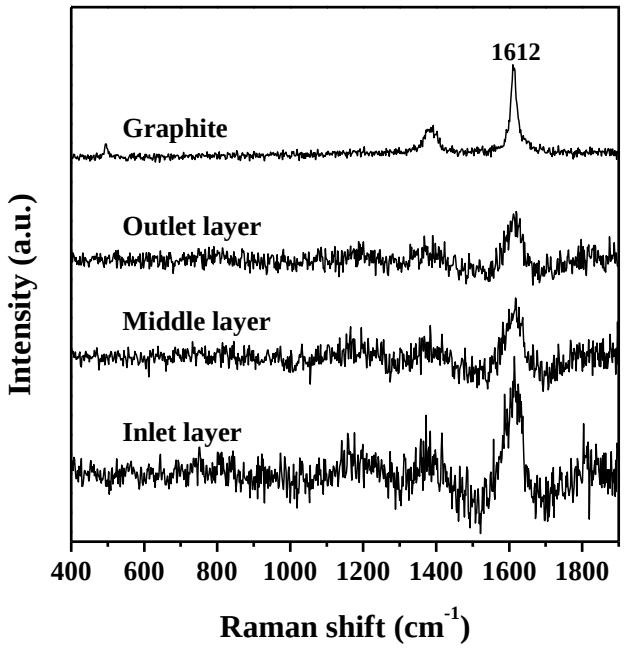

Fig. 4-8 UV-Raman spectra of the spent samples recovered after a 40 min test in

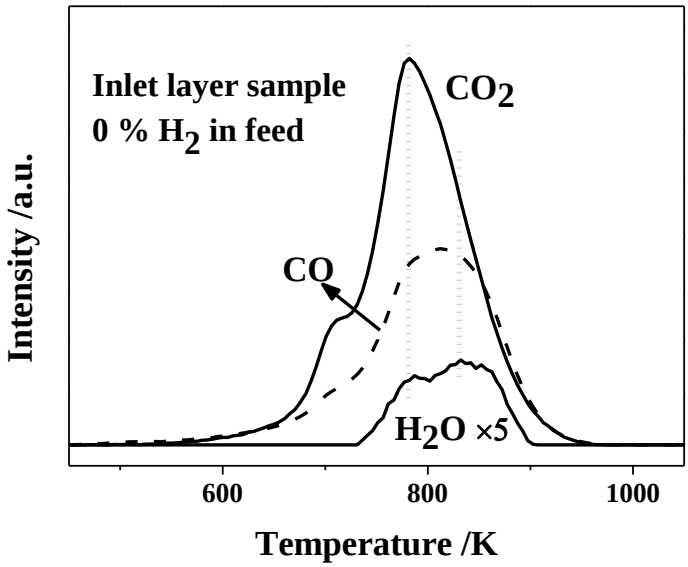

Fig. 4-9. CO_2, CO and H_2O profiles recorded in the TPO measurement of a spent sample recovered after the test of 40 min in the feed of 10%Ar/CH_4 at 1073 K.

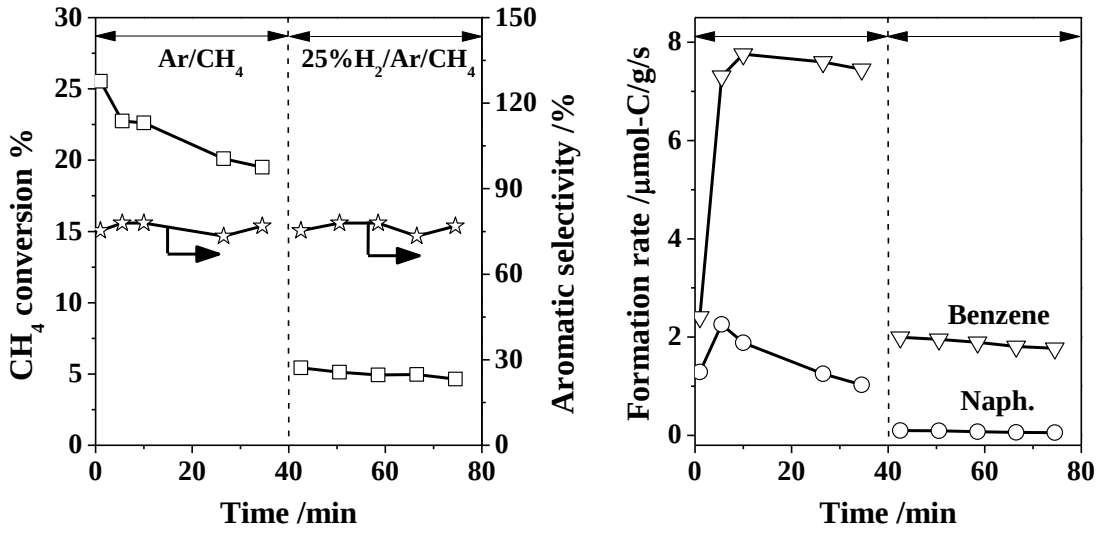

Fig. 4-10. Catalytic performance of the catalyst in a test of 80 min in a feed-switching mode.

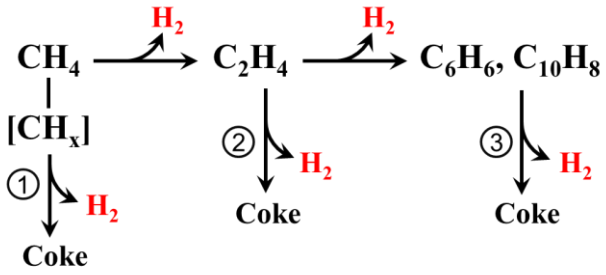

Fig. 4-11. Schematic diagram of proposed coking pathways

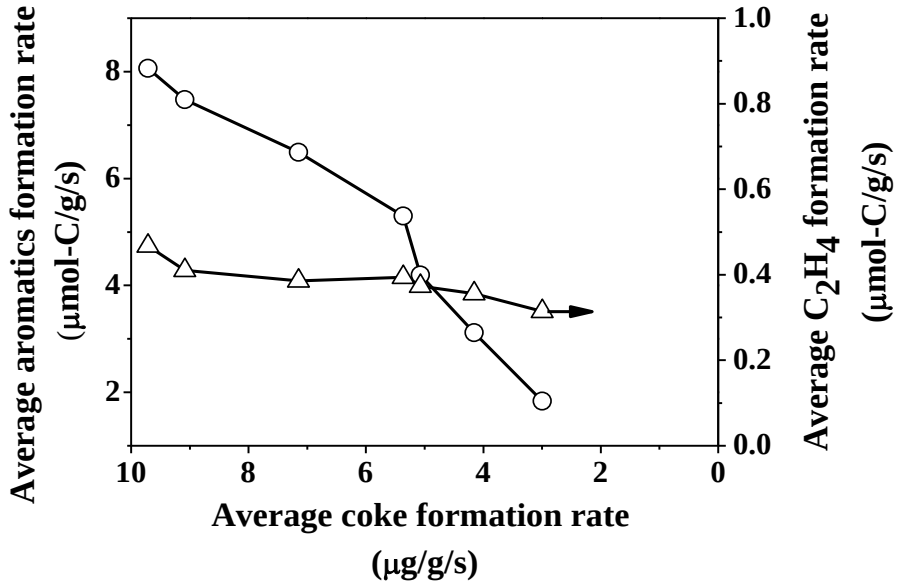

Fig. 4-12. Dependences of the average C_2H_4 and aromatics formation rates on the average coke formation rate in the stable aromatics formation period.

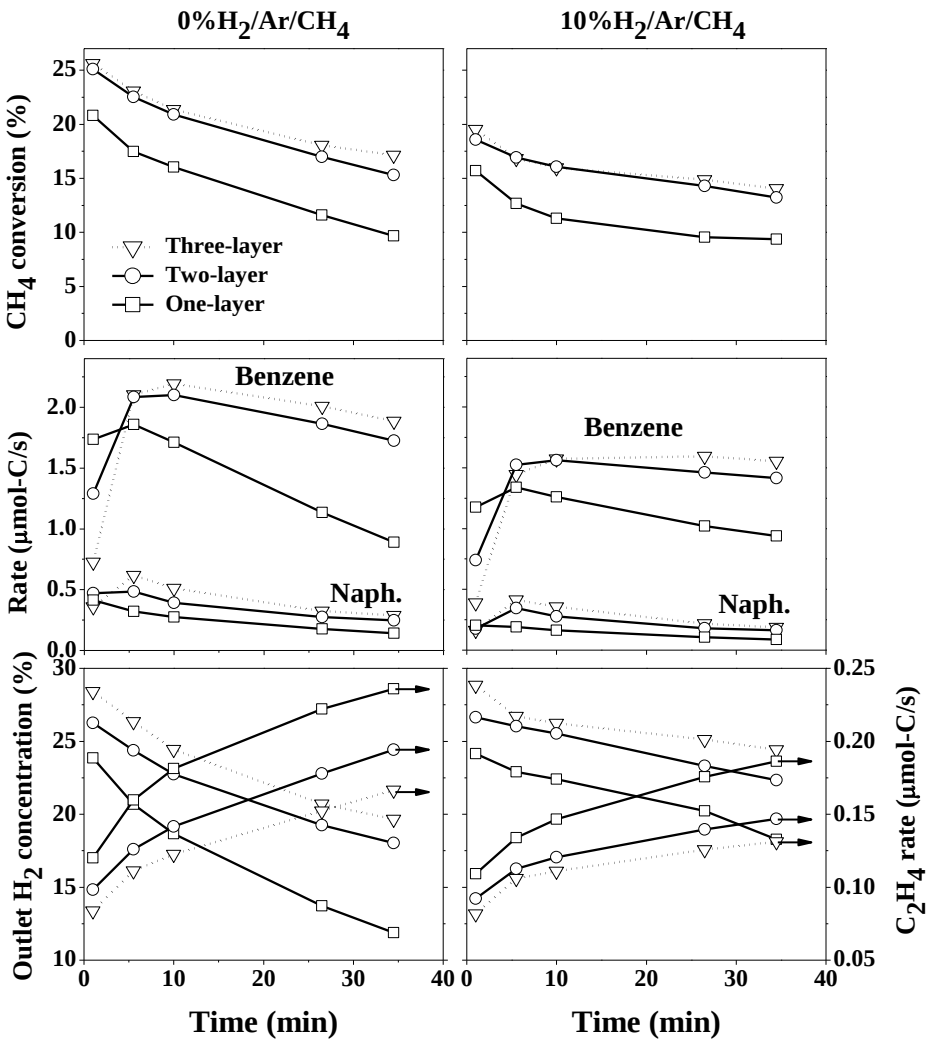

Fig. 4-13. Time-dependences of the catalytic performances of the beds packed with 100, 200 and 300 mg catalyst in the streams of Ar/CH_4 and $10\%H_2/Ar/CH_4$ at 1073 K.

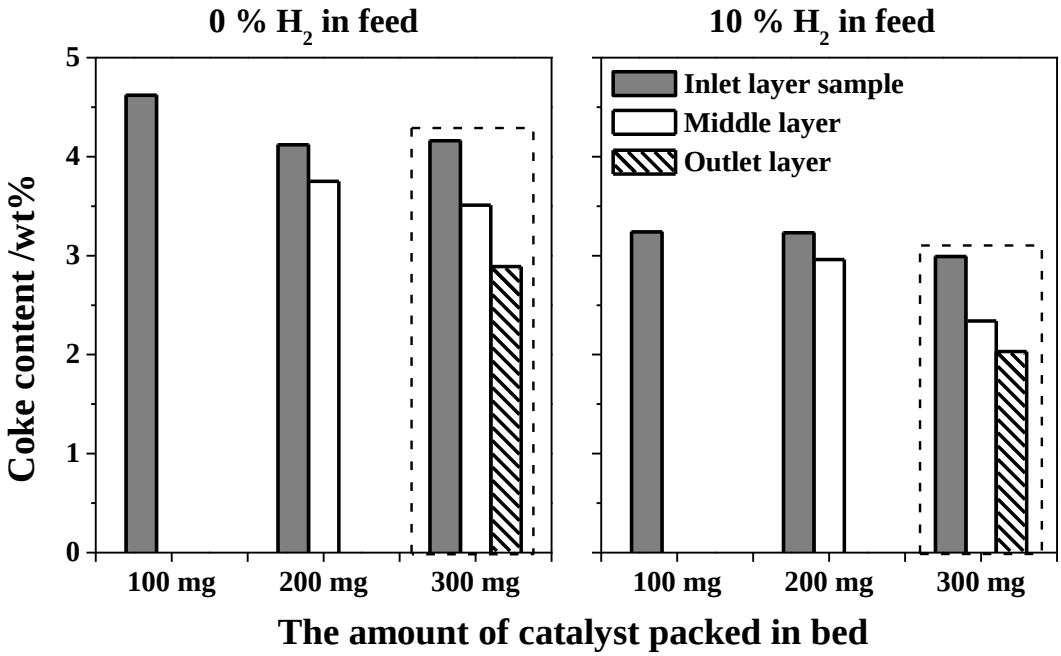

Fig. 4-14. Coke contents of the spent samples recovered after the tests described in Fig. 4-13.

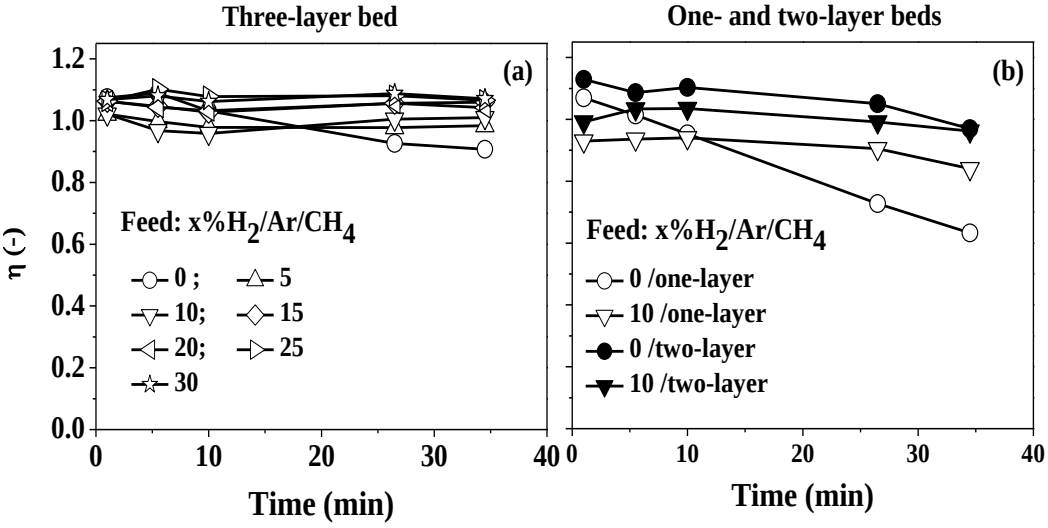

Fig. 4-15. The degree of C2H4 approach to equilibrium for reaction $CH_4 \rightarrow 1/2C_2H_4 + H_2$ (Keq = 0.0193) at the outlets of one-, two- and three-layer bed in the feeds of different H_2 concentrations at 1073 K.

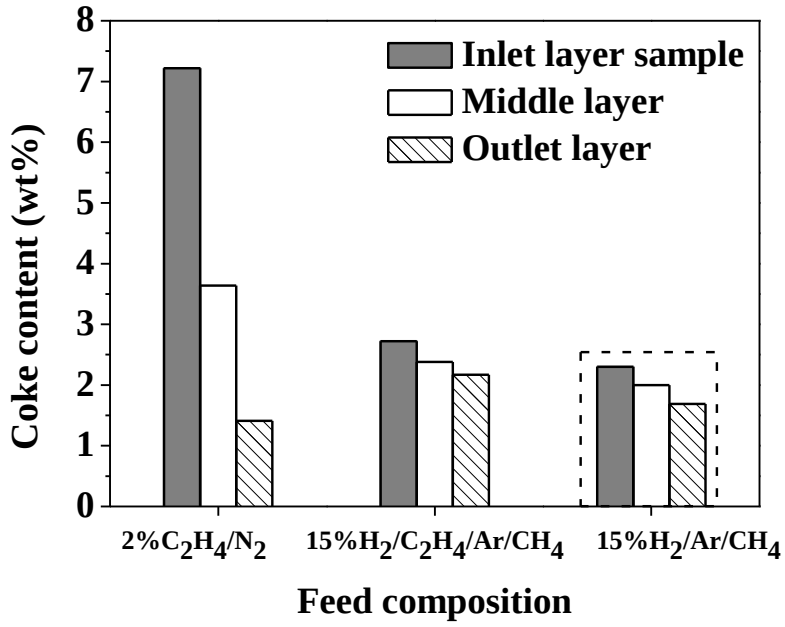

Fig. 4-16. Coke contents of the spent samples recovered after the tests in the feeds of $2\%C_2H_4/N_2$ and $15\%H_2/C_2H_4/Ar/CH_4$ (a mixture of H_2 and $2\%C_2H_4/10\%Ar/CH_4$) at 1073 K.

Chapter 5

Coke formation over Mo/HZSM-5 in the non-oxidative methane dehydroaromatization reaction under CH_4-H_2 switching mode: identification of the coke responsible for deactivation

5.1. Introduction

The non-oxidative methane dehydroaromatization (MTB) to value-added chemicals was first reported at 1993. [1] Although many meaningful and inspiring works were reported in the past two decades [2-5], how to solve coke-caused in the catalyst deactivation still remains a formidable challenge from both fundamental research and engineering practice. At least three types of coke have been observed to form over Mo/HZSM-5 by X-ray photoelectron spectroscopy: adventitious or graphitic-like C, carbidic-like C, and hydrogen-poor sp-type C, but what type is responsible for deactivation is still a controversial issue [6].

Ma et al [7]. also reported three types of carbonaceous deposits form during the MTB reaction but they are described in a different way as: carbidic carbons (in isolated Mo ions or in external Mo particles), molybdenum-associated coke, and aromatic-type cokes on acid sites. These authors pointed out that the aromatic-type coke, formed inside the zeolite channels and burnt at high temperature in the TPO, could be easier removed by hydrogen than the molybdenum-associated, low-temperature burning coke. They believed that the aromatic-type coke was the key factor to control the deactivation rate, since the catalyst activity increased significantly after most of this type of coke was cleaned off through TPH treatment. For example, after a H_2-TPR treatment, while about 90% of the aromatic-type coke and about 60% of the molybdenum-associated coke were removed, the catalyst recovered nearly its full activity. Moreover, some other methods such as added metal

promoters to the catalyst, modification of the acid property of the zeolite or co-feeding a small amount of H_2, CO and /or CO_2 [8.9] to the methane stream also could partly suppress the aromatic coke formation inside the channels, and stablize the catalyst activity in the MTB reaction. Therefore, some researchers considered that accumulation of the aromatic coke inside the channels is responsible for the catalyst deactivation.

On the other hand, there are some studies saying that the coke on the zeolite surface is responsible for the catalyst deactivation. The title catalytic reaction is said to occur according to a bifunctional mechanism: activation of methane over Mo sites to the intermidate C_2H_4 followed by its cyclization to aromatics on the Bronsted acid sites. If there was no spatial constrains of zeolite channels[10], bulky aromatics and coke deposition could form easily over the free Bronsted acid site. As previously reported, the selective elimination of external surface acid sites through silanation treatment or dealumination could lead to a significant improvement in the activity stability of Mo/HZSM-5 and its selectivity to aromatics. This suggests the coke on the zeolite surface was closely related to the catalyst deactivation.

While the above controversial issue still exists, there is also another question to be answered of what type of coke among all reported types of coke is mainly responsible for the catalyst deactivation. If we can design and conduct tests at a specific condition where only one type of coke is allowed to form while the others are suppressed, we may get a clear answer to the question. The results given in the Chapter 3, have shown that the Mo/HZSM-5 catalyst undergoes the three-stage deactivation over its lifetime, and also that the benzene selectivity remains high and constant in the second deactivation stage, but in the third stage it decreases very rapidly with coke formation at a higher rate. This means the aromatic-type of coke forms more rapidly in the last stage of catalyst deactivation, not in the second stage where the benzene selectivity remains constant [11]. Moreover, it was known that the aromatic-type of coke could be easily removed by H_2 in a TPH treatment. This means that under cyclic CH_4-H_2 switch operation mode, the formation of aromatic-type of coke may be suppressed to allow the selective coke formation on

the zeolite surface. Therefore all tests in this chapter were conducted under cyclic CH_4-H_2 switch operation mode [4,12]. The purpose aims to clarify what type of coke is really responsible for the catalyst deactivation.

5.2. Experimental

5.2.1. Catalyst preparation and characterization

A 6wt%Mo/HZSM-5 was prepared by traditional impregnation method. A commercial HZSM-5 with a Si/Al ratio of 20 (TOSOH Co., Japan) was used as a parent zeolite, and it was impregnated with an aqueous solution of ammonium heptamolybdate, followed by evaporating the water, drying at 393 K overnight and calcination at 773 K for 5 h. The resulting solid powder was then pressed, crushed and sieved to collect a fraction of 350–500 μm for use. The test catalyst was characterized using various techniques including FESEM, XRD, BET, 27Al-NMR, NH3-TPD and FT-IR. The detailed procedures were described in previous papers [14].

5.2.2. Activity evaluation

Activity evaluation of the catalyst was carried out in an up-flow, fixed bed quartz reactor at 1073 K and a space velocity of 10,000 ml/g /h in a periodic CH_4-H_2 switch mode. 150 mg of a catalyst sample was used for each test. The sample was first treated in a CH_4 stream at 923 K for 10 min for conversion of its MoO_3 to active Mo_2C. Then it was heated in a H_2 stream to 1073 K, and finally subjected to a CH_4 flow to start a periodic 5 min CH_4 - 5 min H_2 switching operation. The effluent out of the reactor was on-line analyzed by two gas chromatographs. The experiments was stopped and rapidly cooled down to room temperature in the methane stream after different reaction time. And then the coked samples were collected for further characterization.

5.2.3. Coke characterization

The coke contents of coked samples were quantified using a TG/DTA analyzer (EXSTAR TG/DTA 6200, Seiko Instruments Inc.). After loaded to a TG cell, the

sample was kept in a dry air stream for 30 min to ensure that the measurement starts with a stable base. Then it was heated to 393 K and held there for 30 min to have an accurate measurement of the weight loss originated from vaporization of physically adsorbed water. Subsequently it was further heated to 873 K at a rate of 10 K/min and kept there for 30 min to obtain the TG profile of the sample. About 10 mg of a spent sample was used for each measurement. The weight loss after around 673K was used to estimate the coke content.

Burning behavior of the coke in the spent samples was characterized using TPO technique. An auto-controlled TPD apparatus (Bel. Japan Inc.) was employed for the purpose and 30 mg of a spent catalyst sample was used for each measurement. The sample was heated from room temperature to 1103 K at a rate of 10 K/min in a 50 mL/min flow of a gas mixture composed of 10 vol% O_2 and 90 vol% He. The mass spectra of the gases evolved during the TPO were monitored by a Q-MASS spectrometer (ULVAC RG-201). The MS signals m/e = 18, 28 and 44 were used for the detection of H_2O, CO and CO_2 evolved in the TPO, respectively.

N_2 adsorption and desorption experiments of fresh and spent catalysts were carried out at 77 K using a BELSORP-max equipment (Bel. Japan Inc.). Prior to the adsorption measurements, all samples were vacuum-degassed at 623K for 5 h to remove adsorbed moisture from their surfaces. Specific micropore surface areas of the spent catalysts as well as their micropore volumes were analyzed by BET method and t-plot method.

5.3. Results and discussion

5.3.1. Activity evaluation

Figure 5-1 shows the activity performances of 6%Mo/HZSM-5 catalysts over 20, 80, 140, 190 and 240 min, which include CH_4 conversion, aromatic formation rate and aromatic selectivity. In the figure the time on stream refers to the accumulated time of CH_4 flowing through the catalyst bed only, not including the flowing durations of H_2. It is clear that the well duplicated data were acquired at each

measure point in these “actually repeated” tests and therefore ensured the precision of further characterization of coked samples.

It can be observed clearly from Figure 5-1 that the test catalyst underwent three stages of deactivation during its lifetime in periodic CH_4-H_2 switch mode, which is similar to that observed in CH_4 continuous-feeding mode: the most rapid decrease in the CH_4 conversion activity in the very initial stage of the reaction (~20 min), followed by a linearly slow deactivation in the period of 20–140 min and then an accelerated deactivation period in the last 100 min. The CH_4 conversions observed at the first two sampling points were over equilibrium values and then decreased rapidly in the initial stage, as shown in figure 5-1(a). This can be attributed to carburization of remaining MoO_3 species to Mo_2C. For this reason the formation rate and selectivity of aromatic recorded in this period were at low levels. After the fast deactivation, the catalyst went into a very slow deactivation stage where benzene selectivity remains essentially stable at about 70 %. At the third deactivation stage both the formation rate and the selectivity to aromatic decreased rapidly. Although the MTB reaction was conducted at a very high space velocity of 10,000 ml/g /h, the reaction period over which the stable aromatics selectivity is maintained was considerably prolonged when compared that recorded in a CH_4 continuous-feeding mode. [11] This fact confirms the periodic CH_4-H_2 switch operation surely improves the catalytic performance of Mo/HZSM-5 catalyst in the MTB reaction.

It is worth pointing out that the benzene formation rate decreases monotonously, but the selectivity remains stable in the second stage of catalyst deactivation. This observation suggests that the aromatics formation mechanism remains unchanged in the stage, which may reflect the intrinsic property of the Mo/HZSM-5 catalyzed MTB reaction. That is to say, the detrimental coke deposition, which led to the slow deactivation, continues in this stage. The data given in the Chapter 3 have demonstrated that the formation of the aromatic type of coke caused by cracking and/or oligomerization of C_2H_4 was accelerated in the last stage under CH_4 continuous-feeding mode [11]. However, under the present periodic CH_4-H_2 switch operation the accumulation of the aromatic type of coke inside the zeolite channels

must be strongly suppressed since during every exposure of the catalyst to H_2 most of the aromatic type of coke formed in the previous exposure to CH_4 is supposed to be removed. [4.12] Therefore, pursuing the lifetime-dependence of the activity performance of the catalyst does allow us to investigate the coking behavior of the catalyst in the periodic CH_4-H_2 switch mode and consequently confirm if the coke on the zeolite surface is mainly responsible for the catalyst deactivation.

5.3.2. Characterization of coked catalyst

The coked catalyst samples collected after the different times on stream were characterized to clarify the relationship between the deactivation and coke deposition rates. TPO technique, as a powerful method, was used to distinguish the types of coke formed in the spent catalysts, and the coke content and structural property of spent catalysts were measured by TG and BET technique, respectively.

TPO profiles of spent catalysts recovered after the reaction periods of 20, 80, 140, 190 and 240 min time were shown in figure 5-2, which were well correlated with the results obtained by TG measurement. As shown in Figure 5-2, all TPO profiles were well deconvoluted into four fitting peaks denoted as I, II, III and IV. They were attributed to the burning of surface reactive carbon, the graphite-coke formed on the external surfaces, the aromatic coke inside the channels and carbon deposits on the free Bronsted acid sites deep inside the channels, respectively. It should be noted that the TPO peak originated from carbidic carbon in a Mo_2C was not detected for the present samples since the amount of C in the form of Mo2C was very limited in comparison with those of the other four types of carbonaceous deposits, although the presence of Mo_2C in these samples were confirmed by XPS measurements and from the corresponding TG weight loss curves.

The TPO profiles of the coked 6Mo/HZSM-5 in Figure 5-2 showed that the intensity of peak III corresponding to the aromatic-type of coke increases more rapidly with time on stream in the period of 140-240 min. Table 5-1 shows that the corresponding coke amount accumulated in the first 140 min was 1.27 wt% while it increased to 2.24 wt% over a reaction frame of 240 min, and also that they

contributed to 16 % and 32 % of the respective totals. Note that the formation of aromatic-type of coke inside the channels in the last stage of catalyst deactivation was dominated by the coking reactions of C_2H_4 [11]. Further note that the selectivity to aromatics formation of catalyst kept stable in the period up to 140 min and then decreased rapidly in the last 100 min reaction period. We may conclude that the formation of aromatic-type of coke which gave the peak III in the TPO was not the cause of the slow deactivation occurring in the second stage.

The TPO profile of the 6Mo/HZSM-5 recovered after the 140 min reaction is quite similar to those obtained for the samples recovered after 20 and 80 min tests: it is dominated by a low temperature peak II at 796 K, which is considered to originate from the burning of the graphite-like coke on the external surfaces. The peak intensity increased obviously and linearly with time on stream in the period up to 140 min, while that of the peak III in the period showed a slight increase. Table 5-1 showed the amount of graphite-like coke accumulated in the period increased from 0.87 to 2.45 wt%. In contrast, the net increase in the amount of aromatic-type of coke in the period was only 0.61 wt%. These TG results confirmed quantitatively that it is the accumulation of graphite-like coke, not that of aromatic-type of coke, dominating the coking process in the second stage of catalyst deactivation. Compared with the cases operated under continuous feeding mode [11], it is obvious that coke formation occurring in the aromatics selectivity-stable stage was dominated by the forming of graphite-like coke. All these facts gave us a confidence to say that the graphite-like coke formed on the external surfaces of the zeolite surface was responsible for the slow deactivation occurring in the second stage.

N_2 adsorption and desorption curves of the fresh and spent catalysts were shown in Figure 5-3, and their specific micropore surface areas and micropore volumes determined by BET method and t-plot method are listed in Table 5-1. With increasing the reaction time, the surface area and micropore volume of the spent sample decreased. This is attributed to continuous coke deposition narrowing or blocking the zeolite channels. However, the decreasing rates of the microporocity were different at different deactivation stages. In terms of the surface area, Table 5-1

showed that it slightly decreased from 295 m^2/g to 271 m^2/g in the period of 20 to 140 min, and then rapidly decreased to 206 m^2/g over the subsequent 100 min reaction period. That is to say, the surface area was reduced by 24 m^2/g in the 120 min aromatics selectivity-stable period, while it was reduced by 65 m^2/g in the last 100 min reaction. This means coke deposition in the aromatics selectivity-stable period caused little change in the micropore volume of the catalyst, while that occurring in the last deactivation was responsible for the narrowing or blocking of the zeolite channels. These results are in reasonable agreement with those observations obtained from TPO patterns, TG measurements and catalytic performances.

5.4. Identification of the coke responsible for deactivation

Thanks to the cyclic CH_4-H_2 switching operation approach, the relationship between the formation rate of the dominant type of coke and the catalytic performance of the catalyst in the selectivity-stable stage could be investigated. The results showed the catalyst gradually deactivated with the accumulation of the graphite-like coke. This suggests that the formation of the graphite-like coke over the external surface of the zeolite crystals is responsible for the catalyst deactivation. If this is true, the activity should restore after part of the graphite-like coke is removed. Thus, another series of experiments was designed and carried out over the same catalyst to make confirmation.

One of these experiments was carried out first under the cyclic CH_4-H_2 switching operation mode for 80 min (cumulative time for methane feed only), followed by 60 min regeneration by H_2. Subsequently the catalyst was subjected to the cyclic CH_4-H_2 switching operation again for another 80 min, followed by a 120 min H_2 regeneration. Finally, the sample was operated in the cyclic CH_4-H_2 switching mode for the third reaction period of 80 min. The whole test was extended for 240 min in total for CH_4 feeding and 180 min for H_2 regeneration. Hereafter, this test is denoted as a 240-180 test. Figure 5-4 shows the results of aromatic formation rate in all three 80 min periodic methane feeding periods. In the first methane feeding (reaction)

period, the time-dependences of aromatic formation rates observed are similar to those obtained from the lifetime tests. The benzene and naphthalene formation rates arrived at maximums in a very short period and then decreased monotonously with time on stream. The two rates decreased to 79 % and 52 % of their respective maxima at the end of the first 80 min reaction. After 60 min regeneration by hydrogen, the benzene formation rate was restored to 89 % of its maximum, and that of naphthalene to 55% of its maximum. During the second 80 min reaction period, the benzene and naphthalene formation rates showed a more rapid decrease. This clearly suggests that not all graphite-like coke accumulated in the first 80 min reaction was removed in the subsequent 60 min regeneration by H_2. One possible reason is that the regeneration time was not enough. As shown in the same figure, as the second H_2 regeneration was extended to 120 min, the benzene formation activity of the catalyst was restored to 99% of its maximum and that for naphthalene to 60%. This repeated test clearly indicated that a sufficient long period of hydrogen regeneration is required to restore the aromatics formation activity of Mo/HZSM-5 to its maximum level.

To further confirm the effect of hydrogen period on removing the graphite-like coke, another additional test was conducted according to the following procedure. The catalyst was first operated in the periodic CH_4-H_2 switching mode for 80 min (cumulative time for CH_4 feed only), then exposed to H_2 for 120 min for removing its coke and finally subjected again to the periodic operation for another 80 min. This test is denoted as 160-120 reaction. As shown in Figure 5-5, the aromatic formation rates in the first and second 80 min reaction periods were well duplicated, suggesting the good reproducibility. The results showed that the benzene formation rate was restored to 95 % of its maximum after 120 min hydrogen regeneration, which is higher than the recovery of 89% obtained after the 60 min hydrogen regeneration. The simultaneous recovery for naphthalene was 63 %, higher than the 55 % reached by the 60 min H_2 regeneration. These two tests strongly illustrated that a long period regeneration is indeed needed to fully restore the activity of the catalyst.

TPO profiles of both samples from 160-120 reaction and 240-180 reaction tests and those obtained for other supplemental samples are showed in Figure 5-6. The TPO profiles of spent samples for 80 min were repeatedly presented in this figure just for the reader's convenience. The two supplemental samples were collected from another two cyclic CH_4-H_2 switching tests: which were composed of a 80 min periodic CH_4-H_2 switching reaction period and a 60 or 120 min continuous H_2 regeneration period. They are denoted as 80-60 test and 80-120 test. N_2 adsorption and desorption curves observed the spent samples are shown in the Figure 5-7, and the corresponding results of micropore property and coke contents are listed in Table 5-1. The TPO profiles of the samples from all 80 min tests clarified again the graphite-like coke dominated the coke deposition during the selectivity-stable stage. The intensity of CO_x signals originated from the burning of the graphite-like coke decreased dramatically to a very low level after the 60 min hydrogen regeneration was preformed, and to a much lower level after 120 min hydrogen regeneration was conducted. It should be noted that the phenomenon of the peak center shifting to higher temperatures with the increase in coke content was quite common. The TG results in the table confirmed that the corresponding coke contents in the samples subjected to 60 min and 120 min H_2 regeneration dropped significantly to 1.47 wt% and 0.82 wt%, respectively. Simultaneously, as a result of the hydrogen regeneration, a slight change in the microporosity was also observed for the two spent samples. For example, the surface area of the sample from the 80 min cyclic test was 279 m^2/g. After its coke was removed during the 60 or 120 min H_2 regeneration it increased by15 m^2/g to 294 m^2/g and further by 7 m^2/g to 301 m^2/g. These facts obviously suggested that the graphite-like coke was indeed removed during the hydrogen regeneration.

Methane in the effluent during hydrogen regeneration in the 80-60 reaction test and the 80-120 reaction test was analyzed by an online GC and the results are shown in Figure 5-8. It was clear that the time-dependence of the outlet CH_4 concentration observed during the 60 min hydrogen regeneration in the 80-60 reaction test overlapped well with that the first part of that obtained from the 80-120 reaction test, which confirmed again the good reproducibility of the tests. Continuous releasing of

methane in the hydrogen regeneration period, although its rate decreased very rapidly, confirmed that the coke reacted with H_2 and was converted to the gaseous product. Furthermore, note that the methane concentration curves firstly dropped quickly and then became relatively flatter. This means part of the coke can be eliminated easily by hydrogen and the remaining part is difficult to be removed. The easily removed coke should be the aromatic-type of coke that deposited in the previous 5 min methane exposure, and the graphite-like coke needs to be removed in a much longer period. This result also agreed well with the results observed for the samples recovered from the 5min CH_4-5min H_2 switching tests, which showed that only one type of coke accumulated and is difficult to be removed.

5.5. Further discussion deactivation mechanism

It is well realized that the Mo species can migrate into the zeolite channels and occupy the Bronsted acid sites during the catalyst preparation process, which is well confirmed by NH3-TPD, and IR. This means that the density of free Bronsted acid sites of the catalyst may be minimized by increasing Mo loading. Most of researchers in the field agreed that the coke formed on the Bronsted acid sites coke leads to the catalyst deactivation. Therefore, one should first make this point clear: if the coke deposited on the Bronsted acid sites is truly responsible for the deactivation.

It is clear from the above the results and discussion, the aromatics formation activity of the Mo/HZSM-5 is decreasing with accumulation of the graphite-like coke, and it will be restored after part of this type of coke is removed by H_2. These facts suggest that the accumulation of the graphite-like coke is most likely to be responsible for the deactivation. According to the XPS results and analysis of H_2O steam released in the TPO process, this type of coke should locate at the mouths of the zeolite channels, be graphite-like and poor in H. Therefore, here a bold but reasonable assumption is proposed: the deactivation is caused by the lamellar graphite-like coke that deposited over the surface of the Mo_2C located at the zeolite channel mouths. Many phenomena suggest the zeolite channels are strongly involved in the benzene production process. It is difficult for one-ring aromatic to

migrate into the deep inside of the zeolite channels having sizes almost idential to the kinetic diameter of benzene and further condense to bulky two-ring aromatics such as naphthalene. If this is true, only the Mo species that locate at the channel mouths enable the graphite-like coke to form over its surface. Note that Mo_2C, even with a certain amount of coke deposits on it, still enables the activation of methane to the reaction intermediate C_2H_4. Moreover, Matus et al [13] have observed the formation of the lamellar graphite-like coke by TEM, meanwhile, the experimental results showed that the activity performance of the catalyst truly decreased with cumulative formation of the graphite-like coke.

5.6. Conclusions

Time-dependent activity evaluations of the 6wt% Mo/HZSM-5 catalyst were carried out under periodic CH_4-H_2 switching operation mode to investigate what type of coke deposits is truly responsible for its deactivation. Pursuing the variation of the amounts of different types of coke formed in the spent samples over the different time frames were performed to clarify the relationship between the activity-decreasing behavior and the cumulative pattern of coke deposits. The TPO technique was used to distinguish the types of coke over the spent catalysts, while the coke contents and the micorporosity of the spent catalysts were measured by TG and BET technique, respectively. The results showed the catalyst gradually deactivated with the accumulation of the graphite-like coke in the selectivity-stable stage under the CH_4-H_2 switch mode. This phenomenon suggests that the graphite-like coke covering the external surface of the zeolite crystals is responsible for the catalyst deactivation. Meanwhile, a few of experiments composed of the periodic CH_4-H_2 switching reaction and the long time continuous H_2 regeneration periods were designed and carried out to confirm that the catalytic activity of the catalyst can be restored when part of graphite-like coke formed in the spent catalyst is eliminated. The results showed that the benzene formation rates were recovered to 91 % and 95 % of its maximum after the 60 and 120 min hydrogen regeneration, respectively. These facts undoubtfully verify that the graphite-like coke formed over the external surface of zeolite crystals was responsible for the deactivation of the test

Mo/HZSM-5 catalyst.

References

[1] L.S. Wang, L.X. Tao, M.S. Xie, G.F. Xu, Catal. Lett. 21 (1993) 35.

[2] P.L. Tan, Y.L. Leung, S.Y. Lai, C.T. Au, Catal. Lett. 78 (2002) 251-258.

[3] H.T. Ma, R. Kojima, R. Ohnishi, M. Ichikawa, Appl. Catal. A 275 (2004) 183-187.

[4] K. Honda, T. Yoshida, Z.-G. Zhang, Catal. Commun. 4 (2003) 21-26.

[5] Y.Y. Shu, H.T. Ma, R. Ohnishi, M. Ichikawa, Chem. Commun., (2003) 86-87.

[6] B.M. Weckhuysen, D.J. Wang, M.P. Rosynek, J.H. Lunsford, J. Catal. 175 (1998) 338.

[7] H.T. Ma, R. Kojima, S. Kikuchi, M. Ichikawa, J. Nat. Gas Chem. 14 (2005) 129.

[8] S.T. Liu, L.S. Wang, R. Ohnishi, M. Ichikawa, J. Catal. 181 (1999) 175.

[9] R. Ohnishi, S.T. Liu, Q. Dong, L.S. Wang, M. Ichikawa, J. Catal. 182 (1999) 92.

[10] C.H.L. Tempelman, V.O. Rodrigues, E.R.H. Eck, P.C.M. Magusin, E.J. Hensen, Micropor. Mesopor. Mat. 203 (2015) 259.

[11] Y. Song, Y.B. Xu, Y. Suzuki, H. Nakagome, Z.-G. Zhang, Appl. Catal., A: Gen. 482 (2014) 387.

[12] Y.B. Xu, J.D. Wang, Y. Suzuki, Z.-G. Zhang, Appl. Catal. A 409-410 (2011) 181-193.

[13] E.V. Matus, I.Z. Ismagilov, O.B. Sukhova, V.I. Zaikovskii, L.T. Tsikoza, Z.R. Ismagilov, Ind. Eng. Chem. Res. 46 (2007) 4063-4074.

Table 5-1. Coke content and BET surface area and micropore volume of fresh and spent samples.

Sample	Coke content /wt%					BET surface area /m^2g^{-1}	Micropore volume /cm^3g^{-1}
	Peak I	Peak II	Peak III	Peak IV	Totally		
6%Mo/HZSM-5	--	--	--	--	--	323	0.136
20 min	0.22	0.87	0.22	0.09	1.40	295	0.121
80 min	0.38	1.73	0.49	0.20	2.80	279	0.115
140 min	0.56	2.45	0.61	0.12	3.74	271	0.108
190 min	0.75	2.59	1.27	0.14	4.75	234	0.094
240 min	0.77	3.68	2.24	0.42	7.11	206	0.084
80-60					1.47	294	0.129
80-120					0.82	301	0.130
240-180	0.60	2.42	0.42	0.10	3.54	260	0.106
160-120	0.49	1.95	0.39	0.09	2.92	272	0.110

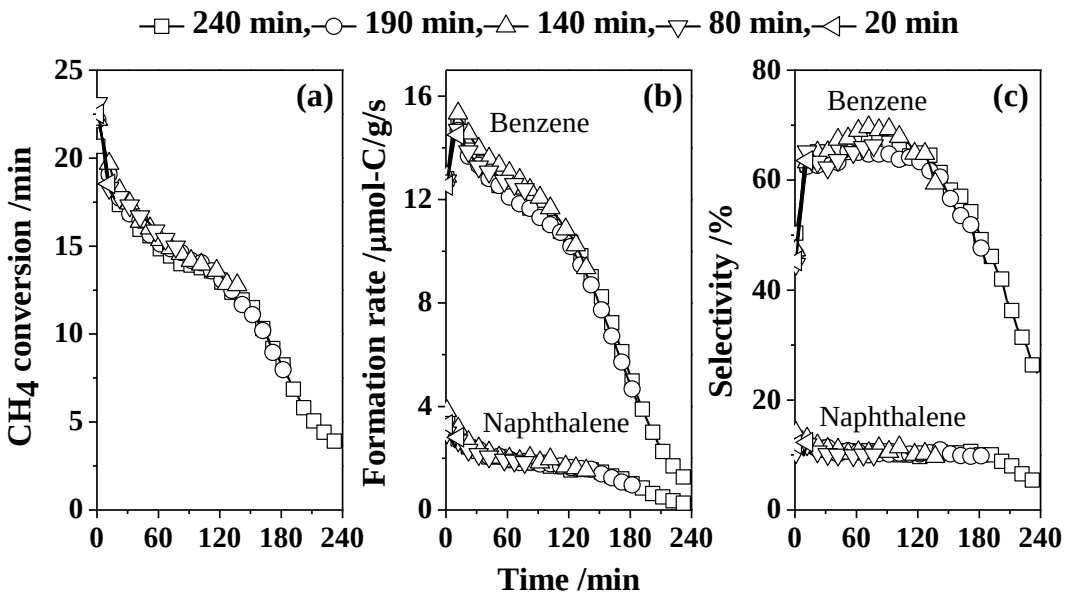

Fig. 5-1. Time-dependences of catalytic performance of 6%Mo/HZSM-5 over different lengths of reaction time at 1073 K and 10000 ml/g/h in periodic CH_4-H_2 switch mode.

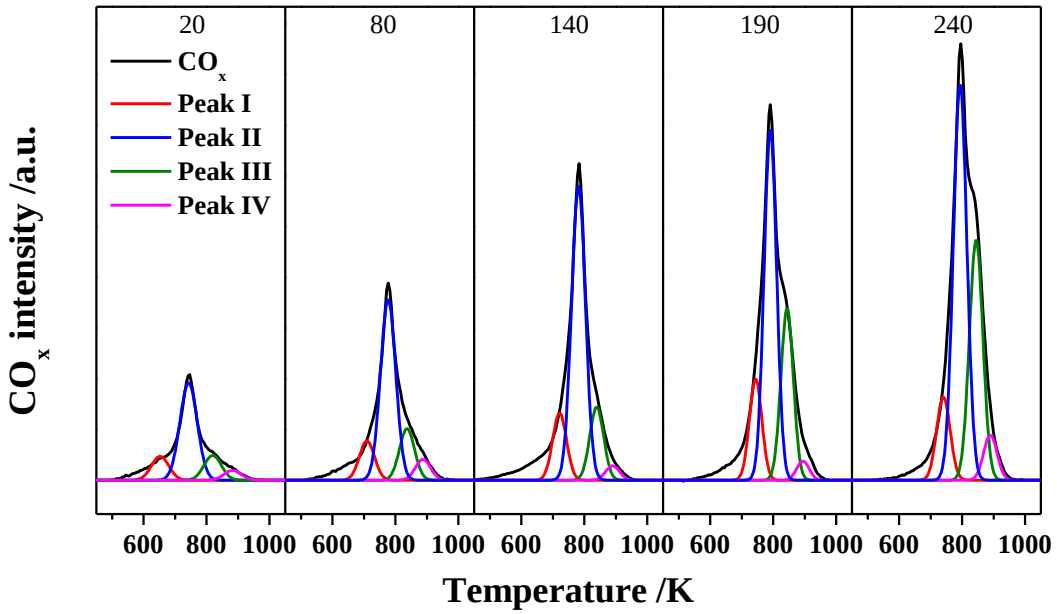

Fig. 5-2. TPO profiles of the spent catalyst samples recovered after the reaction tests over different lengths of time.

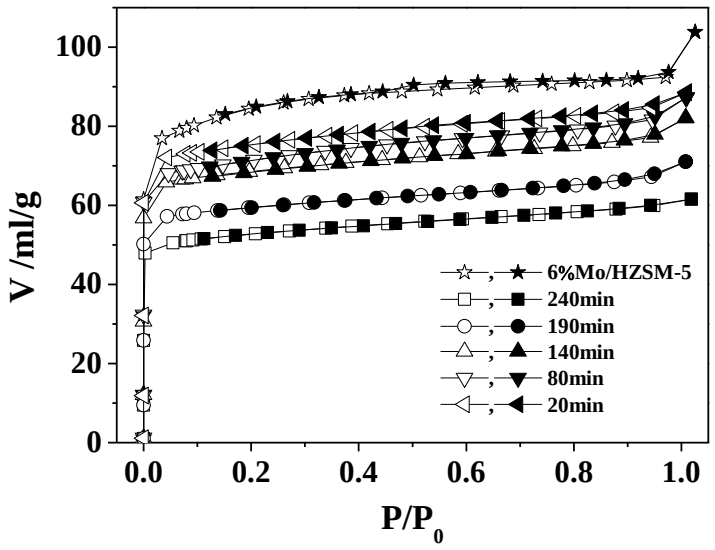

Fig. 5-3. N_2 adsorption and desorption curves of fresh and spent catalysts samples recovered after the reaction tests over different lengths of time.

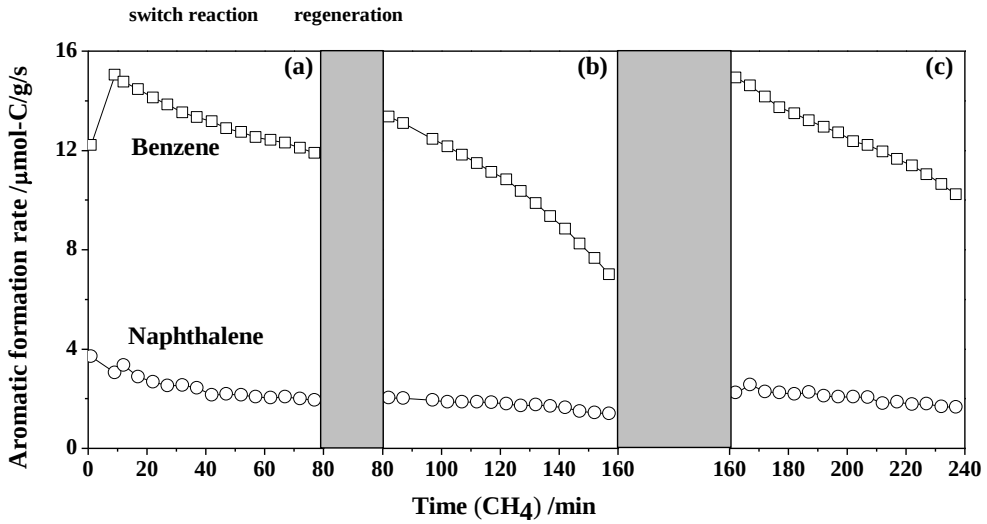

Fig. 5-4. Activity performance of 6%Mo/HZSM-5 under CH_4-H_2 switch mode with 60 min and 120min hydrogen regeneration interval after 80 min and 160min methane reaction, respectively.

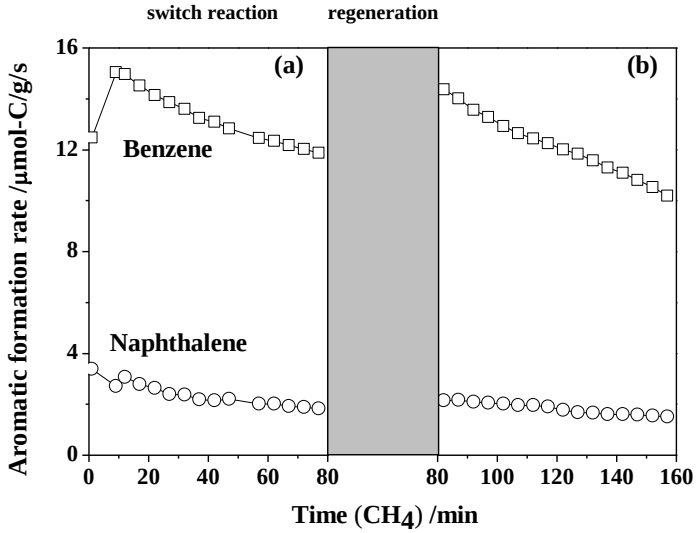

Fig. 5-5. Activity performance of 6%Mo/HZSM-5 under CH_4-H_2 switch mode with an 120min hydrogen regeneration interval after 80 min methane reaction.

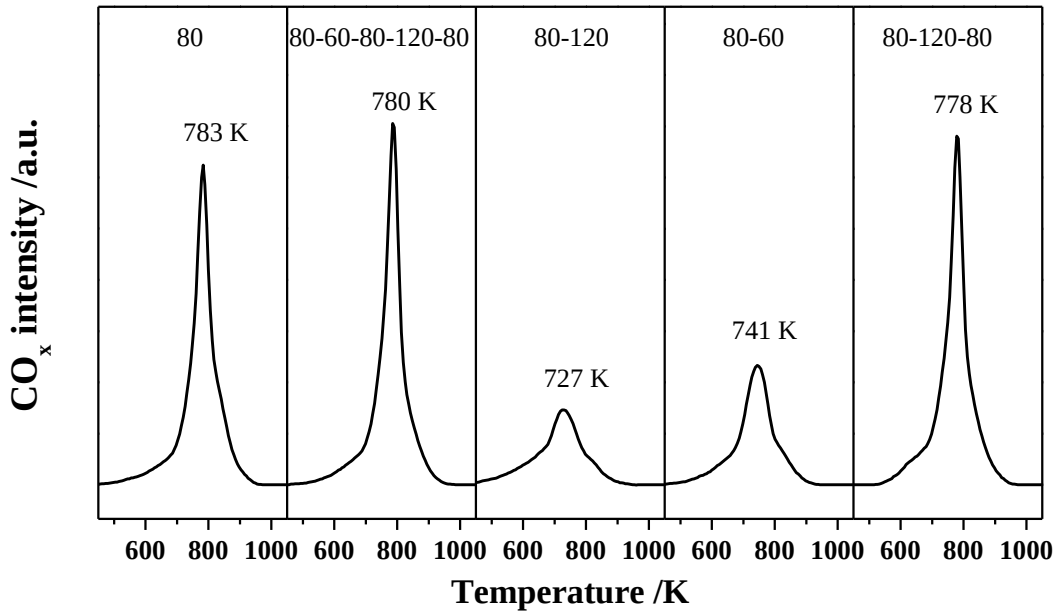

Fig. 5-6. TPO profiles of the spent catalyst samples recovered after the supplemental reaction tests.

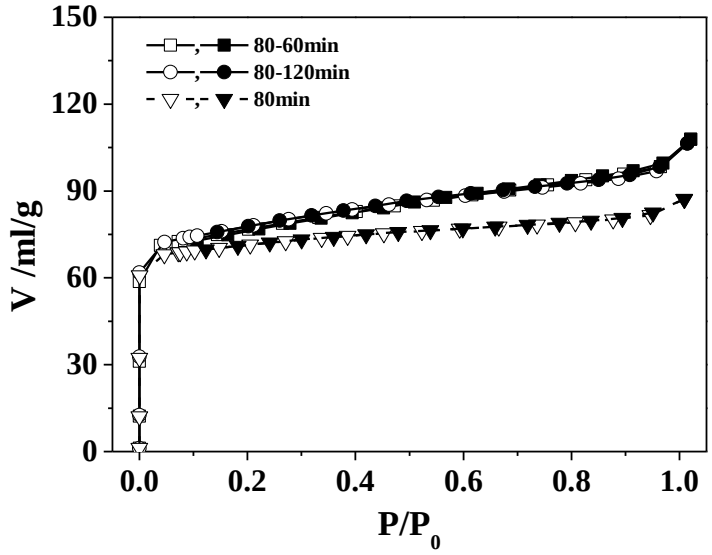

Fig. 5-7. N_2 adsorption and desorption curves of spent catalysts samples recovered after the 80 min and different periods of hydrogen regeneration .

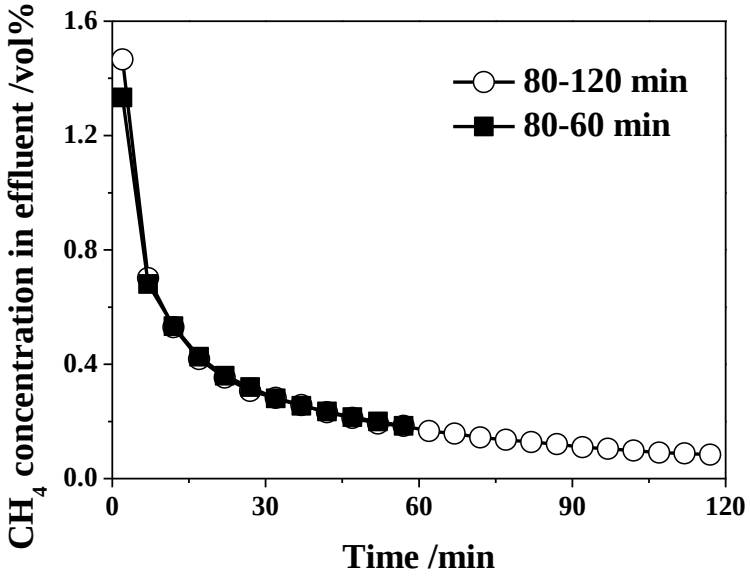

Fig. 5-8. Methane concentration in the effluent during different periods of hydrogen regeneration.

Chapter 6

The catalytic role of Mo in the Temperature-Programmed-Oxidation of the coke

6.1. Introduction

Close attention has been paid to methane dehydro-aromatization over in the past 20 years [1, 2]. However, the rapid deactivation of catalyst caused by carbonaceous deposits in the reaction process remains a tough obstacle for its industrialization [3, 4]. It has reported that some methods and approaches enable to suppress coke formation and improve the activity stability. These include synthesis and use size-suitable HZSM-5 crystals to improve diffusivity of aromatic [5,6], modification of the HZSM-5 to lower its coking sites [7,8], addition of oxygen-containing gases to methane feed to gasify instantaneously the coke [9], doping of other metal promoters to the Mo/HZSM-5 catalyst [10], and regeneration of spent catalysts to restore their activity [11].

However, there are few systematic and detailed studies on characterizing the coke itself formed in the title reaction. Lunsford and co-workers [12] characterized the surface carbon formed over their Mo/H-ZSM-5 catalysts by X-ray photoelectron spectroscopy. The results showed that three different types of surface carbon species are present on an active Mo/H-ZSM-5 catalyst: (a) species A, characterized by a C 1s BE of 284.6 eV, is attributed to adventitious or graphitic-like C and mainly present in the zeolite channel system, (b) species B, defined by a C 1s BE of 282.7 eV, is ascribed to the carbidic like C in Mo_2C and is predominantly located at the outer surface of the zeolite, and (c) species C, defined by a C 1s BE of 283.2 eV, is considered as a hydrogen-poor sp-type or pregraphitic-type of carbon and to be responsible for the catalyst deactivation. Liu and co-workers [13,14] have investigated the chemical nature of the carbonaceous formed on a Mo/HZSM-5 and a Mo/MCM-22 by using the TPSR, TPH, $TPCO_2$ and TPO-TG combined techniques.

They reported that there are at least three different types of coke forming in the title reaction. They are ascribed to the carbidic carbon in molybdenum carbide, the molybdenum-associated coke, and the aromatic-type coke on acid sites, respectively. The TPO profiles of the coked and then TPSR-treated 6%Mo/HZSM-5 catalyst had two peaks at about 776 K and 865 K, while the TPO profile of a 20 min-coked 6Mo/HMCM-22 had a low temperature peak at 694K with a shoulder at the high temperature side. For the form samples the low-temperature and high-temperature peaks were assigned to the molybdenum-associated coke, and the aromatic-type coke on acid sites, respectively. The carbidic carbon in the molybdenum carbide was observed also from the weight increase in the TG profile and the TPO curves of a 10 min-coked 6Mo/HCM-22. The TPH treatment led mainly to a reduction in the coke burning and giving the high-temperature peak. It had little effect on removing the coke burnt-off at the low temperature and giving the low-temperature peak. The $TPCO_2$ treatment was more effective in removing both types of coke burnt-off at low and high temperatures. However, a question still remains of why the type of coke more easily removed by H_2 was burnt off at a higher temperature region in the TPO. Also another question to be answered also remain: why the intensity ratios of CO_2 and CO signals were quite different for the low- and high-temperature TPO peaks. These facts imply that there might exist other factors to influence the TPO behavior of the coke in the spent MO/HZSM-5 catalyst.

Ichikawa and co-workers [9] showed that the addition of the oxidative reagents such as CO and CO_2 to methane feed has a significant improving effect on the catalytic performance. The TPO profiles of spent Mo/HZSM-5 catalyst samples showed that the irreversible or inert coke burning at temperatures above 773 K was greatly suppressed by adding a certain amount of CO or CO_2 to the methane feed gas. These authors made the following proposal and explained the unique role of CO addition in suppressing coke formation. The CO_2 and C are first formed through the Boudart reaction $2CO = CO_2 + C$. The C is then hydrogenated to a reactive carbon species [CH_x], followed by its conversion to aromatic products such as benzene and naphthalene; and at the same time CO_2 reacts with the surface inert carbon species (coke) to form CO, competing a catalytic cycle. Namely, CO functions as a catalyst to

convert the inert coke to aromatic products, which in turn improves the catalytic stability of the catalyst. It is also interesting to point out that the samples exposed to the feed containing a small amount of CO (1.8-12%) or CO_2 (< 4%) had the more reactive coke, giving a TPO peak at temperatures below 673 K.

Ma and co-workers [15] reported that there were three TPO peaks for their spent catalysts operated at high space velocities (≥5400 ml/(g·h)). On the other hand, determined by differential thermal analysis (DTA), Matus [16] reported that only one type of carbonaceous deposits formed in their 2% Mo/HZSM-5 catalyst with its zeolite of a ratio of Si/Al = 17, but for the catalysts based on the zeolites having the higher Si/Al ratios of 30 and 45 the two exothermic peaks were observed.

The difference in the number of burning peaks observed for the samples in these previous studies indicates that the characteristic property of coke formed over Mo/HZSM-5 catalyst in the title reaction, such as coking sites, location, and types of coke is still under debate. Note that the TPO peak of the graphite-like coke, which is thermally stable, poor in H and associated to the Mo species, always appeared at low temperatures when compared with that originated from the aromatic-type of coke. These imply that there may exist other factors to influence the burning behavior of the coke in spent Mo/HZSM-5. Study on the catalytic role of Mo in the TPO of the coke in spent samples is completely missing in previous studies. Therefore, the main aim of this study is to investigate the catalytic effect of Mo in Mo/HZSM-5 on the burning behavior of the coke in it using TG and TPO techniques in combination with FT-IR, NH3-TPD, XPS measurements. The zeolite having an average crystal size of 4 μm was used to prepare the catalysts to be tested. The length of the zeolite channels is sufficient. This allowed us to easily distinguish the external coke from internal coke.

6.2. Experimental

6.2.1. Catalyst preparation

A series of 1, 2, 4, 6 and 8 wt% Mo-loaded HZSM-5 catalysts was prepared by a wet impregnation method, denoted as x/Mo/HZSM-5 (x=1, 2, 4, 6 and 8,

respectively.). A commercial, highly crystalline 4 μm HZSM-5 zeolite (Si/Al ratio=40) was impregnated with a certain amount of ammonium heptamolybdate aqueous solution. The impregnated sample was dried at 393 K overnight and calcined at 773 K for 5 h. All the catalysts with different Mo-loading were prepared by the same condition. Finally, the catalysts were pressed, crushed and sieved to particles in the range of 350–500 μm for use.

6.2.2. Catalyst characterization and evaluation

The NH3-TPD technique was used to measure the acidity of the zeolite and catalysts. The tests were conducted in a TPD-1-ATSP1 (Bel. Japan) instrument. 50mg of the zeolite or a catalyst was used for each measurement. The sample was first heated in a He stream to773 K and maintained at this temperature for 1 h, and then cooled down to 403 K. Then, the ammonia was introduced into the reactor for 30 min to achieve adsorption equilibrium at 40 Torr, and the sample was purged in a He stream for 30 min to evacuate weakly adsorbed NH3.Subsequently, the sample was heated again to 873K at a rate of 10 K/min. The amount of ammonia in the effluent was monitored online by a Q-MASS (ULVAC RG-201). The signal m/e = 17 was used for the detection of NH3.

The activity evaluation tests with all catalysts were performed in a fixed bed reactor system. It is consisted of gas feeding lines, a temperature controller, a upstream fixed bed reactor and two online GCs. analysis part. All tests were carried out at atmospheric pressure in the continuous feeding mode. 150 mg of the catalyst was used for each experiment. The sample was first heated in a H_2 stream at a flow rate of 25 ml/min to 923 K and hold there for 5 min, and then it was switched into a CH_4 stream at a flow rate of 18 ml/min for 12 min at this temperature. Then, the sample was heated again to 1073 K in a H_2 stream at a flow rate of 25 ml/min and hold there for 5 min. A feed gas mixture of 90 % CH_4 and 10% Ar was introduced into the reactor at a flow rate of 25 ml/min (space velocity = 10000 ml/g cat/h) at 1073 K to start the reaction. After undergoing a pre-set reaction period, the sample was cooled down in a He stream to room temperature and then recovered for various measurements. The outlet concentrations of benzene, toluene, naphthalene and methane were analyzed by

an on-line FID gas chromatograph, and those of H_2 and Ar were analyzed by an on-line TCD gas chromatograph. Ar was used as an internal standard for estimate of CH_4 conversion.

6.2.3. Characterization of spent catalyst

Characterization of the spent catalysts was performed using N_2 adsorption, TG, TPO and other techniques.

N_2 adsorption and desorption experiments were carried out at 77 K using a BELSORP-max equipment (Bel. Japan Inc.). Prior to the adsorption measurements, all samples were vacuum-degassed at 623K for 5 h to remove adsorbed moisture from their surfaces. Specific micropore surface areas of the spent catalysts as well as their micropore volumes were analyzed by the BET method and the t-plot method, respectively.

TG profiles were recorded on an EXSTAR-TG/DTA 6200 instrument (Seiko Instruments Inc.). 100 mg of a spent catalyst sample was used for each measurement. The flow rate of air used was 25 ml/min. The sample was heated from 313 K to 393 K and held there for 30 min, and then heated again to 923 K at a rate of 10 K/min and held therefore for 30 min.

The TPO technique was used to analysis the burning characterization of the spent catalysts. The TPO reactor was heated in a flow of 50 ml/min feed gas mixture of 90 % He and 10 % O_2 at a heating rate of 10 K/min from room temperature to 1103 K. The amounts of CO, CO_2 and H_2O in the effluent were continuously monitored online by a Q-MASS (ULVAC RG-201). The signal at m/e= 18, 44 and 18 were used for the detection of CO, CO_2 and H_2O, respectively.

6.3. Results and discussion

6.3.1. Fresh catalyst characterization

The NH_3-TPD profiles of the HZSM-5 zeolite and Mo/HZSM-5 catalysts with

different Mo loadings are shown in Figure 6-1. It can be seen that the TPD profile of the HZSM-5 zeolite has two typical desorption peaks, whose centers are at about 510 K and 690 K. The desorption peak at about 690 K is attributed to the ammonia adsorbed on the Bronsted acid sites. It is very obviously that the intensity of the desorption peak at about 690 K decreased with increasing the Mo loading. If we assume the integral area of the peak at 690 K obtained for the zeolite being 100, the integral areas of the corresponding TPD peaks estimated the catalysts of for 1,2,4,6 and 8wt% Mo were 65, 52, 40, 35 and 30, respectively. This indicated that Mo species loaded on the catalysts migrated into the zeolite channels and occupied the Bronsted acid sites of the zeolite. It is interesting to point out that the ratio of Mo-occupied to free Bronsted acid sites in these catalysts decreased gradually with increasing Mo loading. The results might also suggest the Mo in the 8 wt% Mo/HZSM-5 catalyst exceeded the required amount.

The FT-IR adsorption bands of the zeolite and all catalysts were also measured. Indeed, the Bronsted acid sites were certainly occupied by Mo. As shown in Figure 6-2, the strong absorption at 1550 cm^{-1} was assigned to the Bronsted acid sites. The absorbance decreasing with increasing Mo loading indicated that the Bronsted acid sites were consumed and interacted with Mo, which is in agreement with the NH3-TPD results. If the Mo loading exceeds the required amount estimated from the acid sites of the zeolite support, the excessive Mo will anchor to the acidic sites at the external surface of the zeolite crystals. If this is the case, the excessive Mo maybe agglomerate to form large particles on the external surface of the zeolite. For Mo dispersed inside the zeolite channels, it is unlike to agglomerate due to spatial limitations. From the XRD patterns of all spent catalysts shown in Figure 6-3, it is clear that no detectable crystalline phase other than that of the zeolite was formed in the 1, 2 and 4/Mo/HZSM-5 catalysts. However the XRD patterns of the 6/Mo/HZSM-5 and 8/Mo/HZSM-5catalysts showed a weak and an obvious diffraction peak at 27.3 ^{o}, indicating the presence of crystalline MoO_3 in these two catalysts. These results confirmed again that the excessive Mo would not migrate into the zeolite channels after the Bronsted acid sites inside the channels all are occupied

by Mo, but stay at the external surface of the zeolite and agglomerate to crystalline MoO_3.

^{27}Al MAS NMR spectra shown in Figure 6-4 give information on structures and properties of the zeolite and the Mo loaded catalysts. It is clearly that there are two obvious peaks at 52 ppm and 0 ppm in each spectrum. 52 ppm and 0 ppm are attributed to tetrahedrally coordinated framework aluminum and octahedral non-framework Al, respectively. Intensity at 52 ppm in these spectra decreases sharply with increasing Mo loading, but that of 0 ppm keeps invariable. This suggests that the Mo species indeed interacted with framework aluminum. Note that the test microsized zeolite has a very low concentration of external Bronsted acidic sites. Further note most of the loaded Mo in the test catalysts were dispersed and associated with framework aluminum in the zeolite channels. This result is consistent with the NH_3-TPD as well as FT-IR results. For the 6 and 8%Mo/HZSM-5 catalysts the spectra also show a weak peak at -14 ppm. This peak is ascribed to octahedral aluminum in crystalline $Al_2(MoO_4)_3$. This fact means that an excessive Mo loading would lead to a negative effect due to dealumination of the zeolite framework.

6.3.2. Catalytic reaction

Figure 6-5 shows the catalytic performances of the test catalysts versus time on stream at 1073 K. The catalytic lifetimes of the 1, 2, 4, 6 and 8/Mo/HZSM-5 catalysts were 40 min, 100min, 150 min, 150 min, and 150 min, respectively. The methane conversion, the formation rates of benzene and naphthalene and their selectivity were calculated on carbon base. It can be seen from Figure 6-5(a) that methane conversion recorded over all test catalysts decreased rapidly with the reaction time on stream. The initial methane conversion, also the highest one, observed over1/Mo/HZSM-5 is only 13.28 %, whereas it increased remarkably with increasing Mo loading and attained 23.26 % over the 6/Mo/HZSM-5. The initial methane conversions recorded over the catalyst with the low Mo loadings of 1 % and 2 % are far away from the thermodynamic equilibrium conversion. Although the methane conversion recorded over all the test catalysts decreased sharply with time on stream, the catalysts with low Mo loadings deactivated more quickly than those having the higher Mo loadings.

Meanwhile, the formation rate and selectivity of aromatic hydrocarbon products such as benzene and naphthalene obtained for the catalysts of the low Mo loadings (1 % and 2 %) were also significantly lower than those observed over the other catalysts (Figure 6-5(b) and 6-5(c)). The highest formation rate of benzene was observed over the 6/Mo/HZSM-5 and was almost three times higher than that recorded over 1/Mo/HZSM-5. Comparison in the performance between the catalysts having the higher Mo loadings (4 %, 6 % and 8 %) suggests that the catalytic performance provided by 8/Mo/HZSM-5 was reversely lower than those given by the other two catalysts. In generally, 4-6 wt% Mo loaded HZSM-5 catalysts give the best catalytic performance for the title reaction.

6.3.3. BET of spent catalyst

The textural properties of the fresh and spent catalysts undergoing the different periods of the reaction are shown in Table 6-1. The BET surface areas and micropore volumes of the fresh catalysts were all less than those of the blank HZSM-5 zeolite, 404 m^2/g and 0.1733 cm^3/g. They decreased with increasing Mo loading. This again indicated that Mo species migrated into the channels and occupied the Bronsted acid sites inside the zeolite channels. Moreover, the longer the reaction time the catalyst underwent is, the smaller the BET surface area and micropore volume of the spent sample are. For example, the BET surface areas of the spent 6/Mo/HZSM-5s that underwent the 6, 30, 60, 100 and 150 min of the reaction were 300, 267, 253, 228 and 219 m^2/g, and their micropore volumes were 0.1134, 0.1027, 0.0929, 0.0818 and 0.0675 cm^3/g, respectively. Since the BET surface area of the test zeolite is governed bgy its internal surface area, and its decrease is essentially caused by coke deposition inside its channels, the change in micropore volume given in the table represents the variation of the microporosity of spent catalyst. The micropore volumes of the spent 6/Mo/HZSM-5s recovered from the tests of 6, 30, 60, 100 and 150 min accounted for 16%, 24%, 31 %, 39 % and 50 % of that of the fresh catalyst. Namely, the micropore volume of the spent sample decreased almost linearly with time on stream. These results suggested that the decrease in microporosity observed for the fresh catalysts is resulted from Mo loading, whereas that for the spent samples is caused by coke deposition occurring in the reaction. Further, in addition to the catalytic performances

showed in Figure 6-5, the change in the catalyst microporosity with the time on stream indicates that the catalyst deactivation was certainly resulted from the blocking of the zeolite channels by coke.

6.3.4. TG of spent catalysts

TG technique was used to measure the coke amount in the spent catalysts. The TG weight loss curves recorded for all spent samples are displayed in Figure 6-6. The temperature profiles recorded simultaneously are also showed in the figure. The weight loss observed below 623 K was attributed to the absorbed water. Then, a distinct increase in the 623-723 K was observed in all TG curves for all the samples. It became more obvious for the samples with higher Mo loadings. This weight increase was attributed to the oxidation of carbidic Mo to MoO_3. Such an increase was confirmed by the TG measurement of a standard Mo_2C sample. Finally the weight decreased dramatically till all coke in the sample was burnt off at a high temperature. In short, the coke burnt off in the TG measurement consists of C in Mo2C and coke in the sample. According to the assignment above, the total coke amount in the spent catalyst (M, %) was calculated according to the following formula:

$$\mathrm{M} = \mathrm{M1} + \mathrm{M2}$$

$$\mathrm{M1} = \frac{(\mathrm{m2} - \mathrm{m1}) * \frac{2 * 12}{2 * 144 - 204}}{\mathrm{m3}} * 100$$

$$\mathrm{M2} = \frac{m2 - m3}{m3} * 100$$

Where M1 is carbon in Mo_2C, M2 accounts for the deposited coke, m1 is the lowest weight percent read from the TG curve in the region of < 623 K, m2 is the peak weight percent readable in the region of 623-723 K, m3 is the end weight percent, 12, 144 and 204 are molecular weights of C, MoO_3 and Mo_2C, respectively. The calculated results of M1 and M2 are showed in Table 6-2.

It was obvious that the coke content formed in the test catalysts depended on the

reaction time. The coke contents given in the table showed a large increasing tendency with increasing the reaction time. Compared with M2, however, M1 in amount was so small that its contribution to the total coke content could be neglected foe all samples. For example, for the 6 min-coked 6/Mo/HZSM-5 sample its M2 accounted for 1.02 %, while the M1 only weighted 0.16 %. Such difference became further larger for the sample subjected to the reaction for a longer period. In accord with the results from the BET measurements, the coke amount in the spent catalysts showed a linear increase with increasing the time on stream. This suggests that coke deposition was indeed responsible for the blocking of the zeolite channels and the catalyst deactivation. Moreover, the coke amounts deposited in the catalysts with the Mo loadings of 1, 2, 4, 6 and 8wt% were measured to be 5.68 %, 9.22 %, 16.09 %, 17.31 % and 8.55 %, respectively. The highest coke contents were formed in the 4 and 6/Mo/HZSM-5, while they exhibited the best catalytic performance (methane conversion, aromatic formation rate, and lifetime). This fact implied that not all coke deposited causes the catalyst to deactivate. It is interesting to point out that the M1 in amount, the C in carbidic Mo, increased with increasing reaction time, but it never attained the expected theoretical value. The highest weight increase in the amount of M1 accounted for only 50% of the theoretical amount for all spent catalysts. This indicated that not all MoO_3 in the fresh catalyst was carbonized to Mo_2C.

As mentioned above, the coke amount accumulated in a specific catalyst showed a significant increase with increasing the reaction time. Nevertheless, BET and TG data did provide any information on the types of coke and their respective contributions to the total amount of coke. The temperature-program oxidation technique is a powerful approach to investigating the burning behaviors of various types of coke. In order to reveal the types of coke and their burning temperature regions, all spent catalysts were subjected to the TPO measurements. The TPO profiles obtained are shown in Figure 6-7.

It can be seen from the figure that the intensity of the CO and CO_2 peaks from all the spent catalysts showed a significant increase with increasing the reaction time. This is consistent with the BET and TG results. For the catalysts with the higher Mo

loadings, the TPO curves exhibited more than one TPO peak.

As shown in Figure 6-7, the spent 2/Mo/HZSM-5 recovered after a 6 min reaction, exhibited a weak single CO_x peak without detectable H_2O releasing. For the samples subjected to the reaction for the longer periods of 30, 60 and 100 min, their TPO profiles were composed of the two CO_x peaks at 792 K and 855 K, 807 K and 870 K, and 818 K and 884 K, respectively. When the reaction time was extended over 100 min, the resultant samples exhibited the two-peak TPO patterns with a broad shoulder at the temperatures above 884 K. This shoulder may represent a type of coke different those represented by the two main low-temperature peaks. Meanwhile, it could be seen that the intensity of H_2O signal in the TPO profiles in Figure 6-6 is closely related to the high-temperature CO_x peak (855-884 K) and also increased with increasing the reaction time. It was also worthy pointing out that the peak intensity of CO_2 was always stronger than that of CO for the lower-temperature CO_x peak, but for the higher-temperature peak the ratio of CO_2 to CO peak intensity became lower, as shown in Figure 6-9.

For the spent 4 and 6/Mo/HZSM-5 samples, very similar to the cases of the spent 2%Mo/HZSM-5, the intensities of CO, CO_2 and H_2O peaks increased with increasing the reaction time. After a shorter reaction time, 6 min, the spent catalyst didn't show any strong TPO peak, whereas subjected to the reaction for 30 min or a longer time, the samples showed the TPO patterns with three eye- distinguishable peaks. For the 4%Mo/HZSM-5 catalyst, the three peak temperatures were 775 K, 823 K and 874 K for the 30 min-reacted (coked) sample, 793 K, 832 K and 900 K for the 60 min- coked sample, and 796 K, 844 K and 908 K for the 100 min-coked sample, and 806 K, 871 K and 908 K for the 150 min-coked sample, respectively. It should be noted that a large increase in the peak intensity was observed for the 150 min-coked sample. For the spent 6/Mo/HZSM-5 samples, a similar increase in the peak intensity was observed with increasing the reaction time, and three eye- distinguishable TPO peaks were observed. The corresponding peak temperatures are 790 K, 838 K and 858 K for the 60 min-coked sample, 804 K, 832 K and 869 K for the 100 min-coked sample, and 818 K, 849 K and 910 K for the 150 min-coked samples, respectively. The

intensity of H_2O peak closely related to the higher-temperature CO_x peak also increased with increasing the reaction time for these two catalysts with the higher Mo loadings of 4 and 6 wt%. The ratios of CO_2 to CO peak intensity were always higher than 1, especially for the samples with higher Mo loadings. This fact implied that the coke in the catalysts with higher Mo loadings is more easily burned to form CO_2 than CO.

It can be seen from the TPO patterns in Figure 6-6 that at least three types of coke formed in the test catalysts: they are attributed to the origins of the three TPO peaks centered at the temperatures given above for the 4 and 6/Mo/HZSM-5 samples, the first type poor in H_2, the second rich in H and the third one poor in H again.

6.4. Discussion

To reveal the catalytic role of Mo in the TPO process of the different types of coke in the spent catalysts, a specially designed test was conducted with a mixture of 150 mg of the 6/Mo/HZSM-5 in sizes of 180–250 μm and 150 mg of the HZSM-5 zeolite in sizes of 350-500 μm to collect some coked HZSM-5 sample. The reaction was performed at the same temperature for 100 min. At the end of the test, the spent sample was recovered and sieved to the portions of coked-6%Mo/HZSM and coked-HZSM-5. The latter portion was then subjected to a TPO measurement. The resultant TPO profile is shown in Figure 6-8, and only one single sharp TPO peak appeared at about 930 K. Comparison of the TPO pattern from the coked HZSM-5 with all those from Mo-loaded samples thus strongly suggests that the TPO process of all types of coke formed in the test catalysts are catalyzed by Mo and therefore occur at lower temperatures.

The ratio of CO_2 and CO peak intensity in all the cases, as shown in Figure 6-9, first increased to a maximum at temperatures where the lower-temperature-CO_x peaks appeared, then decreased to a minimum at temperatures where the higher-temperature-COx peaks appeared, and turned to increase again. Note the TPO of all types of coke were Mo-catalyzed. Only in the case that the coke is difficultly

accessible to O_2, its oxidation rate will be decreased and more CO may form, which leads to a lower ratio of CO_2 to CO peak intensity. That is to say, the coke giving the higher temperature CO_x peaks is most likely to reside inside the zeolite channels. Thus the type of coke giving the lower-temperature peaks can be reasonably considered to form on the external surface of the zeolite crystals. For the type of coke giving the peaks at the temperatures above 870 K may be considered to form deep inside the zeolite channels, and it is inaccessible to O_2 unless the coke on the zeolite surface and inside the channel but near the channel mouths is burned off. This explains it always burns off at the highest temperatures during TPOs. All these suggest that the mass transfer factor, in addition to the catalytic effect of Mo itself, must be considered when we argue the TPO behavior of the coke formed on the microsized HZSM-5-based Mo/HZSM-5 catalysts.

6.5. Conclusions

Time-dependences of catalytic performance over a series of Mo/HZSM-5 catalysts (nominal Mo = 1, 2, 4, 6 and 8 wt%) were investigated at severe conditions (1073 K and 10,000 mL/g/h). Characterization of the coke in all spent samples recovered after different periods of the reaction was performed using TG, BET, XPS and TPO techniques. The TPO peak temperatures of coke shifted to the lower ones for the catalysts of higher Mo loadings, and the ratio of CO_2 to CO released in the high temperature range of > about 800 K during the TPO of all spent catalysts increased obviously with increasing the Mo content. This suggested that Mo catalyzes the burning of the coke on coked Mo/HZSM-5 catalyst in TPO.

References

[1] L.S. Wang, L.X. Tao, M.S. Xie, G.F. Xu, Catal. Lett. 21 (1993) 35.

[2] F. Solymosi, J. Cserényi, A. Szöke, T. Bánsági, A. Oszkó, J. Catal. 165 (1997) 150.

[3] Y.B. Xu, J.Y. Lu, J.D. Wang, Y. Suzuki, Z.-G. Zhang, Chem. Eng. J. 168 (2011)

390.

[4] Y.B. Cui, Y.B. Xu, J.Y. Lu, Y. Suzuki, Z.-G. Zhang, Appl. Catal., A: Gen. 393 (2011) 348.

[5] C.L. Zhang, S. Li, Y. Yuan, W.X. Zhang, T.H. Wu, L.W. Lin, Catal. Lett. 56 (1998) 207-213.

[6] S. Burns, J.S.J. Hargreaves, P. Pal, K.M. Parida, S. Parija, Catal. Today 114 (2006) 383-387.

[7] C.H.L. Tempelman, V.O. Rodrigues, E.R.H. Eck, P.C.M. Magusin, E.J. Hensen, Micropor. Mesopor. Mat. 203 (2015) 259.

[8] S. Burns, J.S.J. Hargreaves, P.Pal, K.M. Parida, S. Parija, J. Mol. Catal., A-Chem. 245 (2006) 141.

[9] R. Ohnishi, S.T. Liu, Q. Dong, L.S. Wang, M. Ichikawa, J. Catal. 182 (1999) 92.

[10] Y.B. Cui, Y.B. Xu, Y. Suzuki, Z.-G. Zhang, Catal. Sci. Technol. 1 (2011) 823.

[11] K. Honda, T. Yoshida, Z-G Zhang, Catal. Commun. 4 (2003) 21-26.

[12] B.M. Weckhuysen, D.J. Wang, M.P. Rosynek, J.H. Lunsford, J. Catal. 175 (1998) 338.

[13] H.M. Liu, T. Li, B.L. Tian, Y.D. Xu, Appl. Catal., A: Gen. 213 (2001) 103.

[14] D. Ma, D.Z. Wang, L.L. Su, Y.Y. Shu, Y.D. Xu, X.H. Bao, J. Catal. 208 (2002) 260.

[15] H.T. Ma, R. Kojima, S. Kikuchi, M. Ichikawa, J. Nat. Gas Chem. 14 (2005) 129.

[16] E.V. Matus, I.Z. Ismagilov, O.B. Sukhova, V.I. Zaikovskii, L.T. Tsikoza, Z.R. Ismagilov, Ind. Eng. Chem. Res. 46 (2007) 4063-4074.

Table 6-1. BET surface areas and micropore volumes of fresh and spent catalysts

Reaction time	BET surface areas of x/Mo/HZSM-5 [m^2/g][b]					Micropore volumes of x/Mo/HZSM-5 [cm^3/g][c]				
[min]	1	2	4	6	8	1	2	4	6	8
Fresh[a]	393	381	312	310	308	0.1700	0.1663	0.1334	0.1344	0.1272
6	--	331	300	279	--	--	0.1435	0.1252	0.1134	--
30	--	318	267	253	--	--	0.1311	0.1076	0.1027	--
40	279	--	--	--	--	0.1129	--	--	--	--
60	--	260	253	234	--	--	0.1051	0.1009	0.0929	--
100	--	219	228	209	208	--	0.0857	0.0887	0.0818	0.0818
150	--	--	180	177	168	--	--	0.0692	0.0675	0.0655

[a] Fresh catalyst

[b] Evaluated by BET method

[c] Evaluated by t-plot method

Table 6-2. Coke amount of spent catalysts

Reaction time	M1 of x/Mo/HZSM-5 [%]					M2 of x/Mo/HZSM-5 [%]				
[min]	1	2	4	6	8	1	2	4	6	8
6	--	0.01	0.03	0.16	--	--	1.70	1.91	1.02	--
30	--	0.04	0.13	0.16	--	--	4.22	4.72	3.73	--
40	0.01	--	--	--	--	5.68	--	--	--	--
60	--	0.06	0.17	0.18	--	--	6.21	7.15	5.49	--
100	--	0.09	0.23	0.27	0.40	--	9.22	8.36	10.22	5.47
150	--	--	0.24	0.31	0.37	--	--	16.09	17.31	8.55

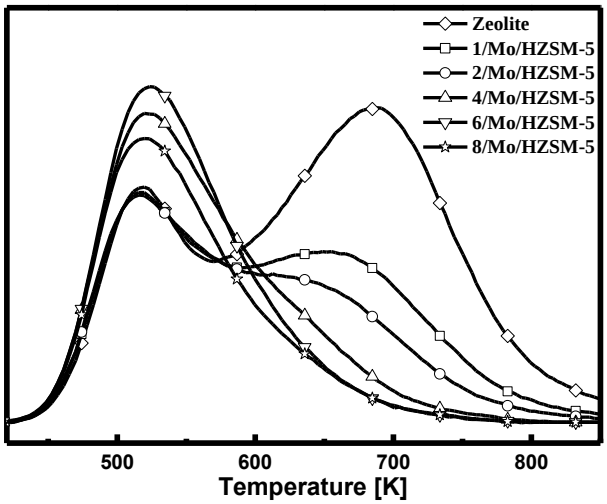

Fig.6-1. NH3-TPD profiles of HZSM-5 zeolite, and all x/Mo/HZSM-5 samples.

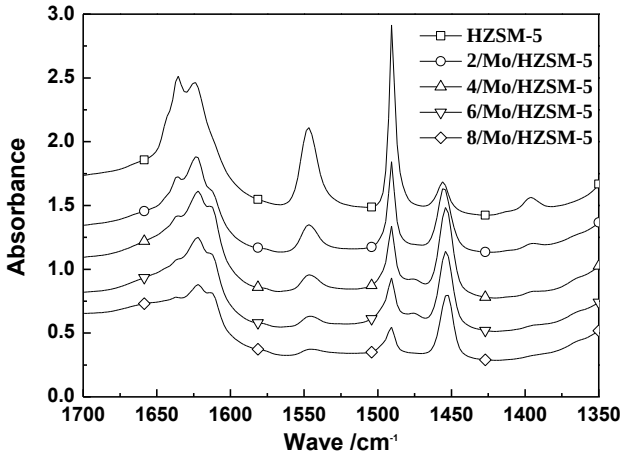

Fig.6-2. FT-IR profiles of HZSM-5 zeolite, and x/Mo/HZSM-5 samples.

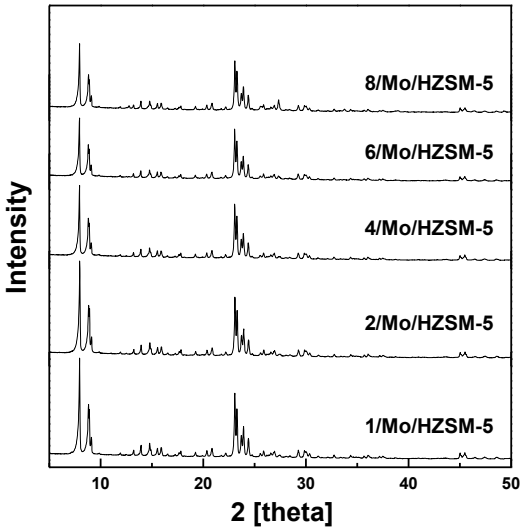

Fig.6-3. XRD patterns of all x/Mo/HZSM-5 samples.

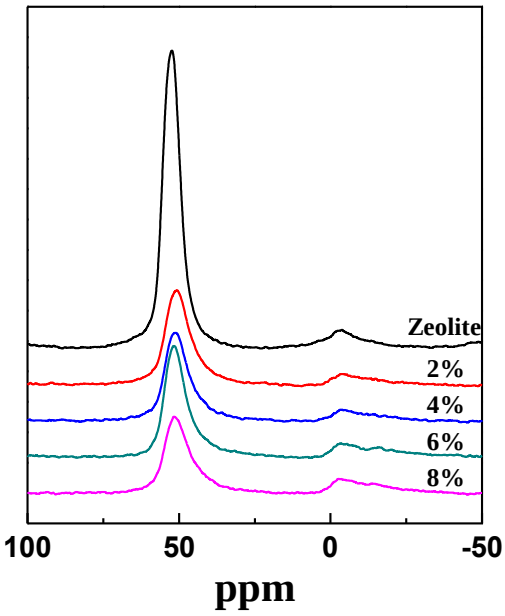

Fig. 6-4. ^{27}Al MAS NMR spectra of zeolite and x%Mo/HZSM-5

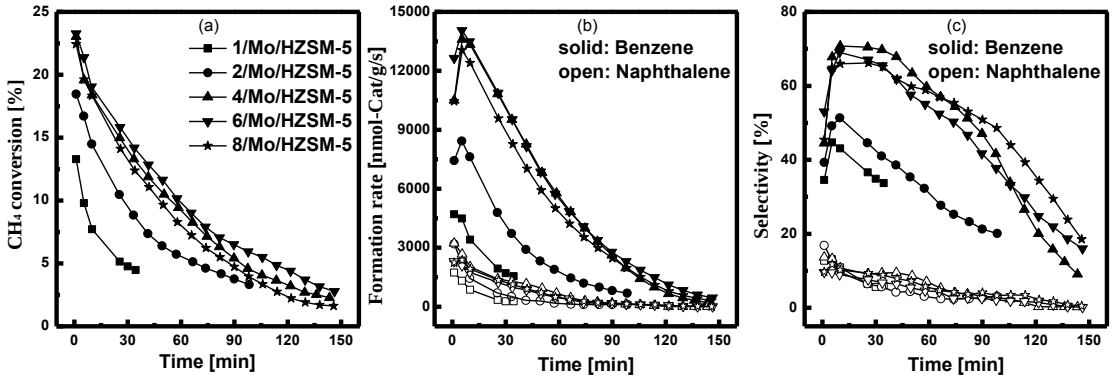

Fig.6-5. A comparison of catalytic performances of Mo/HZSM with different Mo loading. (a) methane conversion. (b) rates of benzene and naphthalene formation. (c) selectivity of benzene and naphthalene. (space velocity = 10000 ml/g cat/h, 1073 K)

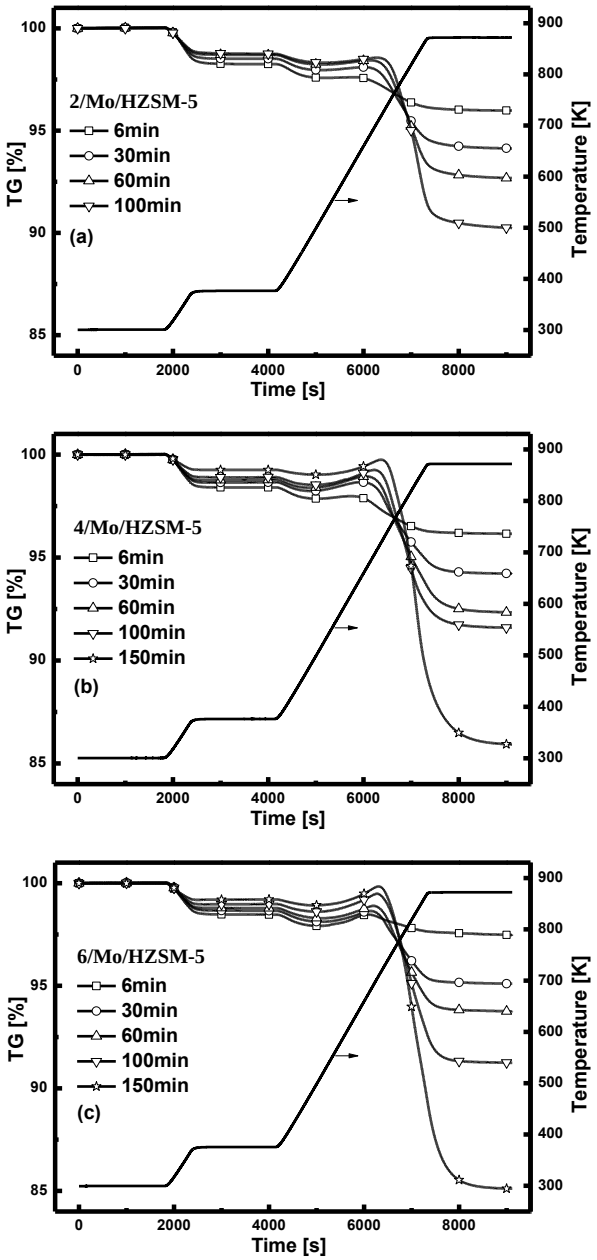

Fig. 6-6. TG profiles of spent catalysts with different reaction time. (a) 2/Mo/HZSM-5, (b) 4/Mo/HZSM-5, (c) 6/Mo/HZSM-5

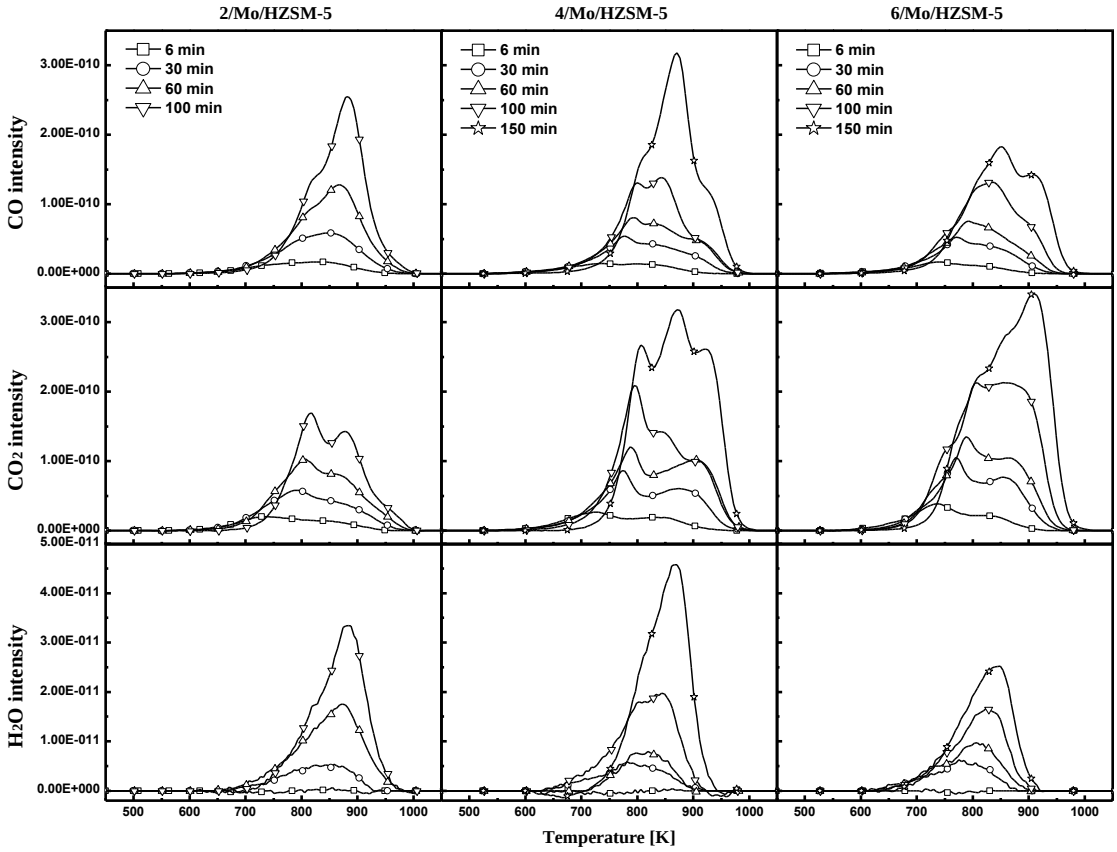

Fig. 6-7. Intensities of CO, CO_2 and H_2O curves from TPO outlet stream of spent catalysts.(in a flow of 50 ml/min feed gas mixture of 90 % He and 10 % O_2 at a heating rate of 10 K/min from room temperature to 1103 K.)

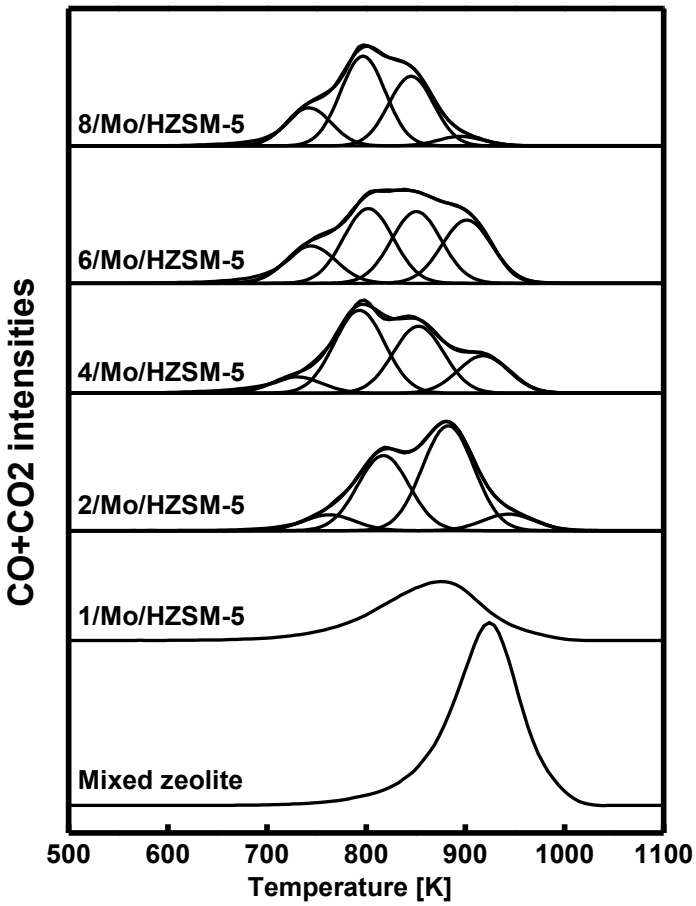

Fig.6-8. The total CO and CO_2 intensities from the TPO outlet stream of different spent catalysts and mixed zeolite. (1/Mo/HZSM-5 after 40 min reaction, and other samples after 100 min reaction)

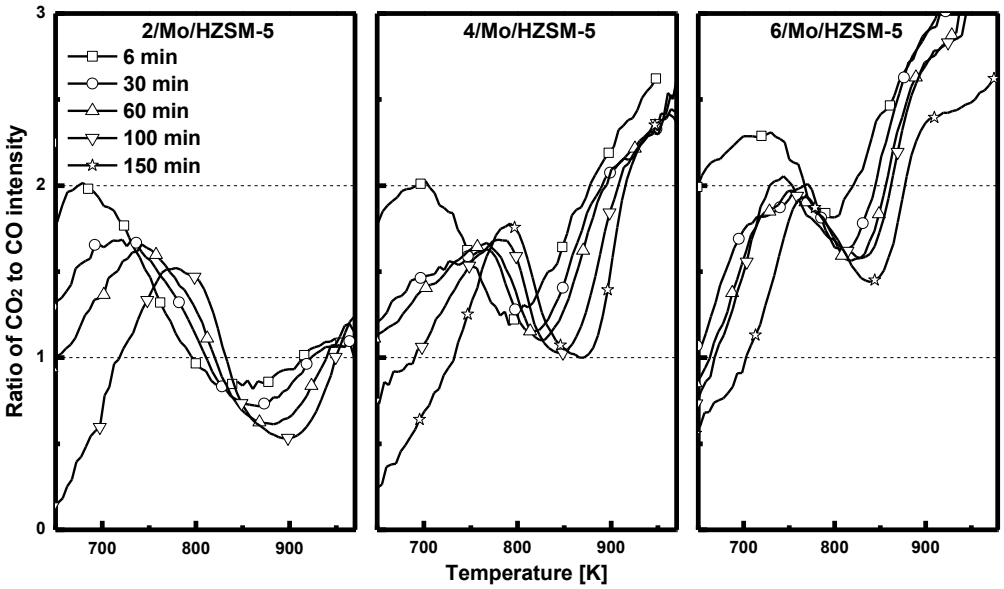

Fig. 6-9. Ratio of CO_2 to CO intensity from TPO outlet stream of different spent catalysts.

Chapter 7

Conclusions

Non-oxidative methane dehydroaromatization reaction (MTB) over Mo/HZSM-5 catalyst is a promising route for direct conversion of methane resources into highly value-added chemicals. However, coking-caused catalyst deactivation problem remains still unsolved. A series of experiments was conducted in this thesis to investigate the coke formation behavior over Mo/HZSM-5 catalyst during the MTB reaction. This thesis focuses mainly on the coking pathways, coking locations, types of coke formed and coke formation behavior in cyclic CH_4-H_2 switching operation mode. First, by pursuing coke formation behavior over the lifetime of Mo/HZSM-5 catalyst and examining the effect of co-fed H_2 in CH_4 feed on the distribution of coke formed in a multi-layer fixed bed reactor, this thesis has successfully proved that not the aromatic product C_6H_6 but the intermediate C_2H_4 is the dominant source of coke deposition. Second, by pursuing coke accumulation behavior in cyclic CH_4-H_2 switching operation mode and coke removal behavior in pure H_2, this thesis has revealed for the first time that the graphite-like coke formed at the channel mouths of the zeolite is responsible for the catalyst deactivation. Third, by using TPO technique and comparing the TPO patterns of spent Mo/HZSM-5 catalysts with that of coked HZSM-5, this thesis has also clarified the catalytic role of Mo species on promoting the coke burning in the TPO process and four types of coke forming on microzeolite-based Mo/HZSM-5 catalyst in the title reaction.

Achievements

Journal publication:

[1] **Yang Song**, Yuebing Xu, Yoshizo Suzuki, Hideki Nakagome and Zhan-Guo Zhang. A clue to exploration of the pathway of coke formation on Mo/HZSM-5 catalyst in the non-oxidative methane dehydroaromatization at 1073 K. *Applied Catalysis A: General*, **482**,387–396 (2014).

[2] **Yang Song**, Yin Wang, Wu Yang, Changbin Yao and Guangwen Xu. Reduction of NO over biomass tar in micro-fluidized bed. *Fuel Processing Technology*, **118**, 270–277 (2014).

[3] Yuebing Xu, **Yang Song**, Yoshizo Suzuki and Zhan-Guo Zhang. Mechanism of Fe additive improving the activity stability of microzeolite-based Mo/HZSM-5 catalyst in non-oxidative methane dehydroaromatization at 1073 K under periodic CH4–H2 switching modes. *Catalysis Science Technology*, **4**, 3644-3656 (2014).

[4] Yuebing Xu, **Yang Song**, Yoshizo Suzuki and Zhan-Guo Zhang. Effect of superficial velocity on the coking behavior of a nanozeolite-based Mo/HZSM-5 catalyst in the non-oxidative CH4 dehydroaromatization at 1073 K. *Catalysis Science Technology*, **3**, 2769-2777 (2013).

[5] Wu Yang, Yin Wang, **Yang Song**, Changbin Yao, Yuejin Liu and Gaungwen Xu. NO Reduction Characteristics of Biomass Pyrolysis Products in a Drop-tube Reactor. *The Chinese Journal of Process Engineering*, **13**,191-196 (2013).

Conference presentation:

[6] **Yang Song**, Yuebing Xu, Yoshizo Suzuki and Zhan-Guo Zhang. Catalytic effect of Mo on the TPO behavior of coke formed on Mo/HZSM-5 in the non-oxidative methane dehydroaromatization. *Proceedings of 64th Canadian chemical engineering conference*, 19-22. (2014).

[7] **Yang Song**, Yuebing Xu, Yoshizo Suzuki, Hideki Nakagome and Zhan-Guo Zhang. Determination of the location of coke deactivating Mo/HZSM-5 catalyst in the non-oxidative methane dehydroaromatization. *Proceedings of the 114th Japan catalysis symposium*, 3I13 (2014).

[8] Yuebing Xu, **Yang Song**, Yoshizo Suzuki and Zhan-Guo Zhang. Distinguishing of the external and internal coke depositions on HZSM-5 zeolite using temperature-programmed catalytic oxidation technique. *Proceedings of 114th Japan catalysis symposium*, 3I14, (2014).

[9] Changbin Yao, **Yang Song**, Yin Wang, Guangwen Xu. Reduction of NO over biomass tar in micro fluidized bed. *Proceedings of the 7th world congress of particle technology*, (2014).

[10] Gaungwen Xu, Changbin Yao, **Yang Song**, Wang Wang, and Shiqiu Gao. Decoupling combustion based on dual fluidized bed for industrial biomass waste: Fundamentals and application. *Proceedings of the 11th International Conference on Fluidized Bed Technology*, 649-652 (2014).

[11] Zhanguo Zhang, Yuebing Xu, **Yang Song** and Yoshizo Suzuki. Development of a Two Beds Circulating Fluidized Bed Reactor System for Non-Oxidative Aromatization of Methane over Mo/HZSM-5 Catalyst. *Proceedings of 2014 AIChE Annual Meeting*, M101 (2014).

[12] **Yang Song**, Wu Yang, Yin Wang and Guangwen Xu. Characterization of NO reduction by biomass tar in micro fluidized bed. *Proceedings of the 13th international conference on polygeneration strategies*, (2013).

[13] **Yang Song**, Yuebing Xu, Yoshizo Suzuki, Hideki Nakagome and Zhan-Guo Zhang. Catalytic effect of Mo on the TPO behavior of coke formed on Mo/HZSM-5 in the non-oxidative methane dehydroaromatization. *Proceedings of the 112th Japan catalysis symposium*, 3E11 (2013).

[14] Yuebing Xu, **Yang Song**, Yoshizo Suzuki and Zhan-Guo Zhang. Effect of CH4 flow rate and catalyst load on the activity stability of Mo/HZSM-5 in the methane dehydroaromatization at 1073 K in an integral, fixed-bed reactor. *Proceedings of the 12th Japan-China Symposium on Coal and C1 Chemistry*, A102 (2013)

[15] Yuebing Xu, **Yang Song**, Yoshizo Suzuki and Zhan-Guo Zhang. Deactivation behavior of Mo/HZSM-5 in methane dehydroaromatization at 1073 K in an integral, packed-bed reactor. *Proceedings of 112th Japan catalysis symposium*, 3E12 (2013).

Acknowledge

This work, started at October 2012, has been carried out at Professor Hideki Nakagome's laboratory in Chiba University in collaboration with Doctor Zhan-Guo Zhang's group in National Institute of Advanced Industrial Science and Technology (AIST). Without the support and help from many people for this thesis, it cannot be presented to advance knowledge in this research area. I would like to take this opportunity to express my gratitude to all of them.

I would like to express my sincere gratitude to Professor Nakagome. I benefited a lot from his comprehensive guidance. When I discussed my research with him, he always gave me some vital advices and encouraged me to promote my research.

I would like to express my sincere gratitude to Doctor Zhan-Guo Zhang. As a talented and wise supervisor, he not only gave me a thoughtful and thorough guidance in scientific research during my doctoral project, but also enlightened me to give insight into our complex world from new angles. In fact, I feel it is really a great honor for me to spend such an important period with him.

I would like to deeply thank Associate Professor Yuebing Xu. He was doing his post-doctoral work in the same project in AIST when I enrolled in my doctoral program. To me he's truly like a brother and someone who helped me so much when I was starting out at Japan. He always discussed research with me patiently and without reservation, and I truly learnt a lot from him to promote my work.

I would like to thank the members of my thesis committee, Professor Hironao Ogura, Professor Yasuo Sugai and Associate Professor Takaaki Wajima for their precious time and vital advices.

I deeply thank all the people who help me to promote my work and share happiness with me. They are Doctor Renzhong Piao, Doctor Yasumasa Kawabata, Doctor Yoshinori Yanagisawa, Master Ichi Kyo and Ms Sachiko Sugioka from Nakagome's laboratory in Chiba University; Doctor Hajime Yasuda, Doctor Yoshizo Suzuki, Doctor Koichi Matsuoka, Doctor Kuramoto koji, Master Yulien Chen and Ms Makiko Tokuda from AIST; Doctor Hongtao Ma from Meidensha corporation; Doctor Feng Guo and Doctor Lina Gan from Chinese Academy of Sciences, and so on.

I would like to thank my family. I owe a lot of appreciates to my family filled with selfless love. My parents set a good example for my behavior. My grandparents poured their grace on me. My sister is a best partner who I grew up with. When I meet confusion and hesitation, I always get the courage and supports from them to overcome any obstacles. I can also feel their happiness from the heart for me when I make any progress in my study and life.

Yang Song